# Hazard Resilience Testing of US Pipe Ductile Iron TR-XTREME™ Pipe Joints

Submitted to:

Russ Huggins PE
AVP of Product Development and Quality
US Pipe

By

H. E. Stewart
C. Pariya-Ekkasut
B. P. Wham
T.D. O'Rourke
C. Argyrou
T.K. Bond


Cornell University
School of Civil and Environmental Engineering
Cornell University
Hollister Hall
Ithaca, NY 14853

February, 2015

## EXECUTIVE SUMMARY

US Pipe has developed a hazard resistant ductile iron (DI) pipe joint, called the TR-XTREME™ joint. This new joint designed for extreme hazards is based on the TYTON JOINT® design and other US Pipe experiences with the HP LOK® and other US Pipe restraining systems. The TYTON JOINT® has been previously tested at Cornell University. Sections of 6-in. (150-mm) pipes with the TR-XTREME™ joints were tested at Cornell University to 1) evaluate the stress-strain-strength characteristics of the DI, 2) evaluate the bending resistance and moment-rotation relationship of the joint for two positions of the locking clip segments, 3) determine the capacity of the joint in direct compression and tension, 4) investigate the axial soil resistance and pull-out capacity of the pipe-joint when buried in soil with and without a polywrap covering, and 5) evaluate the capacity of a 6-in. (150-mm) DI pipeline with TR-XTREME™ joints to accommodate fault rupture using the Cornell full-scale split-basin testing facility.

It should be noted that the term "rotation" in this report is equivalent to "deflection" as used commonly in the field and commercial pipeline information. Test results are summarized for tensile stress-strain-strength characteristics, bending test results, direct joint compression and tension, axial soil/pipe resistance, pipeline response to fault rupture, and significance of test results under the headings that follow.

### Tensile Stress-Strain- Strength Characteristics

The tensile test data for the DI specimens taken from the pipe with TR-XTREME™ joints show similar tensile stress vs. strain characteristics as specimens taken from DI pipe with the TYTON JOINT®. Given this similarity, there should be little to no difference in the mechanical performance of the DI pipe with the TR-XTREME™ joints relative to other US Pipe DI pipe with similar geometric characteristics. Improvements in the casting and pipe fabrication associated with other US Pipe DI are expected to result in pipeline response to large ground deformation that either equals or exceeds the TR-XTREME™ pipe response.

### Bending Test Results

Four-point bending tests were performed to evaluate the moment vs rotation relationships of the TR-XTREME ™ joints when the locking clips were at the 3 and 9 o´clock positions (Test A) and the 12 and 6 o´clock positions (Test B). Test A failed at an applied moment of 515 kip-in. and at

an average rotation of 8.6 degrees. Test B failed at an applied moment of 480 kip-in. (7% lower than Test A) and at an average rotation of 9.1 degrees (6% higher than Test A). There is no significant moment – rotation difference for the two tests. The test results show that moments in the range of the proportional limit, $M_{prop}$, and the yield moment, $M_{yield}$, were associated with loss of pressure and pipe leakage. Stress concentrations related to spigot-bead contact with the restraining clips are a likely source of local deformations leading to leakage at such moments.

**Direct Joint Compression and Tension**

The compressive testing showed that the TR-XTREME™ joint was able to accommodate axial loads to a compressive level at about the DI proportional limit. After this stress level was reached, progressive bending and local distortion of the pipe occurred. Axial loads of roughly 350 kips were applied to the joint. These results were similar to those from the four-point bending tests in which local deformation developed and subsequent leakage occurred after moments, corresponding to the proportional limit, were applied.

Two tension tests were performed on the US Pipe with TR-XTREME™ joints. Tests T1 and T2 reached a maximum force of 83 kips (369.2 kN) at 2.75 in. (69.6 mm) of axial displacement and an axial load of 78 kips (346.0) at 2.72 in. (69.1 mm) of joint displacement, respectively. The joints began to leak at openings of 3.3 and 3.5 in. (83.8 and 88.9 mm) for T1 and T2, respectively. The overall behavior of T1 and T2 was nearly identical.

The onset of leakage was caused by forces generated between the spigot bead and restraining clips that deform the spigot inward a sufficient distance to allow the bead to slip past the clips, with attendant loss of water pressure. Similar to the compressive and four-point bending test results for the US Pipe TR-XTREME™ joint, leakage occurred in the tensile tests when localized strains resulted in irrecoverable deformation. In this case, those strains are circumferential, and the irrecoverable deformation was reflected in shortening of the spigot diameter caused by forces between the spigot bead and clips.

**Axial Soil/Pipe Resistance**

The axial soil resistance tests confirm axial slip of the TR-XTREME™ joint under conditions in which sufficient soil/pipe shear resistance is mobilized either side of the joint to exceed the force required to initiate joint slip. Once the spigot bead engages the clips that, in turn, engage the bell

mouth, additional resistance to pullout is mobilized from soil reaction at the bell as it is pulled through the soil. The test results provide excellent data with which to quantify the axial pullout loads and displacements when there is relative movement between the adjacent soil and pipelines with 6 in. (150 mm) TR-XTREME™ joints.

The test results show that the polywrap reduced the axial pullout force by about 15% or more at displacements exceeding 4 in. (102 mm) when compared with unwrapped pipe under similar burial conditions. The reduced axial force is caused by the lower interface resistance between the soil and polywrap when compared with the interface resistance between soil and ductile iron pipe.

There is less than 10% difference between the ultimate pullout forces associated with the flat and curved ends of the bell oriented towards the direction of movement. The force vs. displacement data show that the ultimate pullout resistance is mobilized more rapidly when the flat end of the bell is oriented toward the direction of movement, thus contributing to a stiffer reaction.

**Pipeline Response to Fault Rupture**

A 39-ft (11.9-m)-long, five-piece section of a DI pipeline with TR-XTREME™ joints was tested at the Cornell Large-Scale Lifelines Facility. The pipe had four joints, equally spaced about a 50º fault. The pipe was pressurized to approximately 80 psi (552 kPa). The pipe was placed on a bed of compacted partially saturated sand, aligned, instruments checked, and then backfilled with compacted sand to a depth of cover of 30 in. (762 mm) above the pipe crown. The test basin's north section was displaced along a 50º fault at a rate of 12 in. (305 mm) per minute. At a fault displacement of roughly 19.0 in. (483 mm) there was an audible "pop," the pipe lost pressure, and the test was stopped. The 19.0 in. (483 mm) fault displacement corresponds to 12.2 in. (310 mm) of axial extension of the test basin and pipe. Following excavation, a fracture was observed at the west springline of the bell of the south joint.

The test measurements confirm that the pipeline was able to accommodate successfully fault rupture through axial displacements and rotations at all four joints. Moreover, the measurements provide a comprehensive and detailed understanding of how the movement was accommodated at each joint, the sequence of movements, and combined axial pullout and rotation at each joint. The combined joint pullout displacements are 12.2 in. (310 mm), which exceeds the sum of the 2.3 in. (58.4 mm) spigot insertion length for all four joints. On average, the spigot at each joint pulled from the bell on the order of 3.05 in. (77 mm), thus confirming that significant additional pullout

occurs beyond the slip required for the spigot bead to make contact with the restraining clips. This type of additional pullout capacity was observed at comparable levels of movement during previous tension testing of TR-XTREME™ joints. The maximum rotation measured at the joints closest to the fault was nearly six degrees, thus demonstrating the ability of the joints to sustain significant levels of combined axial pullout and rotation. The maximum stresses sustained by the pipeline, corresponding to the largest pipeline deformation, were well within the elastic range of pipeline behavior.

The pipeline with TR-XTREME™ joints was able to accommodate significant fault movement through axial pullout and rotation of the joints. Fault rupture simulated in the large-scale test is also representative of the most severe ground deformation that occurs along the margins of liquefaction-induced lateral spreads and landslides.

**Significance of Test Results**

The amount of tensile strain that can be accommodated with pipelines with TR-XTREME™ joints will depend on the spacing of the pipeline joints. The pipeline used in the large-scale split-basin test was able to accommodate 12.2 in. (310 mm) of axial extension, corresponding to an average tensile strain of 2.61% along the pipeline. Such extension is large enough to accommodate the great majority (over 99%) of liquefaction-induced lateral ground strains measured by high resolution LiDAR after each of four major earthquakes during the recent Canterbury Earthquake Sequence (CES) in Christchurch, NZ. These high resolution LiDAR measurements for the first time provide a comprehensive basis for quantifying the ground strains caused by liquefaction on a regional basis. To put the CES ground strains in perspective, the levels of liquefaction-induced ground deformation measured in Christchurch exceed those documented in San Francisco during the 1989 Loma Prieta earthquake and in the San Fernando Valley during the 1994 Northridge earthquake. They are comparable to the levels of most severe liquefaction-induced ground deformation documented for the 1906 San Francisco earthquake, which caused extensive damage to the San Francisco water distribution system.

The tests confirm that the TR-XTREME™ joints are able to sustain without leakage large levels of ground deformation through axial displacement and rotation. The test results are directly applicable to the performance and behavior of nominal 4-in. (100-mm), 6-in. (150-mm), and 8-in. (200-mm) US Pipe DI pipelines with TR-XTREME™ joints.

## TABLE OF CONTENTS

## TABLE OF CONTENTS (continued)

## TABLE OF CONTENTS (completed)

## LIST OF FIGURES

## LIST OF FIGURES (continued)

## LIST OF FIGURES (continued)

## LIST OF FIGURES (completed)

## LIST OF TABLES

## Section 1

## Introduction and Organization

This report presents testing results performed at Cornell University for 6-in. (150-mm)-diameter US Pipe with a newly designed hazard-resistant joint. The purpose of the testing was to characterize the mechanical behavior of the TR-XTREME™ jointed pipe. The report is organized in eight sections, the first of which provides introductory remarks and describes the report organization. Section 2 presents the results of tensile coupon testing. Several coupons were machined from the ductile iron provided with the test joints. The results for Young' modulus, yield strength, and elongation are given. Section 3 gives the results of two four-point bending tests used to determine the moment-rotation relationships as dependent on locking clip position. Sections 4 and 5 give the results of direct compression and tension tests on pipe joints. The compression and tension capacities of the joints are evaluated, and limit conditions of pipe leakage are provided. Section 6 presents the results of three axial soil resistance tests using 6-in.- (150-mm)-diameter pipe. Tests were performed with the joint facing different directions to determine the sensitivity of axial resistance to joint direction during pull. In addition, a special polywrap was used in one test to investigate the difference in frictional resistance with and without an additional wrap on the pipe. Section 7 presents the results of fault rupture effects on a pipeline performed in the large-scale test basin at the Cornell University Large Scale Lifelines Testing Facility. Section 8 provides summary remarks and draws conclusions for the testing. It should be noted that the term "rotation" in this report is equivalent to "deflection" as used commonly in the field and commercial pipeline information.

# Section 2

# Tensile Coupons

## 2.1 Introduction

This section of the report describes the uniaxial tension testing of ductile iron (DI) from a TR-XTREME™ jointed pipe specimen provided by US Pipe. The test results are used to determine the strength and ductility of the material. Tensile coupons were machined from the DI pipe specimen and tested in tension to determine the yield strength, ultimate strength, and ultimate strain of the material. All testing was completed in accordance with ASTM – E8 2013 standards (ASTM, 2013) to ANSI/AWWA C151/A21.51-09 60-42-10 [60 ksi (414 MPa) ultimate tensile strength, 42 ksi (290 MPa) yield, and 10% elongation] specifications (AWWA, 2009).

## 2.2 Tensile Coupon Testing

### 2.2.1 Specifications and Specimen Type

The tensile coupons were machined from the pipe to obtain the nominal dimensions shown in Figure 2.1. These dimensions comply with ASTM - E8 2013 (ASTM, 2013) for large diameter tubes. Adjustments were also made to four of the original specimens by machining the surface of the reduced area to decrease pitting, as explained in the following section.

### 2.2.2 Pitting

The pipe showed a considerable amount of surface irregularity, as shown in Figure 2.2 below. After machining, the specimen still showed significant surface pitting (see Figure 2.3.) Surface pitting was removed by machining the surface to create a more uniform specimen, as shown in Figures 2.4 and 2.5. The surfaces of four specimens (Test Specimens 1 – 4) were machined to reduce pitting, while two were left in their original state (Test Specimens 5 – 6). A comparison of the test results for the machined and unmachined specimens allows for evaluation of effect of surface pitting on the strength of the DI coupons. The actual thicknesses of Specimens 1 – 6 are given in Table 2.1.

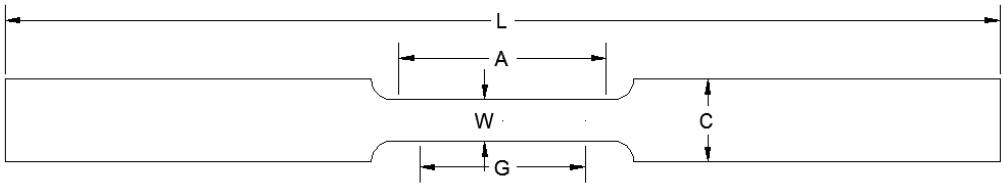


| Sheet-Type, .5 in Wide | |
|---|---|
| *Dimensions* | *Length (in.)* |
| G - Gauge Length | 2.00 |
| W - Width | 0.50 |
| T - Thickness | |
| R - Radius | 0.50 |
| L - Overall Length | 8.00 |
| A - Length of Reduced Section | 2.25 |
| C - Width of Grip Section | 1.00 |

Figure 2.1. Schematic of Tensile Coupon Specimen

Table 2.1. Tensile Coupon Thicknesses

| Test Specimen | Type | Thickness (in.) |
|---|---|---|
| 1 | Reduced Thickness (without Pitting) | 0.245 |
| 2 | Reduced Thickness (without Pitting) | 0.250 |
| 3 | Reduced Thickness (without Pitting) | 0.260 |
| 4 | Reduced Thickness (without Pitting) | 0.257 |
| 5 | Original Thickness (with Pitting) | 0.320 |
| 6 | Original Thickness (with Pitting) | 0.308 |

## 2.3 Testing and Procedure

All testing was performed in accordance with ASTM - E8 2013 (ASTM, 2013). A Baldwin Hamilton 60 BTE Universal Testing Machine was used to apply tensile loads. This load frame was fitted with a pressure sensor to measure force in the system. The machine was calibrated in March of 2014. A

Figure 2.2. Ductile Iron Pipe Specimen with Significant Material Irregularities

Figure 2.3. Surface Pitting on Ductile Iron Coupon before Machining of Reduced Area of Specimen 1

Figure 2.4. Surface of Ductile Iron Coupon after Machining of Reduced Area of Specimen 1

Figure 2.5. Machining of Surface to Reduce Surface Pitting on Specimen 1

Figure 2.6. Baldwin Testing Apparatus

Table 2.2. Tensile Coupon Test Instrumentation

| | Instrumentation | | | | |
|---|---|---|---|---|---|
| Test Specimen | Axial Load | Axial Strain Gage | Axial Laser Extensometer. | Axial Clip-On Extensometer | Transverse Strain Gage |
| 1 | ✓ | ✓ | ✓ | | ✓ |
| 2 | ✓ | ✓ | ✓ | ✓ | ✓ |
| 3 | ✓ | ✓ | ✓ | ✓ | ✓ |
| 4 | ✓ | ✓ | ✓ | | ✓ |
| 5 | ✓ | ✓ | ✓ | ✓ | ✓ |
| 6 | ✓ | ✓ | ✓ | ✓ | ✓ |

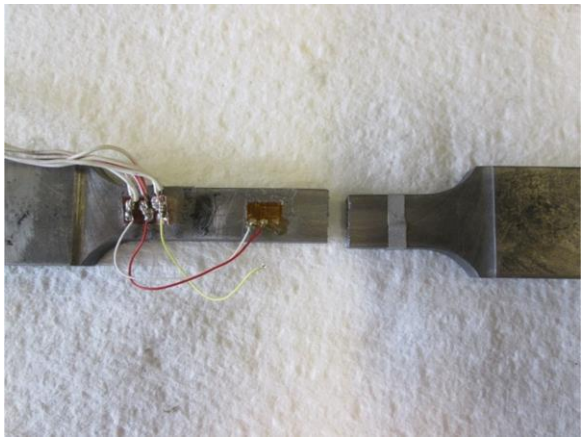

Figure 2.7. Clean and Uniform Break of Test Specimen

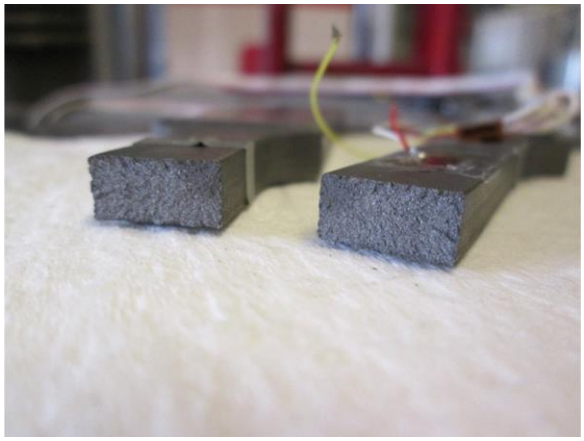

Figure 2.8. Slight Discoloration of at Top-Left Corner of Break of Test Specimen

Bondable axial and transverse strain gages were used in testing to measure small strains. These gages were mounted in the center of the reduced area of the specimen. All measured both axial and transverse strains except on Test Specimen 5, which only measured axial strains. Strain gages were generally used for smaller strains, as they were considerably more accurate at these levels but debonded before failure, rendering them ineffective at larger strains. A laser extensometer was used to measure axial strain to failure. This device was not as accurate at smaller strains as the strain gages, but provided an accurate reading of strain at larger values, specifically those past the failure of the bonded strain gages. Test Specimens 2 - 6 utilized a clip-on extensometer. This proved to be more accurate than the laser extensometer at smaller strains and also provided additional measurements to confirm the DI test results. Table 2.2 lists the instrumentation used during the tensile coupon testing.

## 2.4 Analysis of Specimens 1 – 4 (without Pitting)

Testing on test Specimens 1 - 4 provided data of force, axial and transverse strains of the more uniform material, as these specimens were machined to reduce pitting Specimens 1 - 4 failed relatively uniformly and cleanly, shown in Figure 2.7. As can be seen in Figure 2.8, there was a slight discoloration at the likely start of the break.

### 2.4.1 Stress vs. Strain Curves

The analysis began with the development of stress vs. strain curves. Applied stress throughout the uniaxial test was computed by dividing the measured force by the original cross-sectional area of the

tensile coupon. This generally is referred to as engineering strain. The uniaxial stress vs. axial strains for Specimens 1 – 4 are shown in Figures 2.9 – 2.12

### 2.4.2 Young's Modulus, Yield Strength, and Proportional Limit

Young's modulus was computed using the elastic region of the stress - strain curve and the bonded axial strain gage data. These data are shown to a strain of 0.006 in Figure 2.13. Young's Modulus was determined by performing a linear regression for stress vs. strain from 5 ksi to 30 ksi (34 to 207). The yield strength, $\sigma_y$, was then computed using the offset method, in which the computed slope was used to create a line from 0.2% strain. The intersection of this line and the stress-strain curve provided an estimate of the yield point for each specimen. However, Figure 2.13 shows that the stress-strain curves are linear at stresses well below 0.2% strain. Then, the tensile coupons tend to have a significant increase in strains with little change in stresses before reaching the yield point from the 0.2% strain offset method. The yield strains derived from the 0.2% offset are about 0.40%, which is double 0.2% strain. The 0.2% strain is taken as a proportional limit, beyond which the relationship between stresses and the strains is no longer linear. The 0.2% strain is defined as a proportional strain, and the corresponding stress is called a proportional strength. The Young's modulus, yield stress, and proportional limit for the specimens are presented in Table 2.3. The average Young's Modulus is 22,650 ksi (156 GPa) with a standard deviation of 520 ksi (0.36 GPa). The average yield stress is 52.5 ksi (362 MPa) with a standard deviation of 0.8 ksi (5.5 MPa). The average proportional stress is 42.0 ksi (289.6) MPa with a standard deviation of 0.9 ksi (6.2 MPa).

### 2.4.3 Ultimate Tensile Strength and Strain

Ultimate strength and strain were determined by finding the maximum stress and strain in testing, or the point of fracture for test specimens 1 - 4. Axial stress - strain data from the laser extensometers were used as shown in Figure 2.14. Table 2.4 gives the failure tensile stress and failure strain for these four specimens. The average ultimate tensile stress was 81.1 ksi (559.2 MPa) with a standard deviation of 5.0 ksi (34.5 MPa). The maximum strains for specimens 1 – 4 ranged from 3.7 to 12.1%. The average value was 7.1% with a standard deviation of 3.6%.

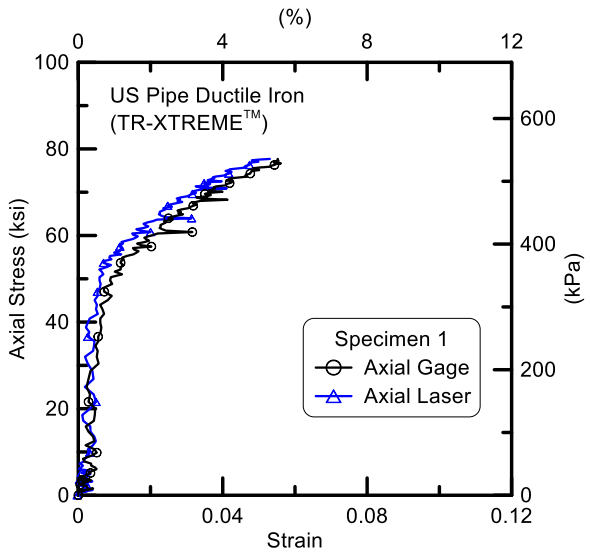


Figure 2.9. Stress – Strain Curve for Specimen 1

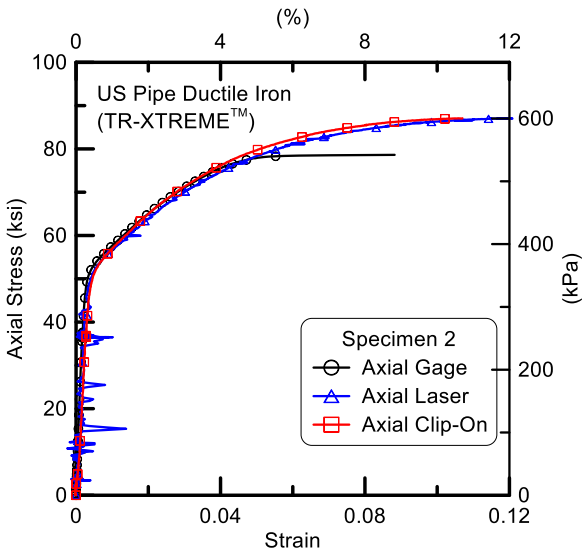


Figure 2.10. Stress – Strain Curve for Specimen 2

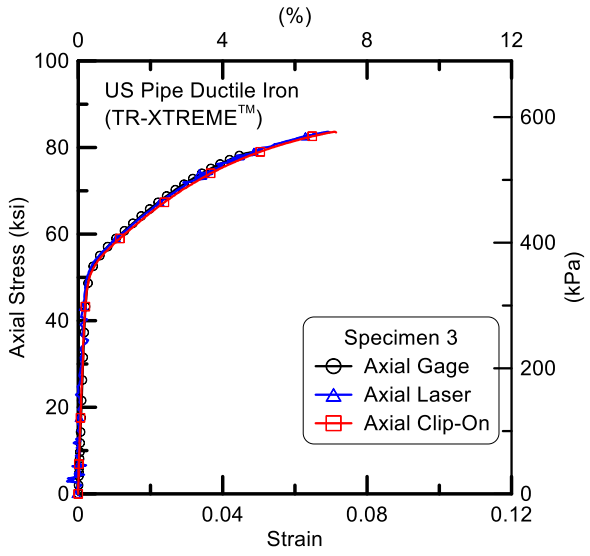


Figure 2.11. Stress – Strain Curve for Specimen 3

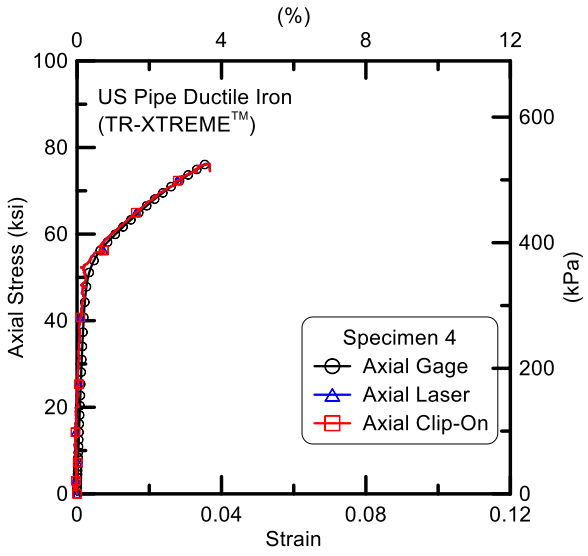


Figure 2.12. Stress – Strain Curve for Specimen 4

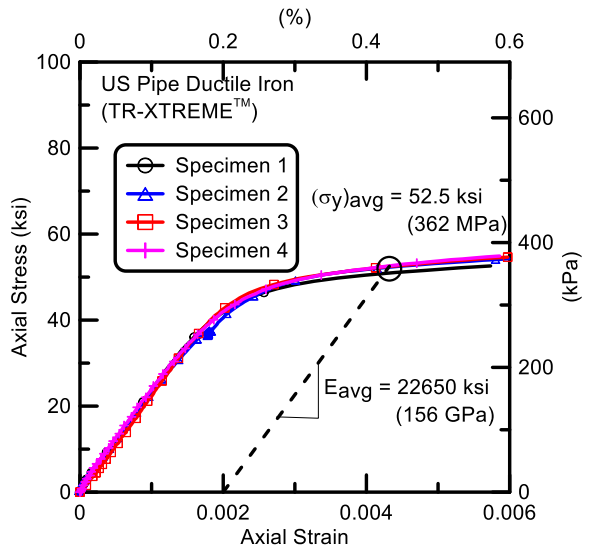


Figure 2.13. Average Young's Modulus and Yield Stress for Specimens 1 – 4

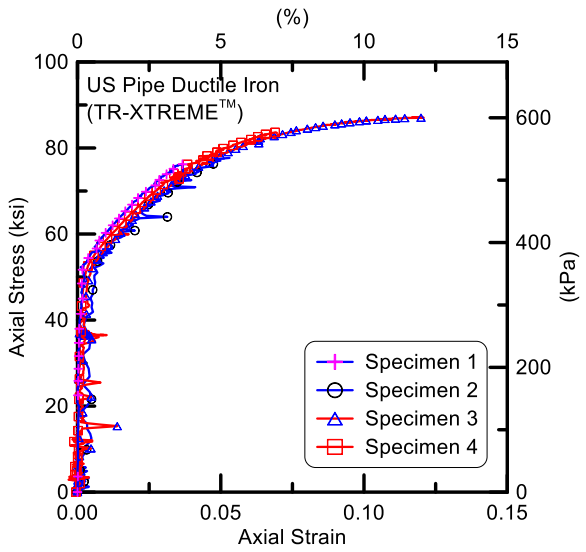


Figure 2.14. Stress - Strain Curve to Failure Using Laser Extensometer Data

Table 2.3. Young's Modulus and Yield Point for Specimens 1 - 4

| Specimen | Young's Modulus, E (ksi) | Offset Yield, $\sigma_y$ (ksi) | Proportional Limit, $\sigma_{prop}$ (ksi) |
|---|---|---|---|
| 1 | 22990 | 51.3 | 42.4 |
| 2 | 21780 | 53.0 | 40.5 |
| 3 | 23090 | 52.8 | 42.8 |
| 4 | 22730 | 53.0 | 42.1 |
| Average | 22650 | 52.5 | 42.0 |
| Standard Deviation | 520 | 0.8 | 0.9 |

1 ksi = 6.89 MPa

Table 2.4. Summary of Ultimate Tensile Stress and Strain for Specimens 1- 4

| | Ultimate Tensile | |
|---|---|---|
| Specimen | Strength (ksi) | Strain (%) |
| 1 | 78.5 | 5.6 |
| 2 | 87.0 | 12.1 |
| 3 | 83.2 | 7.0 |
| 4 | 75.6 | 3.7 |
| Average | 81.1 | 7.1 |
| Standard Deviation | 5.0 | 3.6 |

1 ksi = 6.89 MPa

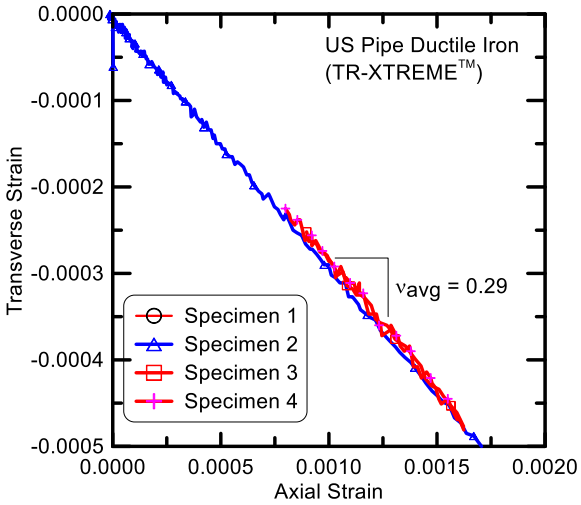


Figure 2.15. Transverse vs. Axial Strain in Elastic Range for Test Specimen 1-4

Table 2.5. Poisson's Ration in Elastic Range for Specimens 1 – 4

| Specimen | Poisson's Ratio, ν |
|---|---|
| 1 | 0.288 |
| 2 | 0.291 |
| 3 | 0.292 |
| 4 | 0.297 |
| Average | 0.292 |
| Standard Deviation | 0.004 |

### 2.4.4 Poisson's Ratio

Poisson's ratio, ν, is the negative ratio of transverse strain to axial strain for uniaxial loading. Figure 2.15 show the transverse and axial strain gage data for Specimens 1 – 4 while the stresses were in the elastic range of roughly 20 to 37 ksi (140 to 255 MPa). Tabulated data are given in Table 2.5. Poisson's ratio for all specimens was approximately 0.29 with a very small standard deviation of 0.004.

Figure 2.16. Uneven Fracture of Test Specimen 5

Figure 2.17. Fracture of Test Specimen 5 with Multiple Ridges

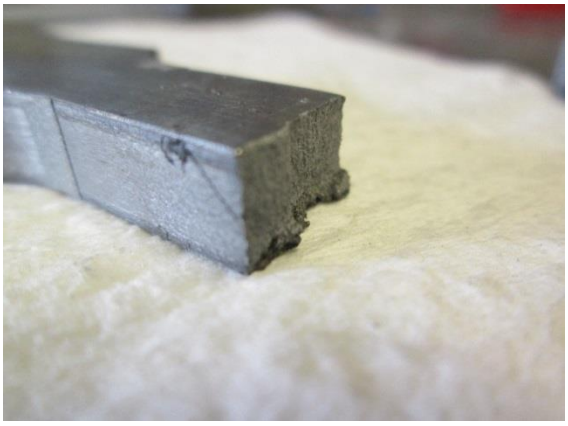

Figure 2.18. Failure of Specimen 5 Begins from Pitting Outside Fracture

## 2.5 Analysis of Test Specimens 5 and 6 (with Surface Pitting)

Two coupons, test Specimens 5 and 6, were tested with their original surface to investigate the effect of surface pitting on the material properties. Unlike the clean breaks of Test Specimens 1 – 4, the fractures of test Specimens 5 and 6 were severely uneven with a number of deep ridges stemming from the irregularities of the pitting. This can be seen in Figures 2.16 and 2.17. A closer observation yielded the discovery of a failure surface originating from a pit outside of the fracture, shown in Figure 2.18.

### 2.5.1 Stress vs. Strain Curves

Figures 2.19 and 2.20 show the axial stress-strain data from strain gages, laser extensometer, and clip-on extensometer for Specimens 5 and 6, respectively. The scales in Figures 2.19 and 2.20 are the same as those used in Figures 2.9 through 2.11 for Specimens 1 – 4 to illustrate the markedly smaller strains in the pitted specimens.

### 2.5.2 Young's Modulus, Yield Strength, and Proportional Limit

Young's modulus for Specimens 5 and 6 was determined from the slope of the stress vs. strain curve in the elastic range, as was done for Specimens 1 – 4. The axial strain gage data up to strains of 0.006 are shown in Figure 2.21. The yield strength was then computed using the offset method as described previously. The proportional strength was found from the corresponding strength at 0.002 strain. Young's moduli, the yield strengths, and the proportional strengths for these pitted specimens are given in Table 2.6. The average Young's modulus is 22,300 ksi (154 GPa), the average offset yield is 51.0 ksi (352 MPa), and the average proportional limit is 37.9 ksi (262 MPa). Standard deviations are not given because there are only two samples. The average modulus for Specimens 5 and 6 is only about 1.5% lower than for Specimens 1 – 4. The average yield strength for Specimens 5 and 6 is roughly 4.8% lower than for Specimens 1 – 4. The average proportional strength for Specimens 5 and 6 is roughly 10.8% lower than for Specimens 1 – 4. Thus, at relatively small strains the pitting does not appear to significantly affect the elastic response.

### 2.5.3 Ultimate Tensile Strength and Strain

Although the Young's modulus and yield strength of all specimens are in reasonable agreement, there is a significant difference in the ultimate tensile strength and strain, summarized in Table 2.7. Compared to the results for Test Specimens 1 – 4, the ultimate tensile strength and strain decrease by 25% and 20%, respectively. This dramatic decrease is due to the surface pitting.

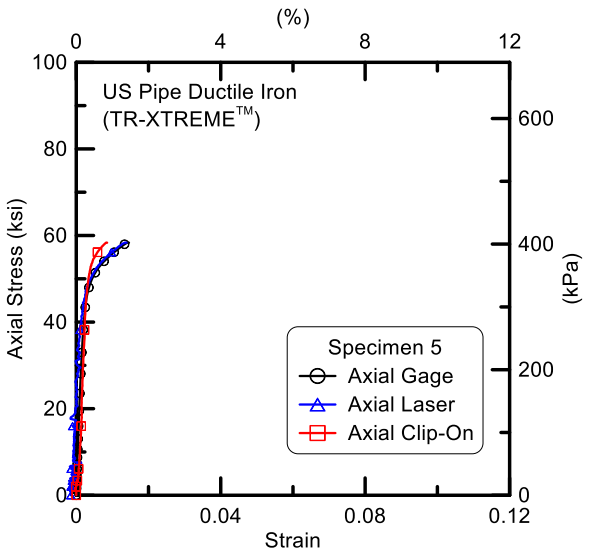


Figure 2.19. Stress – Strain Curve for Specimen 5

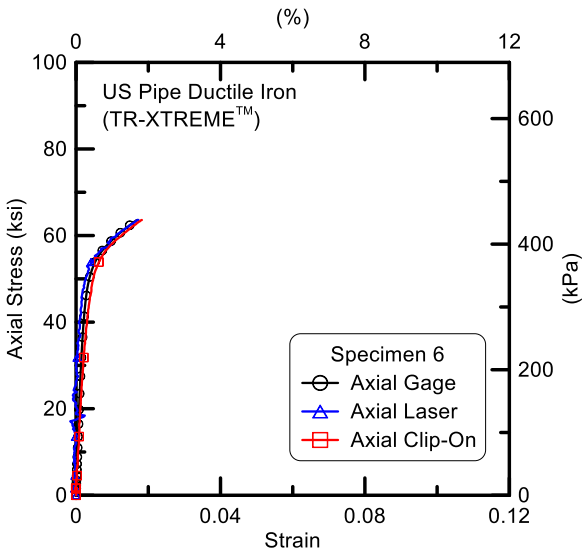


Figure 2.20. Stress – Strain Curve for Specimen 6

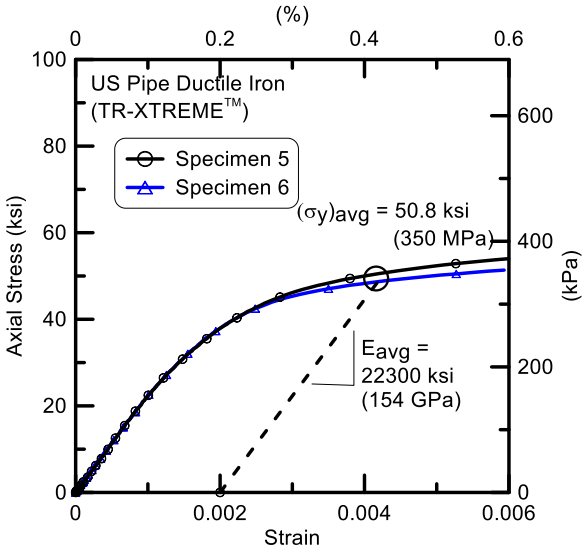


Figure 2.21. Average Young's Modulus and Yield Stress for Specimens 5 and 6

Table 2.6. Young's Modulus and Yield Point for Specimens 5 and 6

| Specimen | Young's Modulus, E (ksi) | Offset Yield, $\sigma_y$ (ksi) | Proportional Limit, $\sigma_{prop}$ (ksi) |
|---|---|---|---|
| 5 | 22650 | 52.5 | 37.9 |
| 6 | 21960 | 49.0 | 37.8 |
| Average | 22300 | 51.0 | 37.9 |

1 ksi = 6.89 MPa

Table 2.7. Summary of Ultimate Tensile Stress and Strain from Test Specimens 5 and 6

| | Ultimate Tensile | |
|---|---|---|
| Specimen | Strength (ksi) | Strain (%) |
| 5 | 58.4 | 4.2 |
| 6 | 65.6 | 7.1 |
| Average | 60.0 | 5.7 |

1 ksi = 6.89 MPa

## 2.6 Comparison of Results to Previous DI Tensile Results

Tensile coupon data were collected in 2011 at Cornell University on another research project using US Pipe ductile iron from pipe with the TYTON JOINT®. Those standard DI pipes were supplied by the Los Angeles Department of Water & Power (LADWP). They were manufactured by US Pipe and coded 06 52 TJ. The tensile coupons were machined from DI pipe specimens with a 6 in. (150 mm) nominal diameter, referred to in this report as "TYTON JOINT®" DI. The data for the TR-XTREME™ pipe tested are referred to as "TR-XTREME™".

Axial stress vs. axial strain curves for both sets of data are shown in Figure 2.22. The moduli, yield stress, ultimate stress, and strain at failure are tabulated in Table 2.8 to highlight differences in material properties. The Young's modulus and strain at failure for the TR-XTREME™ test specimens are both 16% and 32% less, respectively, while yield stress and ultimate stress are 16% and 22% greater, respectively. The material used in the TR-XTREME™ specimens is generally stronger, but less ductile than that of the TYTON JOINT® pipe specimens. This difference may reflect the effects of small differences in mineralogy as well as surface pitting.

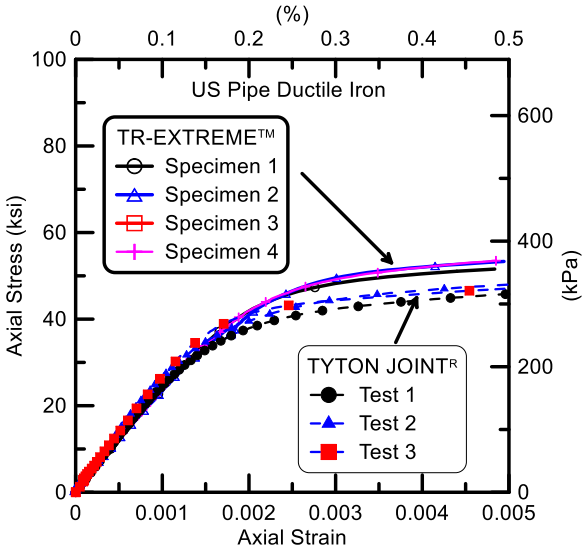


Figure 2.22. Stress – Strain Curves for TR-XTREME™ and TYTON JOINT® Ductile Iron

Table 2.8. Comparison of Material Strengths of TR-XTREME™ Joints and TYTON JOINT® Joints

| Parameter | TR-XTREME™ | TYTON JOINT® | Difference (%) |
|---|---|---|---|
| Young's Modulus (ksi) | 22650 | 27000 | -16 |
| Yield Stress (ksi) | 52.5 | 45.1 | 16 |
| Ultimate Stress (ksi) | 81.1 | 66.7 | 22 |
| Strain at Failure (%) | 7.1 | 10.4 | -32 |

1 ksi = 6.89 MPa

## 2.7 Conclusions from Tensile Coupon Tests

The tensile test data for the DI specimens taken from the pipe with TYTON JOINT® pipe prepared by US Pipe show similar tensile stress vs. strain characteristics as those of other DI pipe commercially available from US Pipe. Some differences between the TYTON JOINT® pipe and TR-XTREME™ test specimens are noted. The Young's modulus and strain at failure for the TR-XTREME™ test specimens are respectively 16% and 32% less than those of the TYTON JOINT® pipe that was tested. In contrast, yield stress and ultimate stress for the TR-XTREME™ test specimens are respectively 16% and 22% greater than those of the TYTON JOINT® pipe. The tensile test results also show that surface pitting associated with the TR-XTREME™ specimens did not significantly affect the material performance at smaller strains, but did decrease the ultimate stress and strain of the DI specimens.

Given the similarity of DI stress vs. strain characteristics of the TR-XTREME™ jointed pipe relative to those of the TYTON JOINT® pipe, there should be little to no difference in the mechanical performance between US Pipe ductile iron with similar geometric characteristics. Minor surface and casting irregularities (e.g., surface pitting) can contribute to local loss of ductility and fracture in the specimens under high loading. Any improvements in casting and pipe fabrication process are expected to result in pipeline response to large ground deformation that either equals or exceeds the TR-XTREME™ jointed pipe response during the full-scale testing at Cornell.

# Section 3

# Four-Point Bending Tests

## 3.1 Introduction

This section of the report describes two four-point bending tests of a ductile iron (DI) TR-XTREME™ joint specimen provided by US Pipe. The test results are used to determine the moment-rotation response of the newly designed TR-XTREME™ bell and spigot pipe sections. Of particular interest was the effect that the location of the locking ring segments had on the rotational response. In this section the special locking segments are referred to as clips and the term "rotation" is equivalent to "deflection" as used commonly in the field and commercial pipeline information.

## 3.2 Locking Clip Locations

During the four-point bending tests the load is applied vertically. For the first test, Test A, the slot was positioned at the top of the pipe and the locking clips are inserted such that they are located near the springline of the pipe (the 3 [blue] and 9 o´clock [red] positions) as seen in Figure 3.1a. It was expected that this test would produce somewhat larger rotations because of the lack of material at the slots at crown and invert. Under the assumption that the slot is usually at the crown of the pipe when installed in the field, this first test is representative of vertical differential soil movement.

Specimen B was rotated 90 degrees such that its slots were located at the springline of the pipe. The locking segments were inserted into one slot and pushed up and down such that they were at approximate 12 (blue) and 6 (red) o´clock positions as seen in Figure 3.1b. Under the assumption that the slots are at the top during regular pipeline installation, the vertical load applied to the pipe is representative of horizontal differential soil displacement. Horizontal soil displacement is typically associated with the most severe conditions of soil-pipe interaction during earthquake induced ground deformation.

In the full-scale split basin tests, the pipeline is constructed with the slots at the top and locking clips at the 3 and 9 o´clock positions as shown in Figure 3.2. Therefore, the second 4-pt bending test (Test B) is representative of the joints' rotational behavior in the split basin test. Before testing, rotation in this direction (with locking segments at 3 and 9 o´clock) was thought to be a worst case scenario for the pipeline due to reduced rotational capacity related to the clip positions.

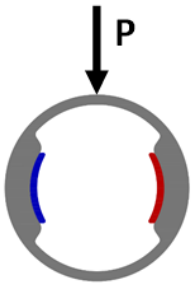


a) Clip Locations at 3 and 9 O´Clock (First Test, Test A)

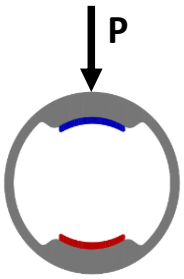


b) Clip Locations at 12 and 6 O´Clock (Second Test, Test B)

Figure 3.1. Orientation of Retaining Clips for the Two Bending Tests

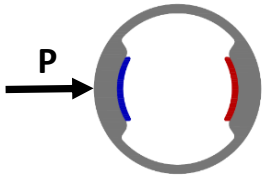


Figure 3.2. Full-Scale Basin Test Setup with Clips at the 3 and 9 O´Clock Positions and Lateral Ground Motion

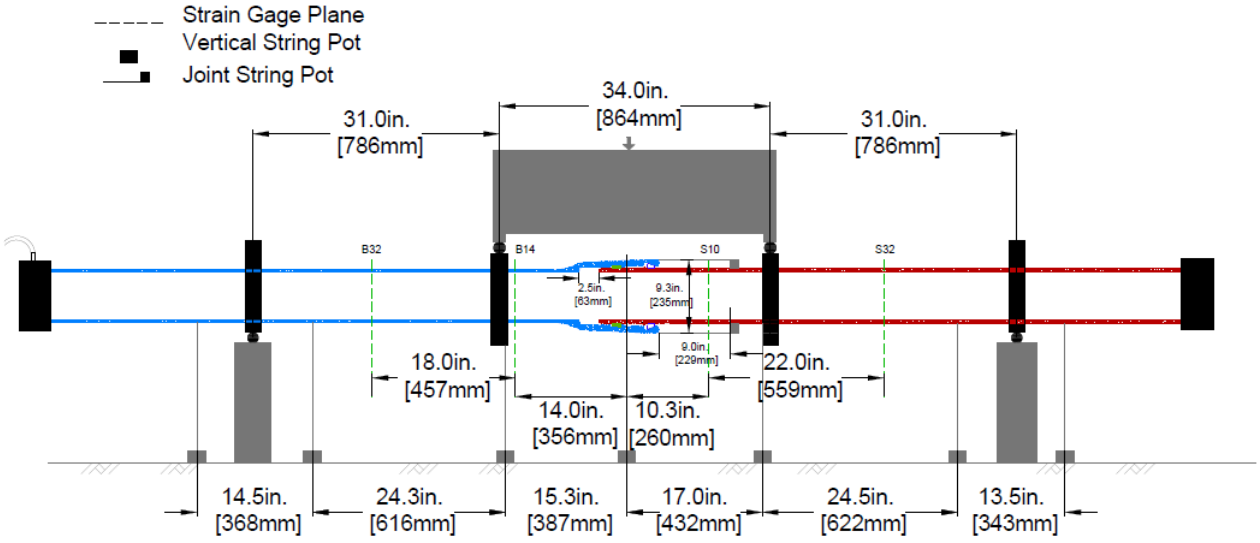


Figure 3.3. Schematic of Instrumentation Locations for Bending Tests A and B

Table 3.1. Instrumentation for US Pipe TR-XTREME™ Bending Test A and B

| Location | Instrument | Local Instrument Name |
|---|---|---|
| 54.1 in. from Joint | Vertical String Pot on Bell End | VSP-B54 |
| 39.6 in. from Joint | Vertical String Pot on Bell End | VSP-B40 |
| 15.3 in. from Joint | Vertical String Pot on Bell End | VSP-B15 |
| 0 in. from Joint | Vertical String Pot on Bell End | VSP-B0 |
| Top of Bell | Horizontal String Pot | HSP Top |
| Bottom of Bell | Horizontal String Pot | HSP Bot |
| 17.0 in. from Joint | Vertical String Pot on Spigot End | VSP-S17 |
| 41.5 in. from Joint | Vertical String Pot on Spigot End | VSP-S40 |
| 55.0 in. from Joint | Vertical String Pot on Spigot End | VSP-S55 |
| 32.0 in. from Joint | Strain Gage at Crown on Bell End | B32C |
| 32 in. from Joint | Strain Gage at Invert on Bell End | B32I |
| 14.0 in. from Joint | Strain Gage at Crown on Bell End | B14C |
| 14.0 in. from Joint | Strain Gage Invert on Bell End | B14I |
| 10.3 in. from Joint | Strain Gage at Crown on Spigot End | S10C |
| 10.3 in. from Joint | Strain Gage at Invert on Spigot End | S10I |
| 32.3 in. from Joint | Strain Gage Crown on Spigot End | S32C |
| 32.3 in. from Joint | Strain Gage at Invert on Spigot End | S32I |
| Center of Load | Load Cell | Load |
| Bell End | Pressure Gage | Pressure |

1 in. = 25.4 mm

Table 3.2. Geometric and Material Properties for Bending Test Specimens

| Property | Value |
|---|---|
| Outside Diameter, $D_o$ (in.) | 6.9 |
| Inside Diameter, $D_i$ (in.) | 6.3 |
| Wall Thickness, t (in.) | 0.3 |
| Distance to Outer Fiber, c (in.) | 3.45 |
| Moment of Inertia, I ($in.^4$) | 33.9 |
| Proportional Limit Stress, $\sigma_{prop}$ (ksi) | 42.0 |
| Yield Stress, $\sigma_y$ (ksi) | 52.5 |
| $M_{prop}$ (kip-in.) | 413 |
| $M_y$ (kip-in.) | 512 |

1 in. = 25.4 mm; 1 ksi = 6.89 MPa; 1 kip-in. = 0.113 kN-m

### 3.3 Instrumentation

A variety of instrumentation was used in the bending tests. Figure 3.3 is a schematic of the test setup for both Test A and Test B. A vertical load was applied at the nominal center of the bell and spigot specimen. The center of rotation for the complex inner geometry of the bell and its interaction with the weld bead connection is not well defined. The spigot end was inserted fully into the bell, and then retracted 2.5 in. prior to bending. Table 3.1 lists the instrumentation used for Tests A and B, and gives the instrument location and local instrument name.

### 3.4 Specimen Geometry, Material Properties, and Calculation Approaches

Table 3.2 presents the geometric and material properties for the ductile iron used in the bending tests. The yield stress $\sigma_y$ = 52.5 ksi (358.5 MPa), is based on the tensile test data from the TR-XTREME™ ductile iron. The proportional limit stress, $\sigma_{prop}$ = 42.0 ksi (289.6 MPa), is the stress near the end of the elastic range, as determined from the tensile coupon test data. The outer fiber stress due to bending, $\sigma_b$, is calculated as

$$\sigma_b = \frac{M\,c}{I} \tag{3.1}$$

Thus, using the stress limits given in Table 3.2 the moments at the proportional limits, $M_{prop}$, and the moments at the yield stress, $M_y$, are as given in Table 3.2.

The length of the test specimens between the outer supports was 96 in. (2.44 m). The central 34-in. (0.86-m)-span had equal lengths of 31 in. (0.78 m) on each side, as shown in Figure 3.3. The moment applied to the central portion of the specimen, $M_{central}$, was calculated as

$$M_{central} = \frac{P}{2}\ell_{central} \tag{3.2}$$

where

P = the applied load and
$\ell_{central}$ = the distance from the support to the central zone, or moment arm, of 31 in. (0.79 m)

Moments outside the central zone, for example, at gage planes B32 and S32, have moment arms of 16 in. (0.41 m)

Two methods were used to calculate joint rotations. One method uses the horizontal string pots (HSPs) at the top and bottom of the bell and the vertical separation distance to calculate the joint rotation. Equation 3.3 gives the method used for this approach.

$$\theta \text{ (degrees)} = \tan^{-1}\left[\frac{(\text{top disp.} - \text{bottom disp.})}{\text{distance between centers of HSPs} = 9.5 \text{ in.}}\frac{180^{\circ}}{\pi}\right] \tag{3.3}$$

An alternate approach is to take the difference between the string pot measurement at the specimen center and the closest bell or spigot pot, and divide by the pot separation distance. The arctangent of this is the rotation of each side. This is given in Eq. 3.4. The overall joint rotation is the sum of the two side angles. For example,

$$\theta \text{ (degrees)} = \tan^{-1}\left(\frac{(\text{VSP} - \text{B0})\text{ in.} - (\text{VSP} - \text{B15})\text{ in.}}{15.3 \text{ in.}}\right) + \tan^{-1}\left(\frac{(\text{VSP} - \text{B0})\text{ in.} - (\text{VSP} - \text{S17})\text{ in.}}{17 \text{ in.}}\right) \tag{3.4}$$

Where (VSP-B0) in., (VSP-B15) in., and (VSP-S17 in.) are the vertical string pot measurements at the string pots listed in Table 3.1.

## 3.5 Test A Results

### 3.5.1 Pressure

Test A was pressurized with water to approximately 80 psi (552 kPa). Internal pressures fluctuated somewhat during bending, and the pressures were readjusted to maintain nearly constant pressure. Rotation was mobilized about the lower half of the joint, causing the spigot to displace into the bell at the top of the pipe. This resulting reduction of volume was accompanied by a pressure increase above 90 psi before the excess pressure was manually reduced. Figure 3.4 shows the pressure-time data from Test A. Test A failed by fracture of the ductile iron just beyond the spigot. The rapid drop in pressure is shown in Figure 3.4.

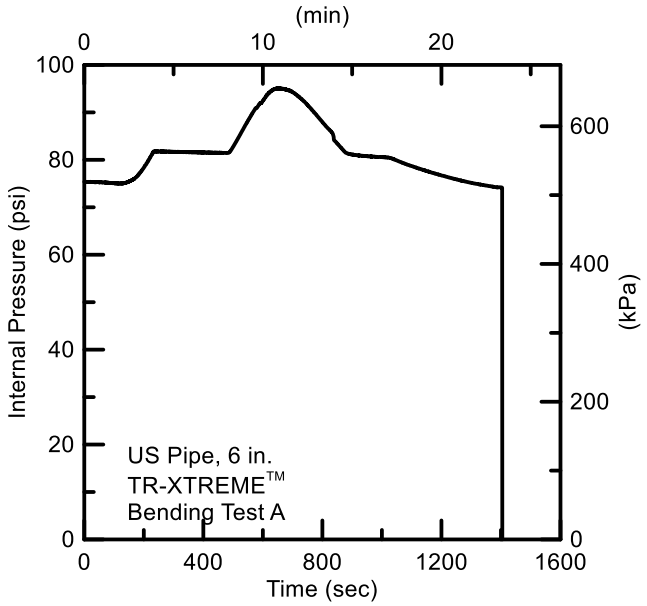


Figure 3.4. Pressure – Time for Test A

### 3.5.2 Moment-Rotation

Figure 3.5 is a photograph of the bending test setup showing the two steel stands (labeled A) supporting the pipe. The central load was applied through a steel beam (labeled B) in the photo. The load was applied using a 400 kip (1780 kN) Baldwin frame.

Figure 3.6 shows the joint rotation in Test A. Moment-rotations for Test A at the central portion of the bell-and spigot joint were calculated using a) the horizontal string pots (HSPs) at the top and bottom of the bell (Eqn. 3.3) and b) using the three vertical string pots (VSPs) in the central portion (Eqn. 3.4.) Figure 3.7 shows the moment-rotation data using both approaches. The moments are those in the central load pipe section, as determined by Equations 3.1 and 3.2. Both measurement methods are in excellent agreement. Shown on Figure 3.7 are the moment limits at the proportion limit of $M_{PL}$ = 394 kip-in. (44.5 kN-m) based on a proportion limit stress of $\sigma_{PL}$ = 40 ksi (275.8 MPa), and at the yield limit, $M_y$ = 512 kip-in. (57.9 kN-m) based on the yield stress of $\sigma_y$ = 52.5 ksi (362.0 MPa). Test A failed at an applied moment of 515 kip-in. (58.2) kN-m) and at an average rotation of 8.6 degrees.

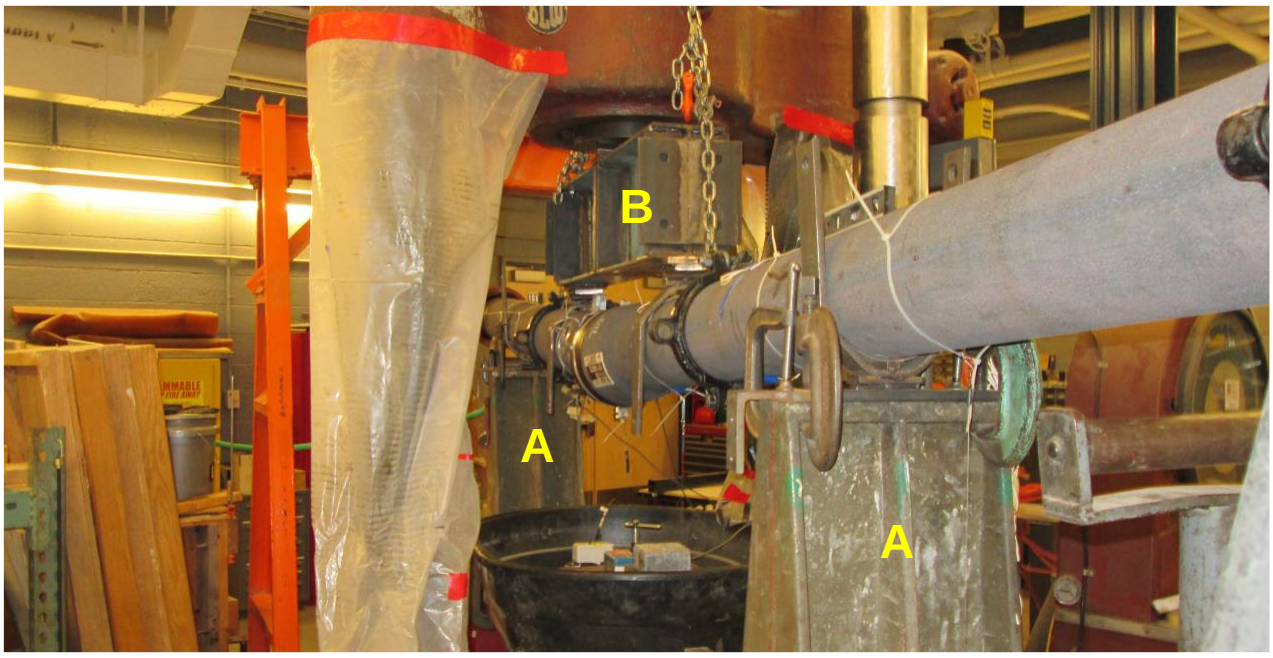


Figure 3.5. Four-Point Bending Test Apparatus

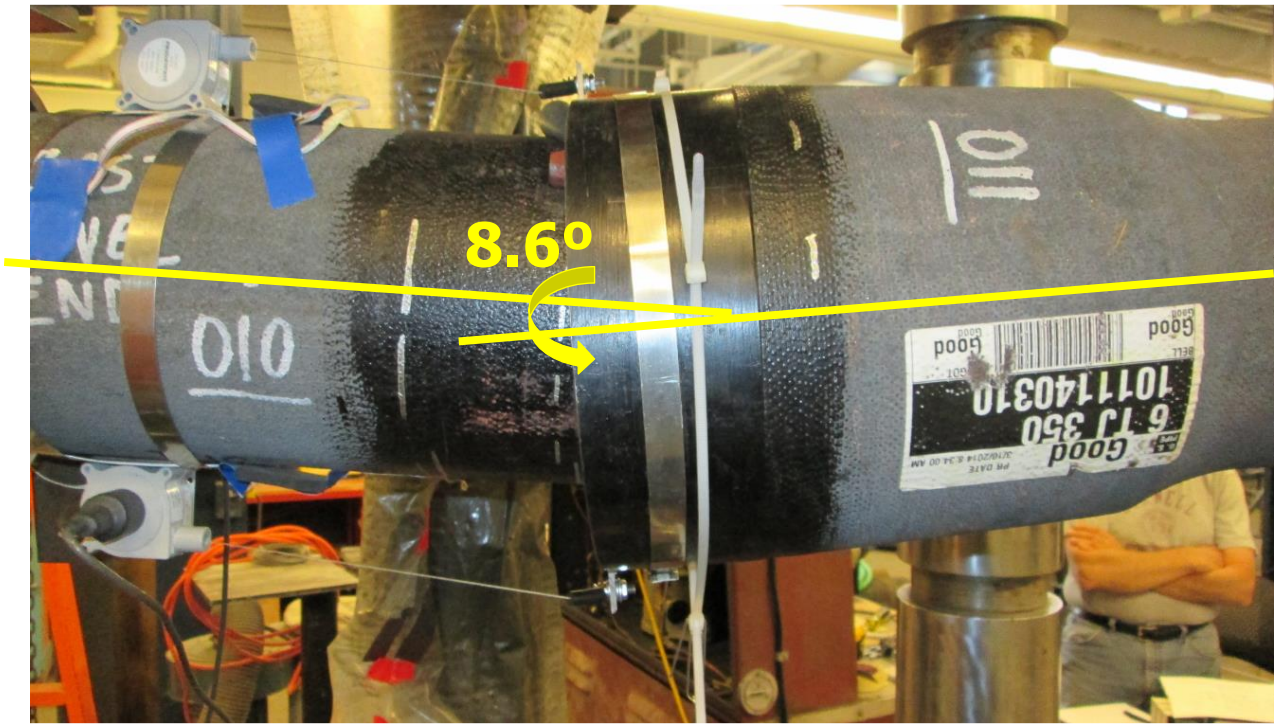


Figure 3.6. Rotation of the Joint in Test A

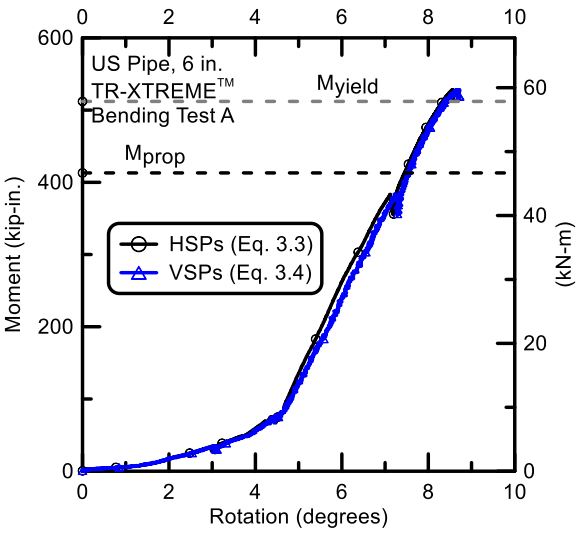


Figure 3.7. Moment-Rotation for Test A

Figures 3.8 and 3.9 show the Test A specimen at pipe rupture. As previously stated, the pipe had a nearly complete circumferential crack at 13 inches away from the bell face behind the bell section. Figure 3.10 shows a feature, which was visible around the entire pipe circumference. Discussions with US Pipe personnel indicated that this is likely due to a buildup of residue from a mold release agent used during casting. It also appeared that the pipe wall was thinner in this zone than in other pipe sections.

### 3.5.3 Displacements

Pipe vertical displacements were measured at several distances along the pipe using VSPs. The VSP readings at these distances (given in Table 3.1) are shown in Figure 3.11. In the figure positive distances along the x-axis represent the spigot portion of the pipe and negative values from the load centerline represent the bell portion. The displacements increase as the load increases, until the specimen failed at a load of approximately 33 kips (147 kN). What is more important in this figure other than the numerical values of the vertical displacement (the relative displacements are used to calculate rotations,) is that the displacements are symmetric about the load centerline and show a linear variation with distance. This validates the assumption of rigid body rotation so that the calculation of rotation can be made from the string VSP measurements.

Figure 3.8. Pipe Failure in Test A


Figure 3.9. Side View of Pipe Failure in Test A

Figure 3.10. Special Feature on TR-XTREME™ Spigot

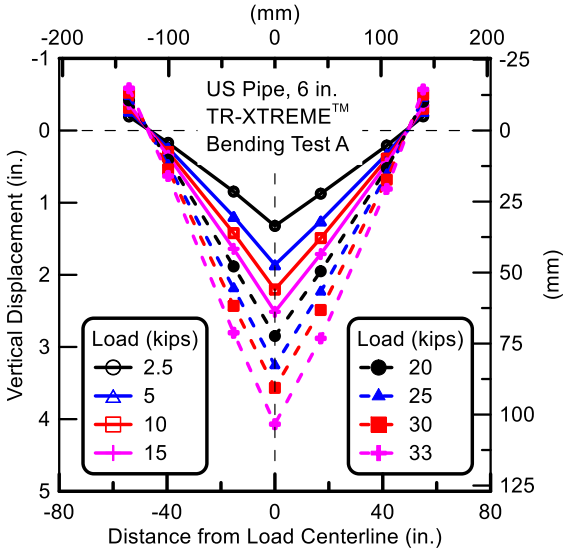


Figure 3.11. Vertical Displacements of Test A Specimen

### 3.5.4 Pipe Strains

Axial strains at the crown and invert vs. moment for Test A are shown in Figures 3.12 a) and b). The strains are dependent on the length of the bell and spigot section, and are a function of the moment arms in the four-point bending test. The moment arms for the gages at the 32 in. (0.83 m) plane are roughly half that for the central portion, so the moments there are roughly half that of the central portion. The strains at all gage planes are nearly the same for equal applied moments.

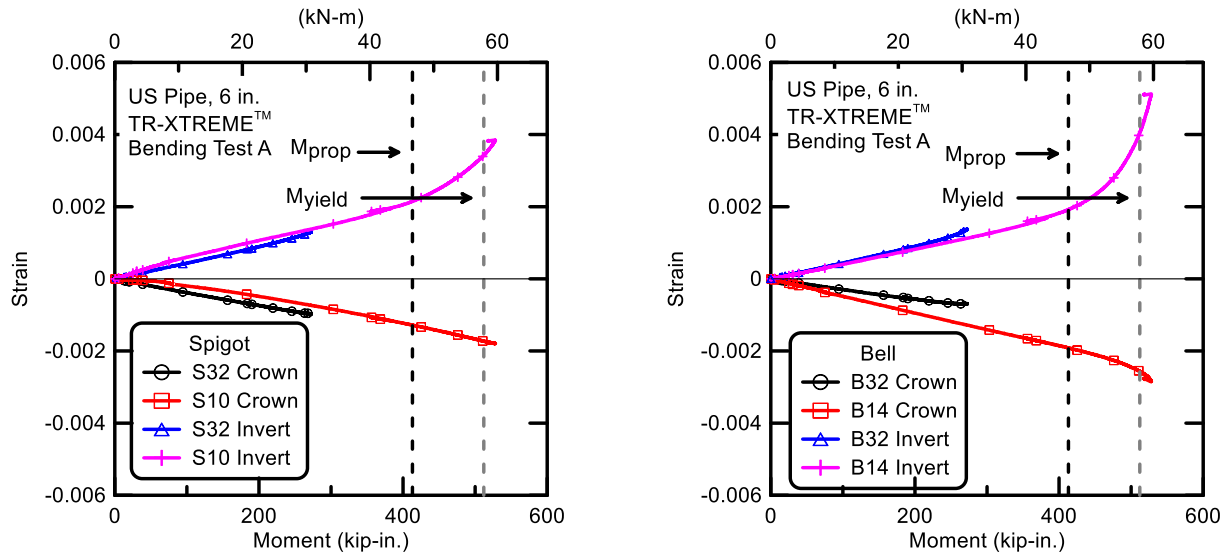


a) Spigot Segment b) Bell Segment

Figure 3.12. Crown and Invert Strains on Spigot and Bell Segment for Test A

## 3.6 Test B Results

### 3.6.1 Pressure

Test B was pressurized with water to approximately 80 psi (552 kPa). Internal pressures fluctuated somewhat during bending, and the pressures were readjusted to maintain nearly constant pressure. The joint rotation was similar to that of Test A in that rotation about the bottom of the joint caused a decrease in volume and an increase in pressure to 100 psi (689 kPa) before manual adjustments reduced the pressure. Figure 3.13 shows the pressure-time data from Test B. Test B developed a slow leak, and the pressure dropped as shown in Figure 3.13.

### 3.6.2 Moment-Rotation

Figure 3.14 shows the joint rotation in Test B. Moment-rotations for Test B for the central portion of the bell-and spigot joint were calculated using the horizontal string pots (HSPs) at the top and bottom of the bell (Eqn. 3.3) and using the three vertical string pots (VSPs) in the central portion (Eqn. 3.4.) Figure 3.14 shows the moment-rotation data using both approaches. The moments are those in the central load pipe section. Only the rotations during the loading phase are shown. As the joint developed a slow leak, the moments (loads) were reduced. As seen in Figure 3.14, both measurement methods are in reasonable agreement. Test B failed at an applied moment of 480 kip-in. (54.2 kN-m) at a rotation of 9.1 degrees, which is the average rotation measured by the HSPs and VSPs. Figure 3.15 shows the Test B leakage.

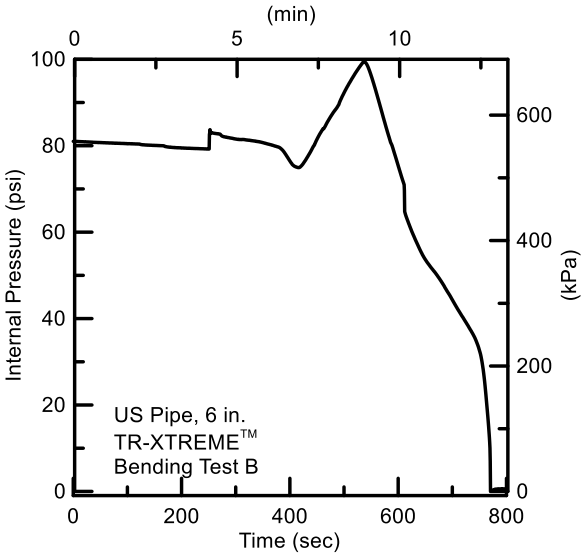


Figure 3.13. Pressure – Time for Test B

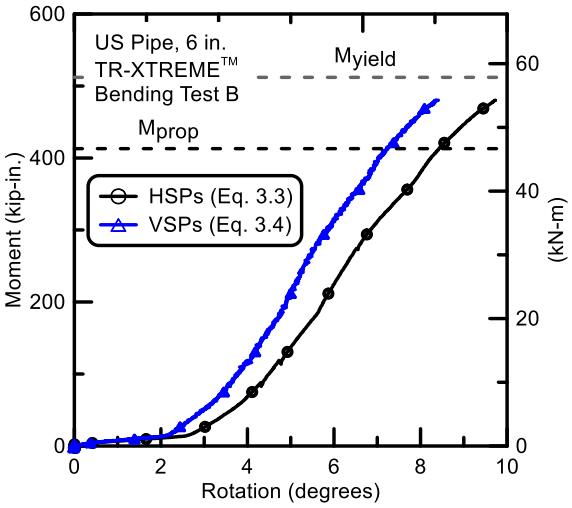


Figure 3.14. Moment – Rotation for Test B

Figure 3.15. Leakage at Peak Moment in Test B

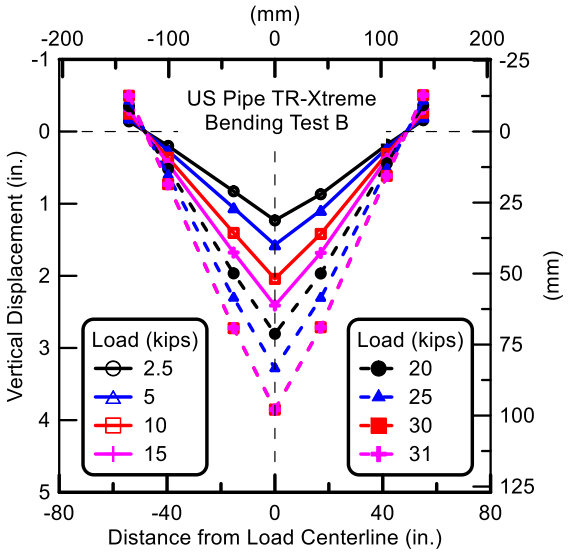


Figure 3.16. Vertical Displacements of Test B Specimen

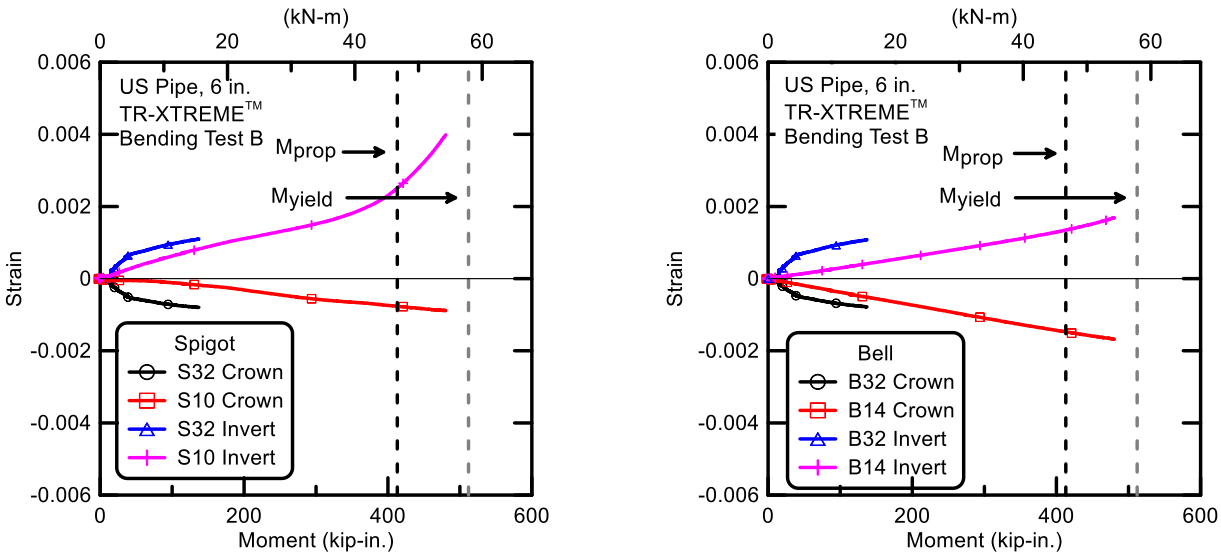


a) Spigot Segment

b) Bell Segment

Figure 3.17. Crown and Invert Strains vs. Moment on Spigot and Bell Segment for Test B

### 3.6.3 Displacements

Pipe vertical displacements for Test B again were measured at several distances along the pipe using VSPs. The VSP readings at these distances are shown in Figure 3.16. In the figure positive displacements are downward and positive distances from the load centerline are on the spigot portion of the pipe. The displacements increase as the load increases, until the specimen failed at a load of approximately 31 kips (138 kN). The pattern of displacements with load for Test B is nearly identical

### 3.6.4 Pipe Strains

Axial strains at the crown and invert vs. moment for Test B are shown in Figures 3.17a) and b). Strains up to the maximum moment are shown. The strains in Test B are similar to those in Test A. They do not, however, reach a yield moment $M_{yield}$, level attained in Test A. In this test, leakage was initiated at a moment between $M_{prop}$ and $M_{yield}$. The maximum rotation for Test B was slightly higher, although consistent with, that of Test A.

## 3.7 Conclusions from Bending Tests

An important reason for performing Test A and Test B was to examine the differences in moment rotation when the locking clips were at the 3 and 9 o´clock positions (Test A) or the 12 and 6 o´clock positions (Test B.) Figure 3.18 shows the average rotations using the HSPs and VSPs for Tests A and B. Test A failed at an applied moment of 515 kip-in. (58.2 kN-m) and at an average rotation of 8.6 degrees. Test B failed at an applied moment of 480 kip-in. (54.2 kN-m) (7% lower than Test A) and at an average rotation of 9.1 degrees (6% higher than Test A). There is no significant moment – rotation difference for the two tests.

The test results show that moments in the range of the proportional limit, $M_{prop}$, and the yield moment, $M_{yield}$, were associated with loss of pressure and pipe leakage. Stress concentrations related to spigot-bead contact with the restraining clips are a likely source of local deformations leading to leakage at such moments.

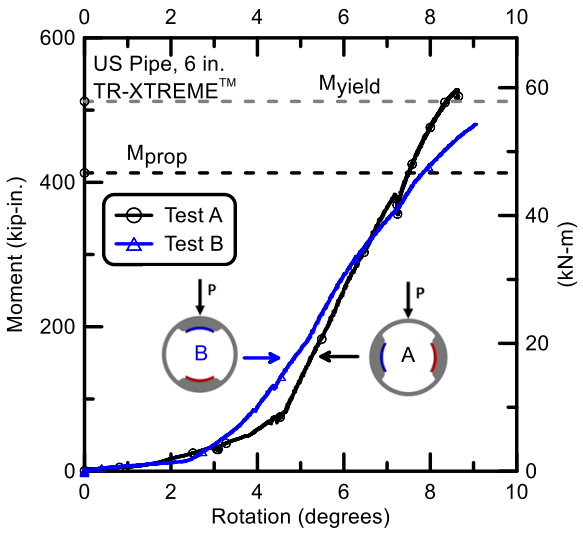


Figure 3.18. Moment – Rotations for Tests A and B

# Section 4

# Joint Compression Testing

## 4.1 Introduction

This section of the report summarizes the results of the US Pipe compression of the TR-XTREME™ joint. The basic pipe was 6 in. (150 mm) ductile iron. One compression test of the joints was completed. It should be noted that the term "rotation" in this section is equivalent to "deflection" as used commonly in the field and commercial pipeline information.

## 4.2 Compression Test

The assembled pipe was 156.7 in. (4.0 m) long and with a wall thickness of 0.3 in. (7.6 mm) and an outside diameter of 6.9 in. (175.2 mm) The pipe was set up on a newly designed load frame so that its retaining clips were at 12 and 6 o´clock (crown and invert) positions. The setup of the compression test is shown in Figure 4.1. Figure 4.2 is a photograph of the testing frame with the pipe installed.

### 4.2.1 Instrumentation

Strain gages were mounted 22 in. (0.56 m) north of the bell face on the bell side of the pipe at the positions of 12, 3, 6, and 9 o´clock (crown, east, invert, and west, respectively). Each location had a pair of axial and circumferential gages. Eight other gages (axial and circumferential pairs) were mounted 14 in. (0.36 m) south of the bell face on the spigot side at the same positions around the pipe. Four string pots were installed near the bell face to measure the displacement of the joint as it closed. The actuator and the load cell also were installed on the load frame to apply the compressive load at the end of the pipe. The instrument locations and local gage names are listed in Table 4.1.

### 4.2.2 Force – Displacement

The pipe was filled up with water and then pressurized at 80 psi (552 kPa), after which the actuator applied load to the pipe. Load vs. time for the compression test is shown in Figure 4.3. In the figures compressive forces and displacements are negative. The test was paused twice to verify procedures and to provide additional safety measures as the load increased. When the load reached -350 kips (-1557 kN), the test was stopped. At this point, there was obvious yielding of the pipe. Figure 4.4 shows compressive force vs. actuator displacements. The maximum actuator displacement was approximately -3.5 in. (-88.9 mm).

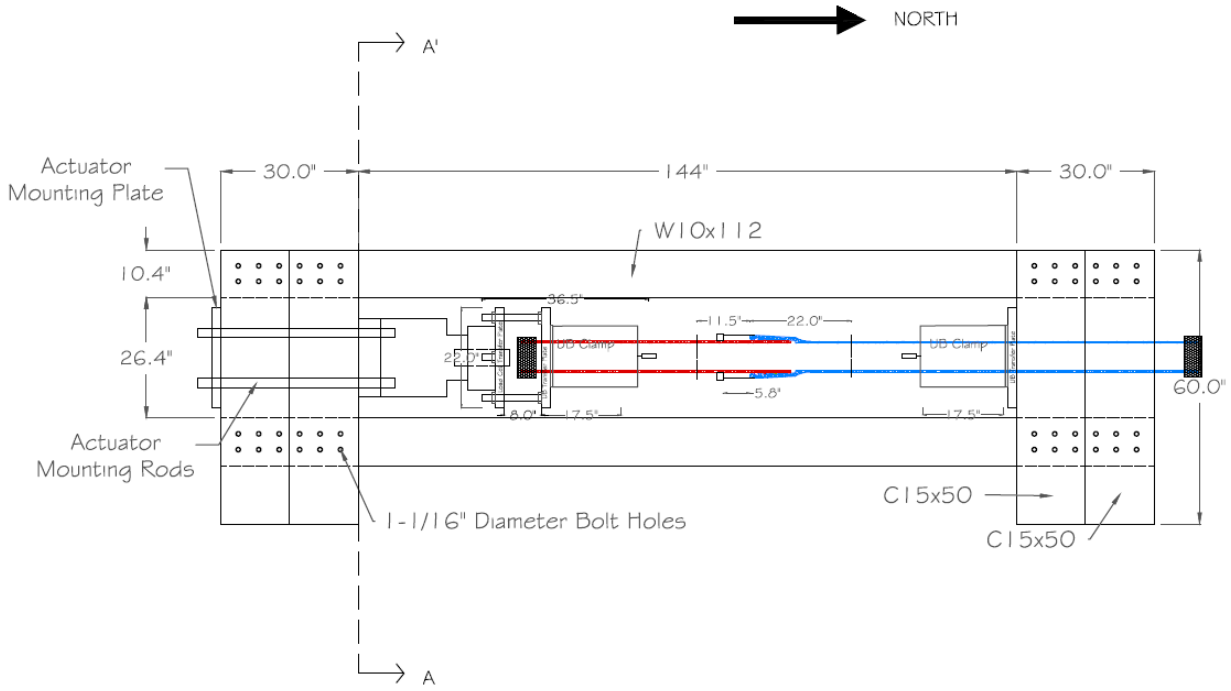


Figure 4.1. Compression Test Layout

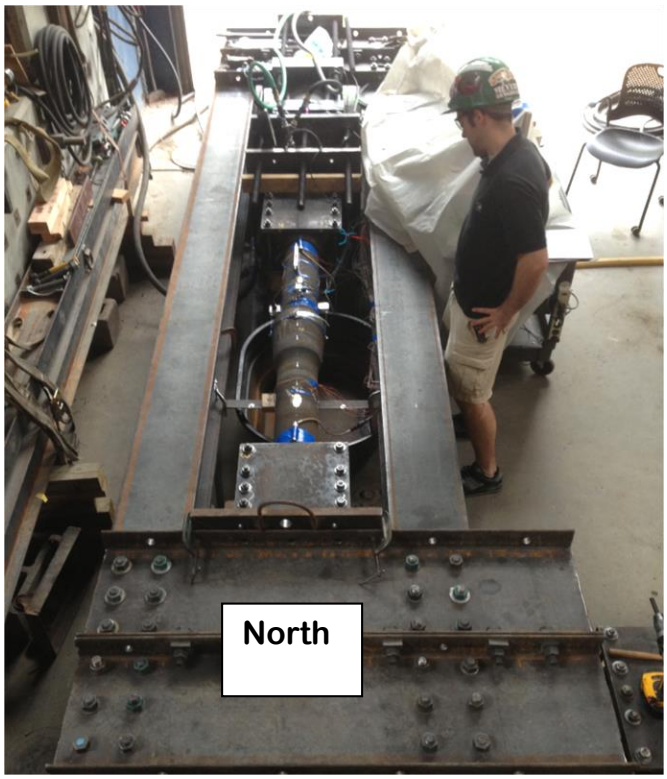


Figure 4.2. Photo of Compression Test

Table 4.1. Instrumentation for US Pipe TR-XTREME™ Joint Compression Test

| Location | Instrument | Local Instrument Name |
|---|---|---|
| 22 in. North of Bell Face | Crown, Axial Strain | ST 22CA |
| 22 in. North of Bell Face | Crown, Circumferential Strain | ST 22CC |
| 22 in. North of Bell Face | Invert, Axial Strain | ST 22IA |
| 22 in. North of Bell Face | Invert, Circumferential | ST 22IC |
| 22 in. North of Bell Face | East Springline, Axial Strain | ST 22EA |
| 22 in. North of Bell Face | East Springline, Circumferential Strain | ST 22EC |
| 22 in. North of Bell Face | West Springline, Axial Strain | ST 22WA |
| 22 in. North of Bell Face | West Springline, Circumferential | ST 22WC |
| 14 in. South of Bell Face | Crown, Axial Strain | ST 14CA |
| 14 in. South of Bell Face | Crown, Circumferential Strain | ST 14CC |
| 14 in South of Bell Face | Invert, Axial Strain | ST 14IA |
| 14 in. South of Bell Face | Invert, Circumferential Strain | ST 14IC |
| 14 in. South of Bell Face | East Springline, Axial Strain | ST 14EA |
| 14 in. South of Bell Face | East Springline, Circumferential Strain | ST 14EC |
| 14 in. South of Bell Face | West Springline, Axial Strain | ST 14WA |
| 14 in. South of Bell Face | West Springline, Circumferential Strain | ST 14WC |
| Bell Face | Crown String Pot | Jnt Closing C |
| Bell Face | Invert String Pot | Jnt Closing I |
| Bell Face | East Springline String Pot | Jnt Closing E |
| Bell Face | West Springline String Pot | Jnt Closing W |
| UB Clamp to Weld Bead | LVDT | Spigot Weld Bead |
| UB Clamp to Weld Bead | LVDT | Bell Weld Bead |
| Actuator | Load Cell | 400 K Load Cell |
| Actuator | Displacement | Act Disp |

1 in. = 25.4 mm

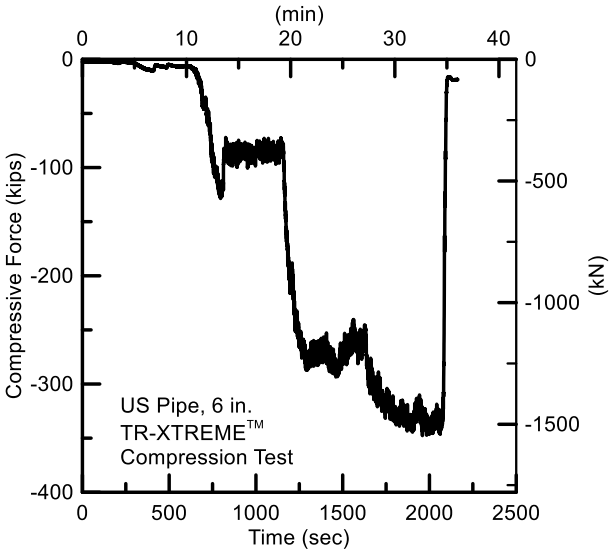


Figure 4.3. Compressive Force vs. Time

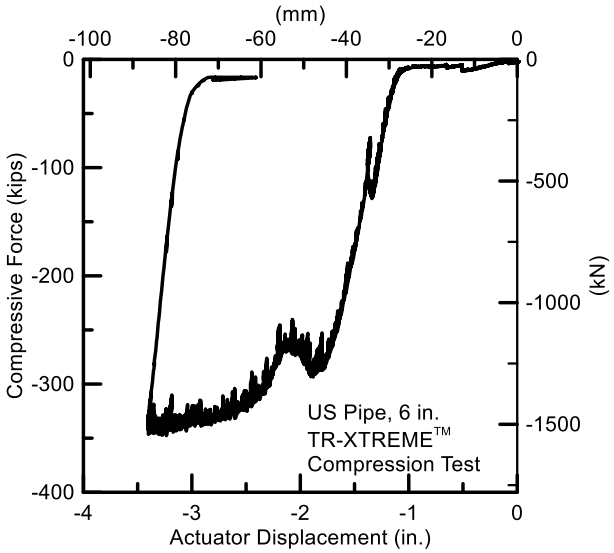


Figure 4.4. Compressive Force vs. Actuator Displacement

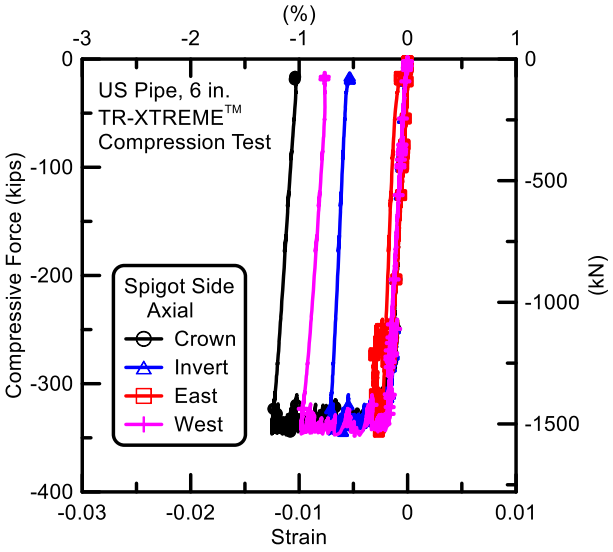


Figure 4.5. Compressive Axial Strains, Spigot Side

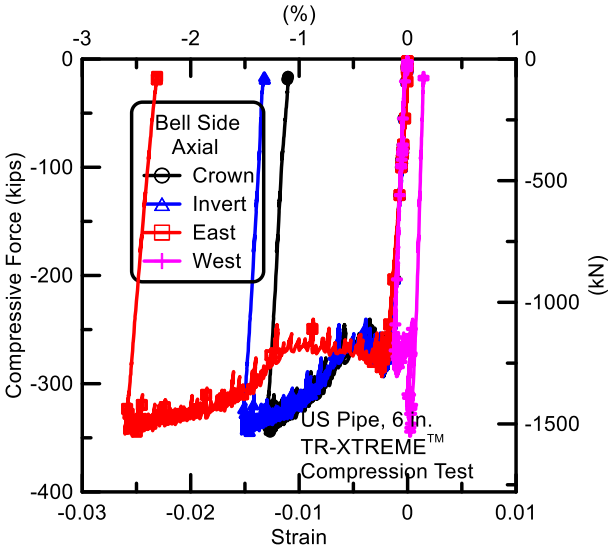


Figure 4.6. Compressive Axial Strains, Bell Side

### 4.2.3 Strains

The axial strains on the spigot and bell sides vs. applied force are shown in Figures 4.5 and 4.6, respectively. The maximum strains on the bell side are larger than those on the spigot side. In Figure 4.6, the largest compressive strains are on the bell section, at the east springline. This location is shown in Figure 4.7. Also shown in Figure 4.7 (see digital indicator), a compressive buckling wrinkle developed where the pipe was fixed in the UB clamp.

Figure 4.8 is an enlargement of the east and west axial strains plotted in Figure 4.6 in the range of 0.005 to -0.005. This location was identified in Figure 4.6. In Figure 4.8, the east and west springline axial strains are both compressive to a load of slightly below -300 kips (-1334 kN). Then, the west side strains shift from compressive to tensile strains because of bending in the pipe. This bending can be seen in Figure 4.7. Longitudinal bending strain, $\varepsilon_b$, at this location can be calculated as

$$\varepsilon_b = \frac{\varepsilon_{EA} - \varepsilon_{WA}}{2} \tag{4.1}$$

where $\varepsilon_{EA}$ and $\varepsilon_{WA}$ are the axial strains measured at the east and west springlines, respectively. (It is arbitrary whether the bending strains are east minus west or west minus east.).

The bending strains are near zero until a compressive force of roughly -150 kips (-167 kN) was applied, as shown in Figure 4.9. The compressive strains at the east springline are higher than they would be if the pipe were in direct compression only.

The actual longitudinal strains at the east springline are calculated as $\varepsilon_{EL} = \varepsilon_{EA} - \varepsilon_b$. Likewise, the actual strains at the west springline are lower than if the pipe were in direct compression only, such that $\varepsilon_{WL} = \varepsilon_{WA} + \varepsilon_b$. These corrected springline strains are shown in Figure 4.10. The corrected strains at the east and west springlines are in excellent agreement.

From the applied load, the axial stress is calculated as:

$$\sigma = \frac{F}{A} \tag{4.2}$$

where

$\sigma$ = axial stress,
F = applied force, and
A = cross-sectional area


Figure 4.7. Photo of Compression Test on TR-Xtreme™ Joint

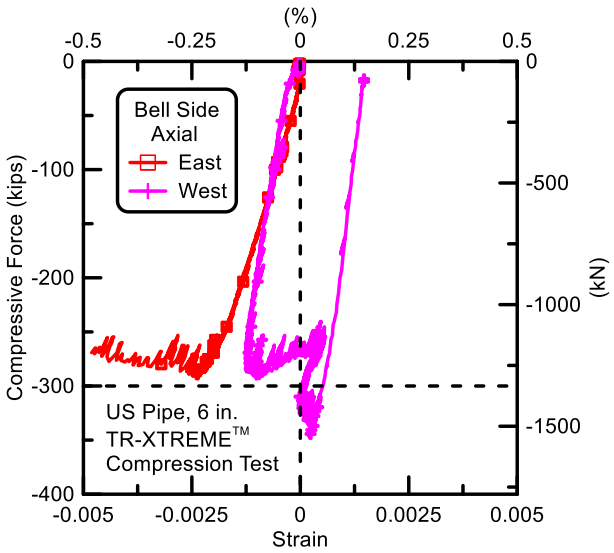


Figure 4.8. Enlargement of East and West Axial Strains, Bell Side

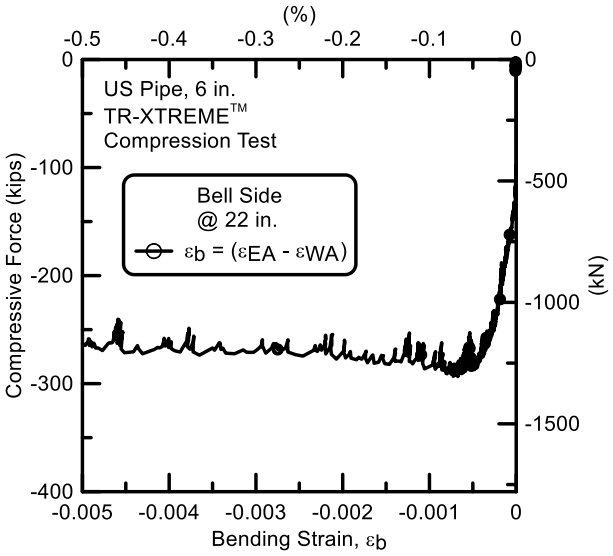


Figure 4.9. Bending Strains, Bell Side

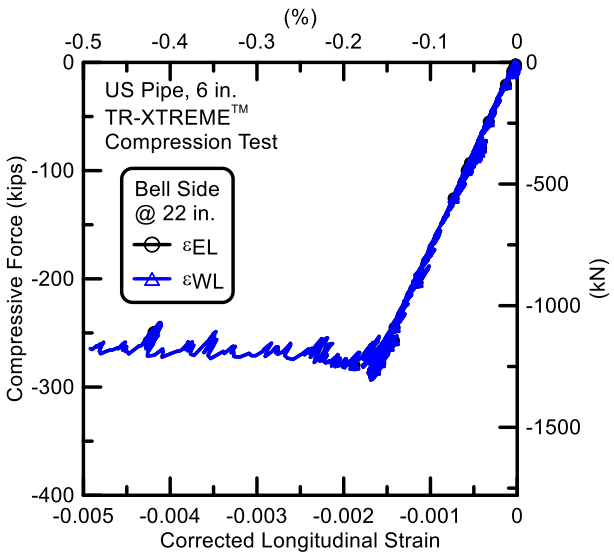


Figure 4.10. Springline Strains Corrected for Bending, Bell Side

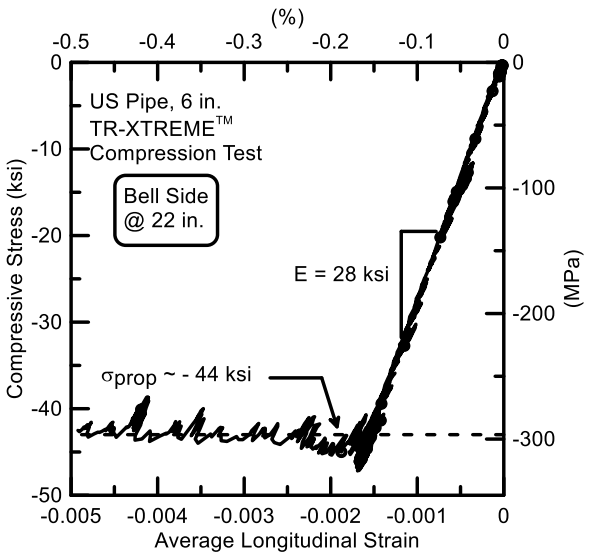


Figure 4.11. Stress vs. Average Longitudinal Strain, Bell Side

The applied force is taken from the force measured by the load cell, and the measured cross-sectional area of the spigot of 6.22 in.$^2$ (4013 mm$^2$) was used. The calculated axial stresses and the corrected average longitudinal strains (corrected for bending) are shown in Figure 4.11. Young's modulus for the linear portion of the data is E = 28,000 ksi (193 GPa). Tensile coupon tests performed at Cornell on other US Pipe DI show Young's modulus in tension as 27,000 ksi (186 GPa). Also shown in Figure 4.11 is an approximate proportional limit stress, $\sigma_{prop}$ of 43 ksi (296 MPa). Again, this is in good agreement with tensile coupon test data on other US Pipe DI.

### 4.2.4 Joint Movements

When the pipe segments were assembled, the actuator was used to push the spigot into the bell. Push forces were kept moderately low to avoid larger axial compression forces prior to the final assembly check. The pipe was pressurized and the compression test started. At the beginning of the test there was an axial separation of roughly 1 in. (25.4 mm) between the weld bead and full contact with the spigot seat.

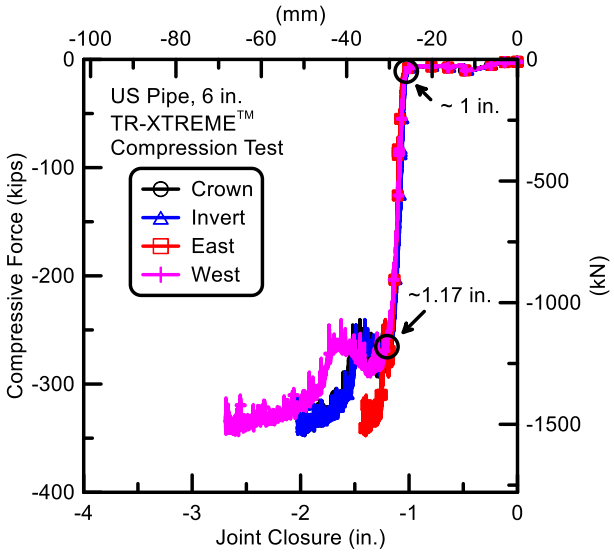


Figure 4.12. Joint Closure vs. Compressive Force

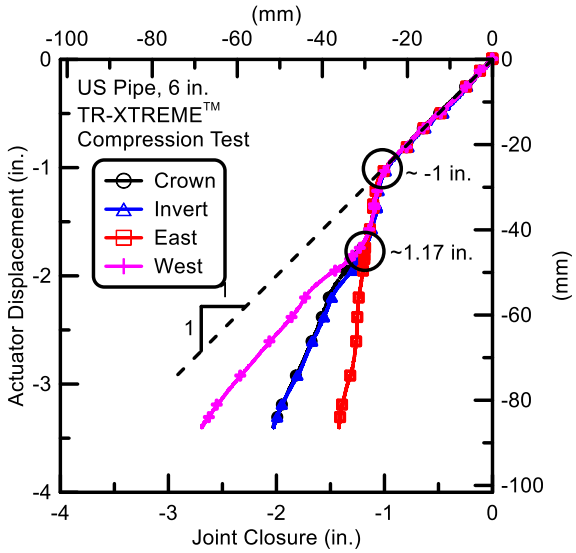


Figure 4.13. Joint Closure vs. Actuator Displacement

Figure 4.12 shows the string pot measurements at the crown, invert, and east and west springlines (Jnt Closing C, Jnt Closing I, Jnt Closing E, and Jnt Closing West in Table 4.1. Until a displacement of roughly 1 in. (25.4 mm) the actuator force stayed constant at approximately 8 kips (35.6 kN). At this point the weld bead on the spigot was in full contact with the internal seat in the bell, and the forces began to rise rapidly. Figure 4.13 shows that the four string pots followed the actuator displacement up to a closure of 1 in. As shown in both figures, there was only about 0.17 in. (4.3 m) of additional joint closure until the pipe began to yield (Fig. 4.12), when a significant divergence between the east and west springline string pot displacements began to develop (Fig. 4.13).

Once the joint was loaded to slightly below -300 kips (-1334 kN), corresponding to the proportional limit of the DI, the pipe started to bend. Tension developed on the west side of the pipe, 22 in. (0.56 m) north of the bell face, and additional compression developed on the on the east side of the pipe, 22 in. (0.56 m) north of the bell face. This also is expressed by the springline strains shown in Figure 4.8.

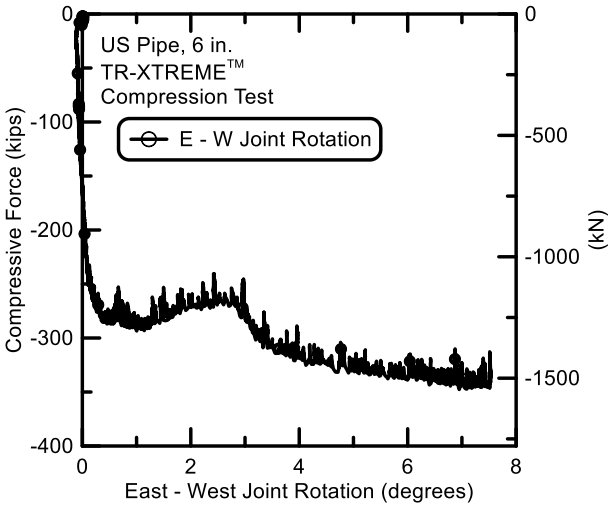


Figure 4.14. Joint Rotation vs. Compressive Force

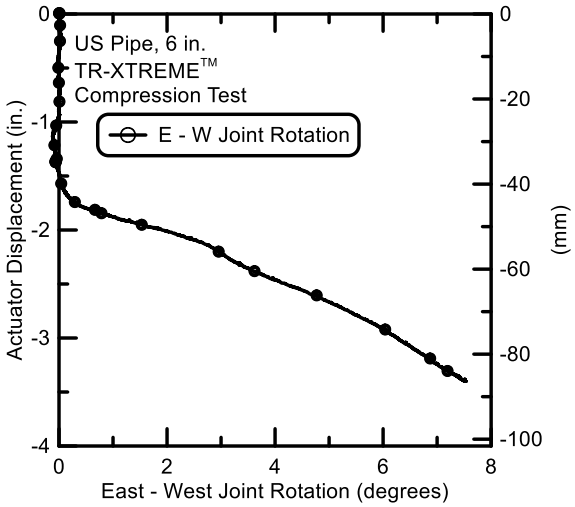


Figure 4.15. Joint Rotation vs. Actuator Displacement

The results confirm the bending direction because the joint closing at the crown and the invert positions are very close to one another. Thus, the center of rotation lay within the plane between the crown and the invert positions. Therefore, the joint rotation can be calculated by taking the difference between the joint displacement of the east and the west sides and the distance between the string pots at the east and the west springlines.

The joint rotation is calculated as

$$\theta\,(\text{deg.}) = \tan^{-1}\left[\frac{\text{Jnt Closing E (in.)} - \text{Jnt Closing W (in.)}}{9.625\,\text{in.}}\frac{180^{\circ}}{\pi}\right] \tag{4.3}$$

where Jnt Closing E (in.) and Jnt Closing W (in.) are the joint closures at the east and west springlines, respectively, and 9.625 in. (244.5 mm) is the horizontal separation between the two string pots.

The joint rotation vs. both compressive force and actuator displacement are plotted in Figure 4.14 and 4.15, respectively. The joint rotation is nearly zero until the compressive force reaches about -250 kips (-1112 kN), after which the rotation increases. Figure 4.15 shows that the rotation is near zero until the spigot penetration into the bell is about 1.5 in. (38.1 mm), after which it increases rapidly.

## 4.3 Concluding Remarks for Joint Compression Test

The compressive testing shows that the TR-XTREME™ joint was able to accommodate axial loads to a compressive level at about the DI proportional limit. After this stress level was reached, progressive bending and local distortion of the pipe occurred. These results are similar to those from the four-point bending tests in which local deformation developed and subsequent leakage occurred after moments, corresponding to the proportion limit, were applied.

# Section 5

# Joint Tension Test

## 5.1 Introduction

This section summarizes the results of the US Pipe tension testing of the TR-XTREME™ joint. Two tension tests were completed.

## 5.2 Tension Test 1

The pipe joint specimen was 168.8-in. (4.28-m)-long and 0.375-in. (9.5-mm)-thick with an outside diameter of 6.9 in. (175 mm). The pipe was set in the load frame so that its retaining clips were at the 3 and 9 o´clock (east and west) positions. The pipe spigot was fully inserted in the bell at the beginning of the test. Fully inserted refers to the position when either the weld bead was in contact with the bell throat, or the end of the spigot was in contact with the base of the bell socket. A schematic of the tension test is provided in Figure 5.1.

### 5.2.1 Instrumentation

Four strain gages were mounted 25 in. (0.64 m) north of the bell face on the bell side of the pipe at the positions of 12, 3, 6, and 9 o´clock (crown, east, invert, and west, respectively). The other four strain gages were mounted 22 in. (0.56 m) south of the bell face on the spigot side at the same positions. Four string pots, mounted to the bell at quarter points around the pipe circumference 12.5 in. (0.39 m) from the bell face, were fixed to the spigot and used to measure axial pullout of the spigot from the bell. The actuator and the load cell were installed on the load frame to apply and measure tensile force at the end of the pipe. The instrument locations and local gage names are listed in Table 5.1.

### 5.2.2 Force – Displacement

The pipe was filled with water and pressurized. The pressurizing sequence is shown in Figure 5.2. As the pressure was increased to 31.4 psi (216.5 kPa), there was a very small pullout movement of the spigot, after which there was a sudden displacement to 2.3 in. (58.4 mm). The pressure was then raised to the target of 80 psi (552 kPa) in preparation for axial loading.

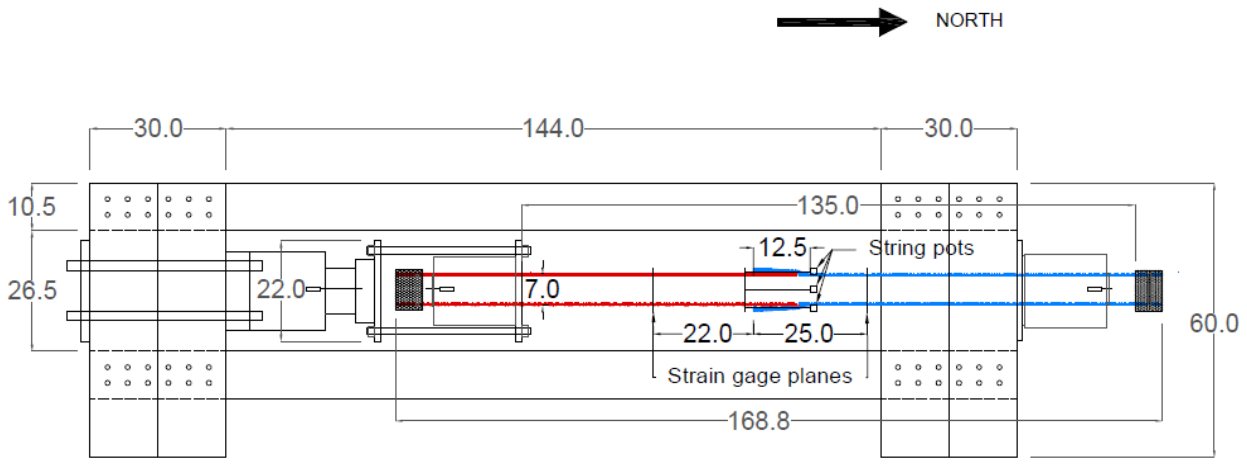


Figure 5.1. Tension Test Layout (Dimensions in inches)

Table 5.1. Instrumentation for US Pipe TR-XTREME™ Joint Tension Test 1

| Location | Instrument | Local Instrument Name |
|---|---|---|
| 25in. North of Bell Face | Crown, Axial Strain | ST 25CA |
| 25 in. North of Bell Face | Crown, Circumferential Strain | ST 25CC |
| 25 in. North of Bell Face | Invert, Axial Strain | ST 25IA |
| 25 in. North of Bell Face | Invert, Circumferential | ST 25IC |
| 25 in. North of Bell Face | East Springline, Axial Strain | ST 25EA |
| 25 in. North of Bell Face | East Springline, Circumferential Strain | ST 25EC |
| 25 in. North of Bell Face | West Springline, Axial Strain | ST 25WA |
| 25 in. North of Bell Face | West Springline, Circumferential | ST 25WC |
| 14 in. South of Bell Face | Crown, Axial Strain | ST 22CA |
| 14 in. South of Bell Face | Crown, Circumferential Strain | ST 22CC |
| 14 in. South of Bell Face | Invert, Axial Strain | ST 22IA |
| 14 in. South of Bell Face | Invert, Circumferential Strain | ST 22IC |
| 14 in. South of Bell Face | East Springline, Axial Strain | ST 22EA |
| 14 in. South of Bell Face | East Springline, Circumferential Strain | ST 22EC |
| 14 in. South of Bell Face | West Springline, Axial Strain | ST 22WA |
| 14 in. South of Bell Face | West Springline, Circumferential Strain | ST 22WC |
| Bell Face | Crown String Pot | Jnt Opening C |
| Bell Face | Invert String Pot | Jnt Opening I |
| Bell Face | East Springline String Pot | Jnt Opening E |
| Bell Face | West Springline String Pot | Jnt Opening W |
| Actuator | Load Cell | 400 K Load Cell |
| Actuator | Displacement | Act Disp |

1 in. = 25.4 mm; 1 kip = 4.448 kN

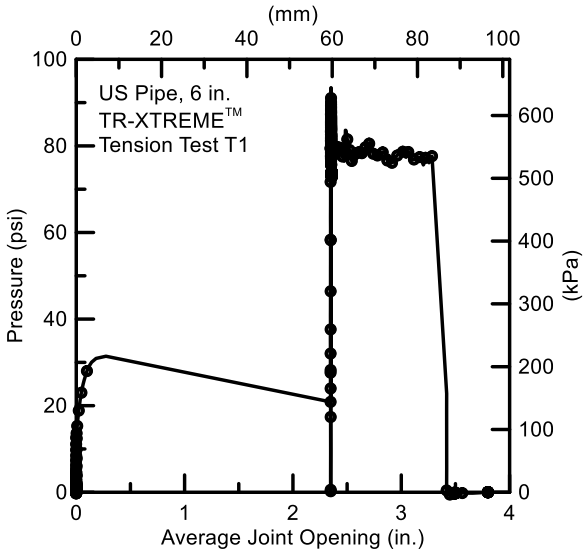


Figure 5.2. Pressure vs. Average Joint Opening

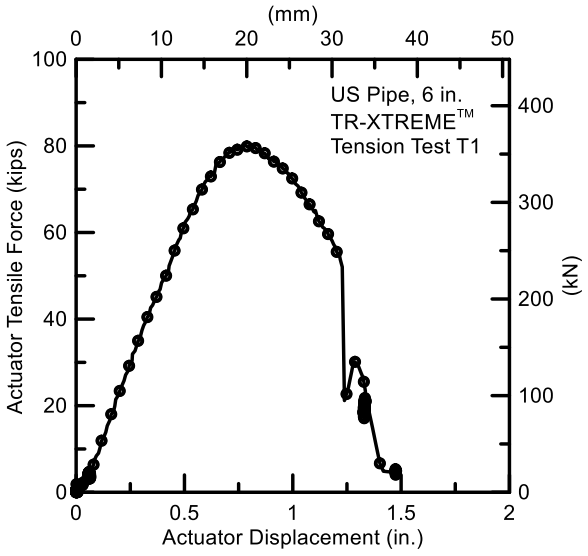


Figure 5.3. Tensile Force vs. Actuator Displacement

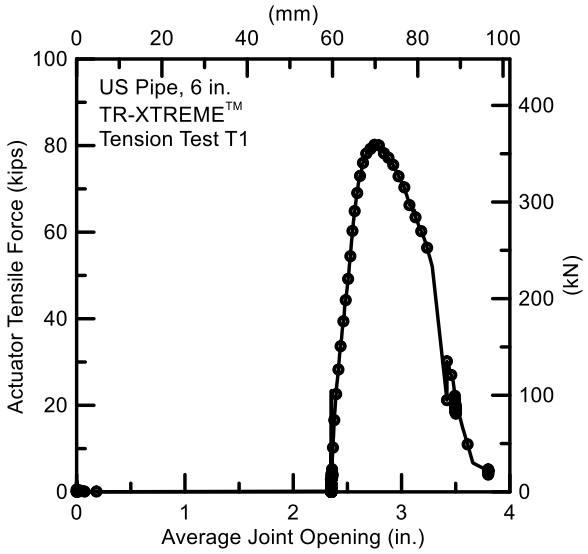


Figure 5.4. Tensile Force vs. Average Joint Opening

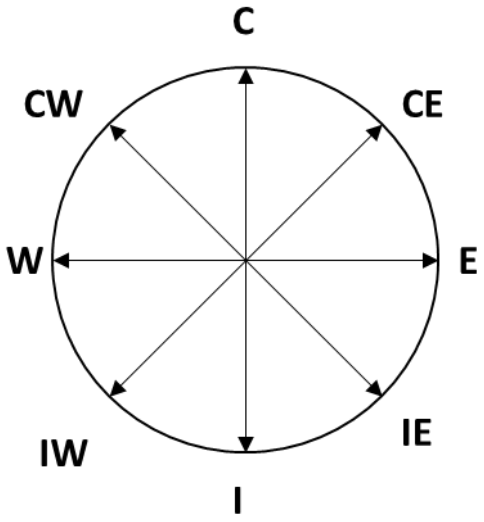


Figure 5.5. Spigot Measurement Locations (Looking North)

The pipe was secured to the actuator, and loading began at a rate of 1 in. (25.4 mm) per minute. A peak load of 80.2 kips (356.8 kN) was attained at 0.78 in. (19.8 mm) of actuator displacement, as shown in Figure 5.3. The load decreased until an actuator displacement of 1.23 in. (31.2 mm), when the retaining clips slid out of the bell and steady leakage at the joint was observed. The measured load at first leakage was 52.0 kips (231.3 kN). Approximately 20 kips (89 kN) remained in the system after this event. Loading was continued until the spigot was dislodged abruptly from the bell. The relationship between the tensile force and average joint opening, as measured by the string pots, is shown in Figure 5.4**.** At the maximum force of 82.2 kips (355.6 kN), there was 2.74 in. (69.6 mm) of total joint opening. At first leakage, there was 3.28 in. (83.3 mm) of total joint opening.

### 5.2.3 Spigot Deformations

The diameter of the spigot was measured at 4 different locations: Crown to Invert (C to I), Crown East to Invert West (CE to IW), East to West (E to W) and Invert East to Crown West (IE to CW) as shown in Figure 5.5.

The outer diameter of the spigot was measured before the tension test. The measurements showed that the spigot had a circular cross-section with a 6.9 in. (175.3 mm) diameter along its length.

Table 5.2. Diameter Measurements on Spigot Section

| Pre-Test | | | | |
|---|---|---|---|---|
| Locations | C-I (in.) | CE-IW (in.) | E-W (in.) | CW-IE (in.) |
| Spigot End | 6.907 | 6.905 | 6.896 | 6.902 |
| Post-Test | | | | |
| Locations | C-I (in.) | CE-IW (in.) | E-W (in.) | CW-IE (in.) |
| Spigot End | 6.865 | 6.903 | 6.910 | 6.907 |
| 2 in. from End | 6.919 | 6.905 | 6.832 | 6.878 |
| 5 in. from End | 7.145 | 6.752 | 6.543 | 6.739 |
| 6 in. from End | 7.184 | 6.602 | 6.570 | 6.585 |
| 32 in. from End | 6.849 | 6.887 | 6.891 | 6.888 |

1 in. = 25.4 mm

As tensile force was applied, the spigot was pulled from the bell, thus causing the weld bead on the spigot to bear against the retaining clips. As the tensile force increased, the load that the retaining clips carried also increased. Load concentration at the E and W locations of the spigot caused the spigot to deform inward from a circular to an oval shape. This inward deformation at the locations of the retaining clips allowed the clips to slide past the weld bead so that the spigot pulled from the bell.

Diameter measurements were taken at 5 different locations along the length of the spigot: at the spigot end, 2 in. (50.8 mm), 5 in. (127.0 mm) (close to weld bead locations), 6 in. (152.4 mm) (clips bearing areas) and 32 in. (812.8 mm) away from the end (strain gage location), as shown in Figures 5.6 a, b, and c. The diameter measurements are presented in Table 5.2.

The C-I diameter measurements are larger than the E-W diameter measurements. Spigot pullout past the restraining clips caused ovaling of the spigot close to the weld bead (6 in. away from the spigot end) where the retaining clips were located.

a) On Spigot Section


b) Close to Spigot End

c) 32 in. (813 mm) from Spigot End

Figure 5.6. Diameter Measurement Locations on Spigot Section

Figure 5.7. Deformed Area of the Spigot Caused by the Load Transferred from the Retaining Clips

As the spigot was pulled from the bell, the clips slid from their positions between the bell and weld bead on the spigot. At this point, the spigot end, which had deformed to a larger diameter in the vertical direction, became wedged at the landing area inside the bell. When the spigot was pulled from the bell after the test, there was some compressive deformation along the C-I direction where the spigot was wedged at a location about 2 in. away from the spigot end. Thus, the change in vertical diameter, which was measured after the spigot was pulled free of the bell, does not represent the maximum increase in diameter during the test. Figure 5.7 is a photo of the deformed area of the spigot caused by the load transferred from the retaining clips.

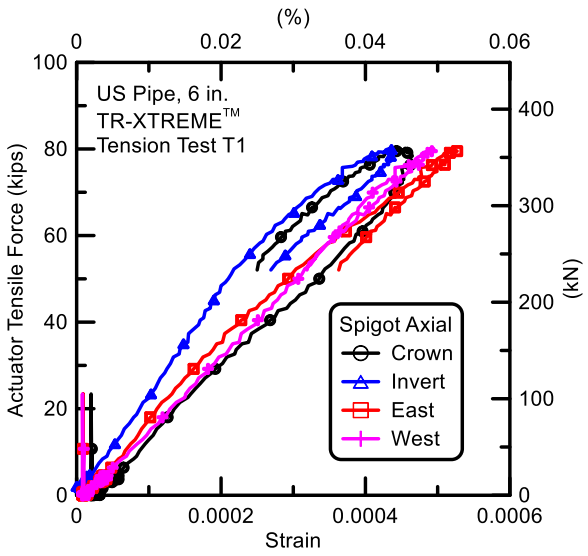


Figure 5.8. Actuator Tensile Force vs. Spigot Axial Strain

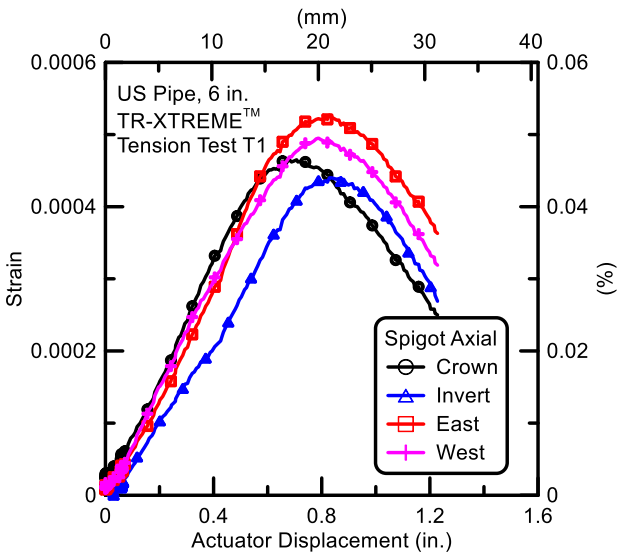


Figure 5.9. Spigot Axial Strain vs. Actuator Displacement

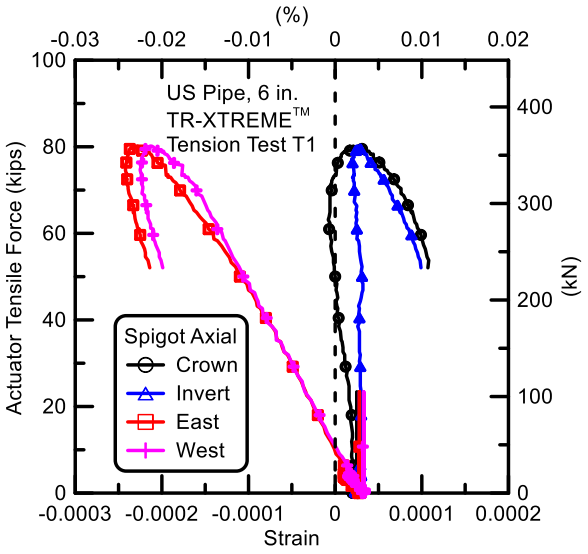


Figure 5.10. Actuator Tensile Force vs. Spigot Hoop Strain

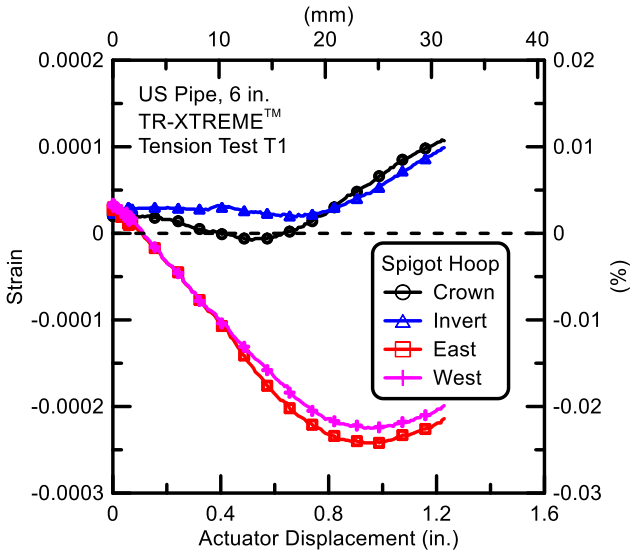


Figure 5.11. Spigot Hoop Strain vs. Actuator Displacement

### 5.2.4 Spigot Axial Strains

The maximum tensile axial strain on the spigot side was 0.00053 (0.053 %) and developed on the east side under an applied load of 80.0 kips (355.6 kN) at 0.82 in. (20.8 mm) of actuator displacement and 2.79 (70.9 mm) in. of joint opening. At the maximum load of 80.2 kips (356.8 kN), the east axial strain on the spigot side was 0.00052 (0.052%).

At first leakage, the east axial strain was 0.00035 (0.035%). The relationships of the spigot axial strains relative to the tensile force and actuator displacement are shown in Figures 5.8 and 5.9. Recall that there was a rapid joint opening of roughly 2.3 in. (58.4 mm) as internal pressure was applied. The axial strains in the spigot were nearly zero as the spigot moved out of the bell under internal pressure.

### 5.2.5 Spigot Hoop Strains

The spigot side had positive (tensile) hoop strains at the crown and invert, whereas the east and the west springlines had negative (compressive) hoop strains. Figure 5.10 shows the tensile force vs. the spigot hoop strain, and Figure 5.11 shows the spigot hoop strain vs. the actuator displacement. As the spigot was pulled from the bell, the retaining clips caused the spigot to deform inward at the springlines, with upward and downward deformation at the crown and invert. This deformation pattern is confirmed by looking at the relative movements at the crown, invert, and springlines. The maximum tensile hoop strain of 0.00011 (0.011%) was measured at the crown, whereas the maximum compressive hoop strain of -0.00024 (-0.024%) was measured at the east springline.

Table 5.2 presents the pre- and post-test diameter measurements, and Table 5.3 provides the relative diameter changes of the spigot near the clip locations. In the table positive represents lengthening and negative represents shortening. The C-I direction lengthened, putting the outer fiber of the crown and invert in tension, while the springline dimension shortened, putting the outside fiber at the springlines in compression.

Table 5.3. Relative Diameter Changes in Spigot Section near Retaining Clip Locations

| | Post-Test | |
|---|---|---|
| Locations | C-I (in.) | E-W (in.) |
| 2 in. from End | 0.012 | -0.064 |
| 5 in. from End | 0.238 | -0.353 |
| 6 in. from End | 0.277 | -0.326 |

1 in. = 25.4 mm

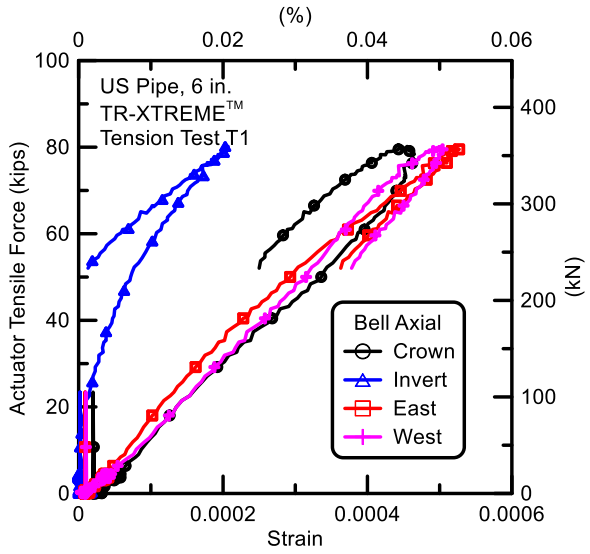


Figure 5.12. Actuator Tensile Force vs. Bell Axial Strain

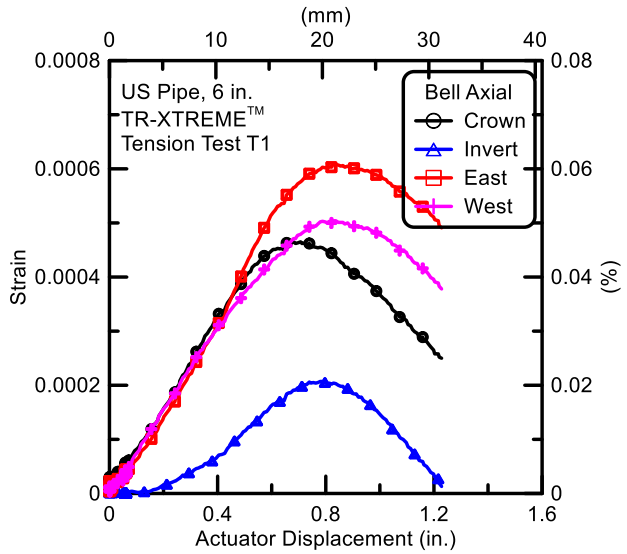


Figure 5.13 Bell Axial Strain vs. Actuator Displacement

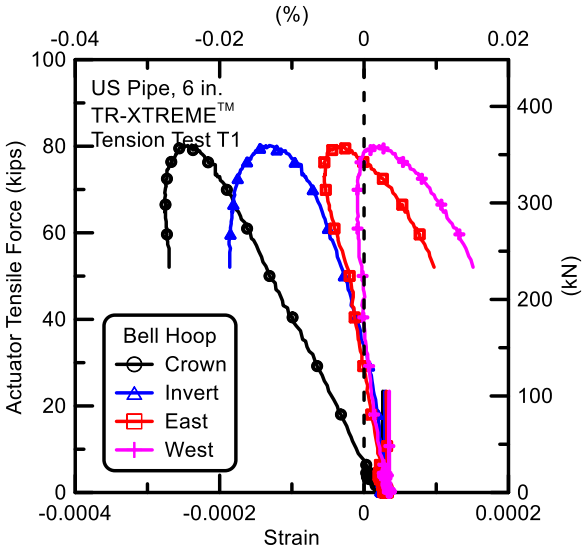


Figure 5.14. Actuator Tensile Force vs. Bell Hoop Strain

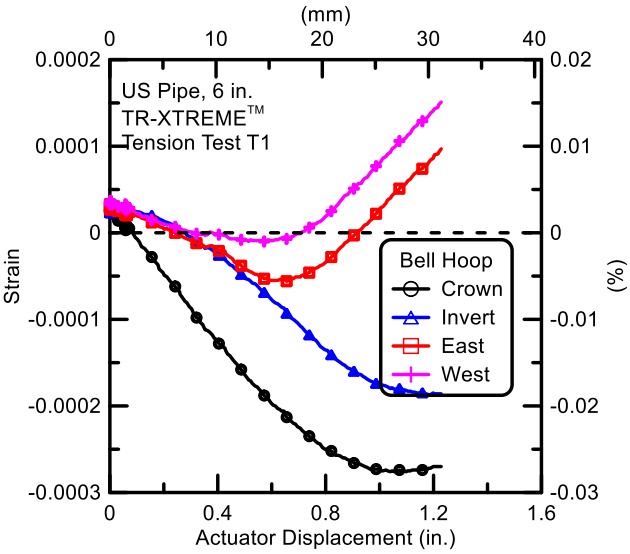


Figure 5.15. Bell Hoop Strain vs. Actuator Displacement

### 5.2.6 Bell Axial Strains

The actuator tensile force vs. bell axial strain and bell axial vs. actuator displacement are shown in Figures 5.12 and 5.13, respectively. The maximum tensile axial strain measured in the bell was 0.00064 (0.064%) at the crown. The axial load was 79.3 kips (352.7 kN), with a corresponding actuator displacement and joint opening of 0.73 in. (18.5 mm) and 2.70 in. (68.6 mm), respectively. The maximum load of 80.2 kips (356.8 kN) developed shortly after the maximum axial strain at an axial tensile strain of 0.00063 (0.063%) at 0.78 in. (19.8 mm) of actuator displacement and 2.74 in. (69.6 mm) of joint opening. When the load dropped to 52.0 kips (231.3 kN), the tensile axial strain at the east side of the bell was 0.00048 (0.048%), and leakage was observed at 1.23 in.(31.2 mm) of actuator displacement, corresponding to a joint opening of 3.28 in. (83.3 mm).

### 5.2.7 Bell Hoop Strains

The actuator tensile force vs. axial hoop strain and axial hoop strain vs. actuator displacement are shown in Figures 5.14 and 5.15, respectively. The crown and invert of the bell had negative (compressive) hoop strains, whereas the east and west springlines had positive (tensile) hoop strains. The outside of the bell crown and invert was in compression, and the east and west springlines were in tension. Just before the onset of leakage, a maximum tensile hoop strain of 0.00016 (0.016%) was measured at the west side of the bell at the same time that the maximum compressive hoop strain of 0.00027 (0.027%) was measured at the bell crown. Shortly after leakage, the tensile and the compressive hoop strains increased rapidly and reached their peaks at 0.00023 (0.023%) and 0.00031 (0.031%), respectively.

## 5.3 Tension Test 2

A second tension test was performed on the US Pipe TR-XTREME™ joint. The purpose of this test was to provide a replicate test to confirm joint behavior and monitor more closely the retaining clip movements at the joint. The pipe was set in the load frame so that its retaining clips were at the 3 and 9 o´clock (east and west) positions. The pipe was initially fully inserted in the bell. The pipe dimensions and instrumentation were identical to that of test T1.

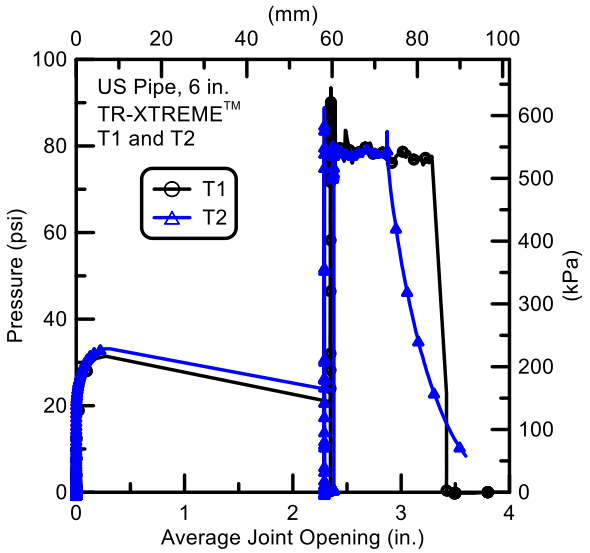


Figure 5.16. Pressure vs. Average Joint Opening for T1 and T2

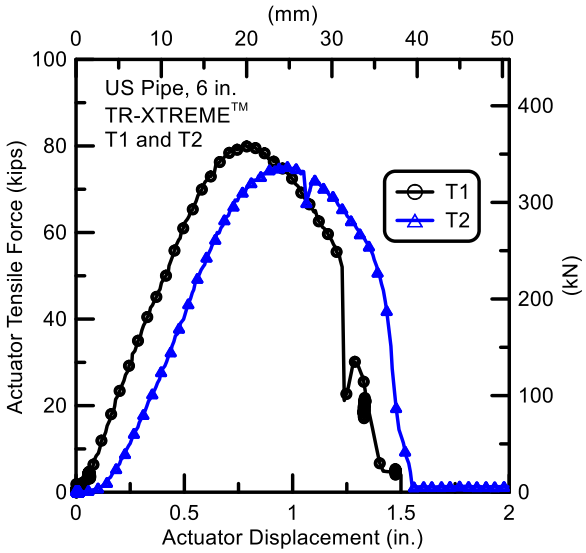


Figure 5.17. Tensile Force vs. Actuator Displacement for T1 and T2

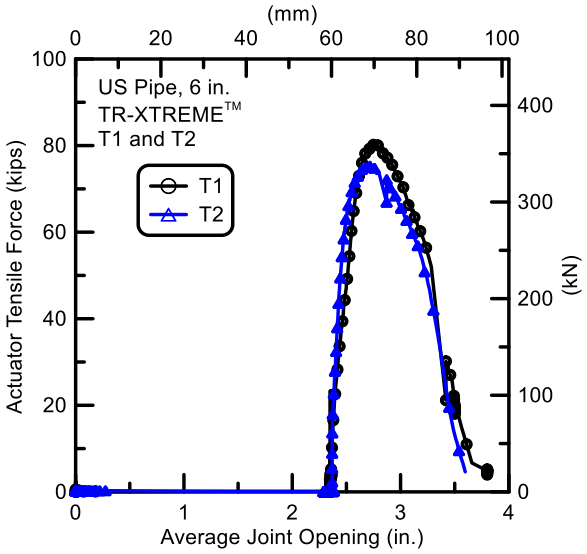


Figure 5.18. Tensile Force vs. Average Joint Opening for T1 and T2

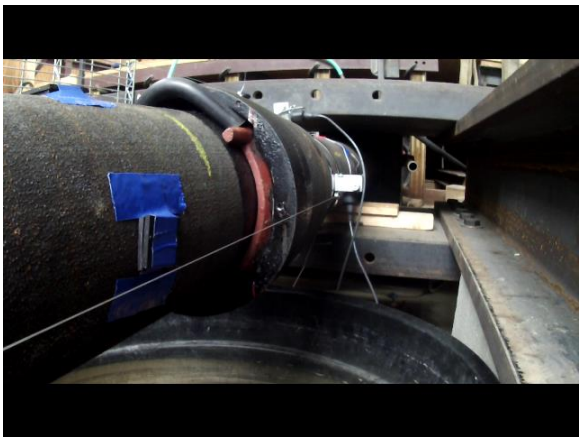

a) Retaining Clip Beginning Outward Movement

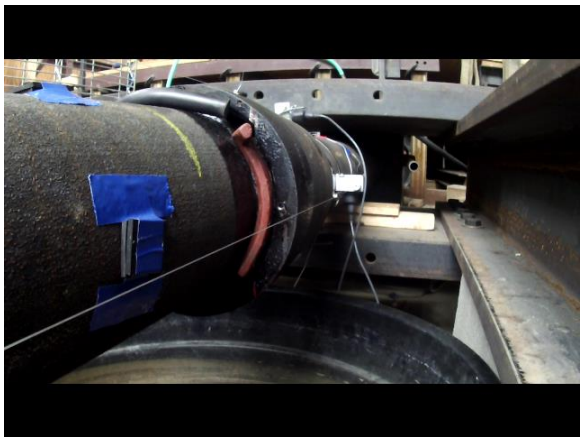

b) Retaining Clip Showing More Outward Movement and Rotation

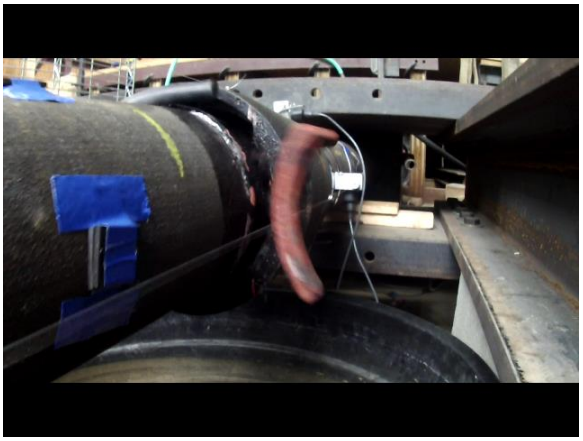

c) Full Clip Displacement

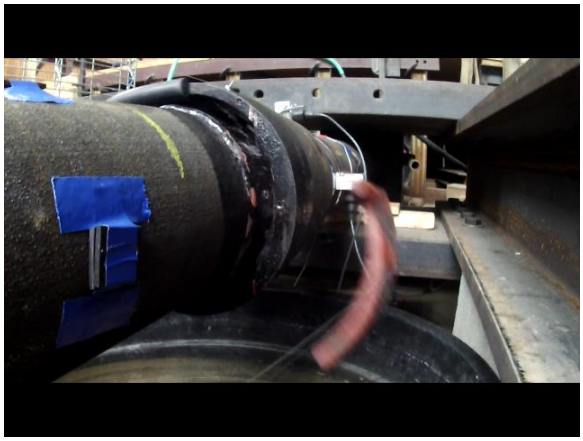

d) Full Clip Displacement and Joint Pull Out

Figure 5.19. Retaining Clip Movements for T2

### 5.3.1 Test 1 and Test 2 Compared

This section presents a comparison of the two test results. Figure 5.16 shows excellent agreement in terms of joint pullout and total load. T1 and T2 reached a maximum force of 83 kips (369 kN) at 2.75 in. (69.6 mm) of axial displacement and a maximum axial load of 78 kips (347 kN) at 2.72 in. (69.1 mm) of joint displacement, respectively. It is important to note that leakage of the joint does not occur

at maximum load. Figure 5.17 shows nearly identical plots of load vs. actuator displacement for the two tests. Figure 5.18 shows tensile force vs. average joint opening for the two tests. Again, the results are nearly identical. Each joint opened approximately 2.3 in. (58.4 mm) upon pressurization. T1 and T2 attained 3.28 in. (83.3 mm) and approximately 3.50 in. (88.9 mm) of total joint displacement, respectively, before leaking.

### 5.3.2 Test 2 Retaining Clip Movements

Figure 5.19 shows the retaining clip on the east springline of Test T2. As the pipe spigot pulls out, the clip exerts lateral force on the pipe, as described previously. Finally, the clip becomes fully dislodged.

## 5.4 Conclusions for Joint Tension Testing

Two tension tests were performed on the US Pipe TR-XTREME™ joints. Both tests began with the spigot fully inserted in the bell. As the pipe was pressurized, the spigot was displaced from the bell seat at approximately 30 psi (207 kPa) internal pressure. The slip was 2.3 in. (58.4 mm) before the weld bead became engaged with the restraining clips. Tests T1 and T2 reached a maximum force of 83 kips (269 kN) at 2.75 in. (69.9 mm) of axial displacement and an axial load of 78 kips (347 kN) at 2.72 in. of joint displacement, respectively. The joints began to leak at openings of 3.3 (83.8 mm) and 3.5 in. (88.9) for T1 and T2, respectively. The overall behavior of T1 and T2 was nearly identical.

The onset of leakage is caused by forces generated between the spigot bead and restraining clips that deform the spigot inward a sufficient distance to allow the bead to slip past the clips, with attendant loss of water pressure. Similar to the compressive and four point bending test results for the US Pipe TR-XTREME™ joint, leakage occurred in the tensile tests when localized strains resulted in irrecoverable deformation. In this case, those strains are circumferential, and the irrecoverable deformation is reflected in shortening of the spigot diameter caused by forces between the spigot bead and clips.

The maximum pullout force was on the order of 80 kips (356 kN) at a joint opening of about 2.75 in. (69.9 mm). Leakage was observed at joint openings between 3.3 and 3.5 in. (83.8 and 88.9 mm). Thus, additional joint pullout capacity was available once the spigot had been pulled 2.3 in. (58.4 mm) from its initial set in the bell. After the weld bead on the spigot made contact with the clips, an additional movement of approximately 1 in. (25.4 mm) was required to generate leakage at the joint.

# Section 6

# Axial Soil Resistance

## 6.1 Introduction

This section of the report summarizes the results from three axial soil resistance tests. The pipes with TR-XTREME™ joints were placed in the north end of the large split basin, and were pulled axially about 18 in. from the north end. This section describes the soil placement, pullout resistances, and measured pipe responses during the tests.

## 6.2 Test Layouts and Instrumentation

Figure 6.1 is a plan view of the experimental setups for Tests 1 and 2. In these tests the bell mouth was facing north. The total length of the TR-XTREME™ joint specimen buried in soil was 149 in., with 71.1 in. and 77.9 in. (3.78, 1.81, and 1.98 m) of the spigot and bell section, respectively, in soil. The bell section was 156 in. long. In Tests 1 and 2 strain gages to measure axial strains were placed at locations B26 and S10, shown in Figure 6.1. Test 1 was set up so that the pipe was pulled at the spigot. The pipe in Test 2 was installed with polywrap surrounding the pipe, and was also pulled at the spigot.

Figure 6.2 is a plan view of the test setups for Test 3. Test 3 had no polywrap. In this test the bell mouth was facing south. The total length of the TR-XTREME™ joint specimen buried in soil was 149 in., with 63.5 in. and 85.5 in. of the spigot and bell section, respectively, in soil.

The instrumentation in the three tests was similar. Tables 6.1 lists the instrumentation for Tests 1 and 2. Table 6.2 summarizes the instrumentation in Test 3. There were two string pots to detect the displacement of the leading end north of the box. Two string pots were installed south of the box to measure the south end displacement. Jack pressure was measured in all tests to determine applied axial force. In Test 3 displacement transducers (DCDTs) were installed at the joint and surrounded by a joint shield. Also, in Test 3 eight cells were installed at the north end. Two load cells were installed in series at each corner of a load transfer plate.

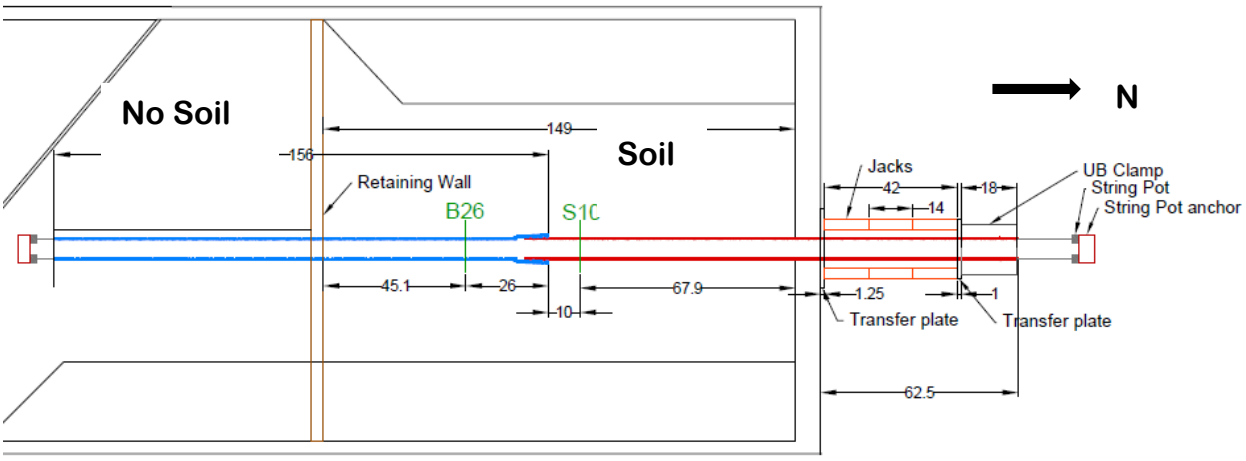


Figure 6.1. Plan View of Tests 1 and 2

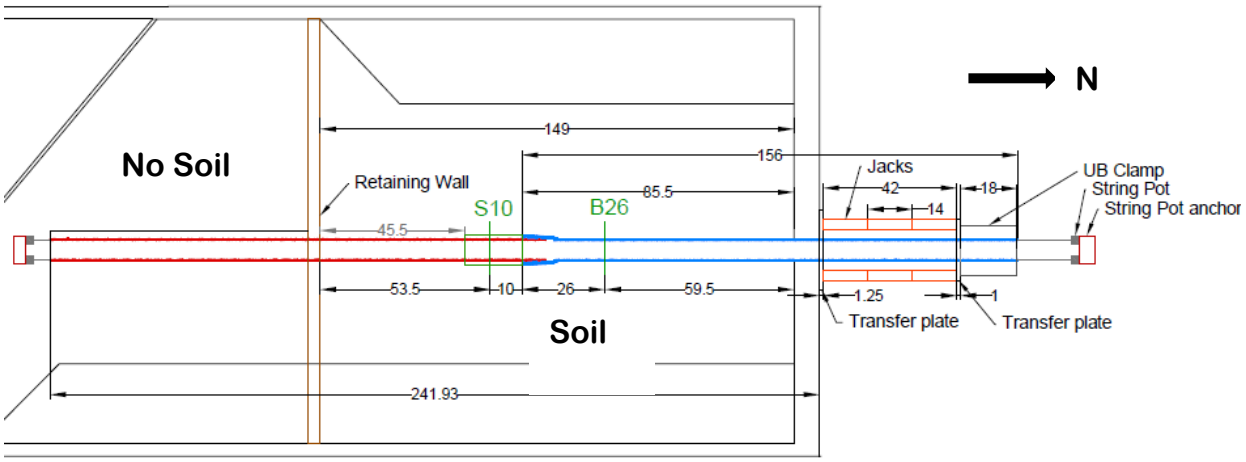


Figure 6.2. Plan View of Test 3

Table 6.1. Instrumentation for US Pipe TR-XTREME™ Joint Axial Pull Tests 1 and 2

| Location | Instrument | Local Instrument Name |
|---|---|---|
| 26 in. South of Bell Face | Crown, Axial Strain | B26C |
| 26 in. South of Bell Face | Invert, Axial Strain | B26I |
| 26 in. South of Bell Face | East Springline, Axial Strain | B26E |
| 26 in. South of Bell Face | West Springline, Axial Strain | B26W |
| 10 in. North of Bell Face | Crown, Axial Strain | S10C |
| 10 in. North of Bell Face | Invert, Axial Strain | S10I |
| 10 in. North of Bell Face | East Springline, Axial Strain | S10E |
| 10 in. North of Bell Face | West Springline, Axial Strain | S10W |
| Southwest Side of Pipe, Outside Test Basin | String Pot for Axial Displacement of Bell Section | SP_SW |
| Southeast Side of Pipe, Outside Test Basin | String Pot for Axial Displacement of Bell Section | SP_SE |
| Northwest Side of Pipe, Outside Test Basin | String Pot for Axial Displacement of Spigot Section | SP_NW |
| Northeast Side of Pipe, Outside Test Basin | String Pot for Axial Displacement of Spigot Section | SP_NE |
| North Transfer Plate to Test Basin | Hydraulic Jacks for Load | Load |

1 in. = 25.4 mm

Table 6.2. Instrumentation for US Pipe TR-XTREME™ Joint Axial Pull Test 3

| Location | Instrument | Local Instrument Name |
|---|---|---|
| 10 in. South of Bell Face | Crown, Axial Strain | S10C |
| 10 in. South of Bell Face | Invert, Axial Strain | S10I |
| 10 in. South of Bell Face | East Springline, Axial Strain | S10E |
| 10 in. South of Bell Face | West Springline, Axial Strain | S10W |
| 26 in. North of Bell Face | Crown, Axial Strain | B26C |
| 26 in. North of Bell Face | Invert, Axial Strain | B26I |
| 26 in. North of Bell Face | East Springline, Axial Strain | B26E |
| 26 in. North of Bell Face | West Springline, Axial Strain | B26W |

1 in. = 25.4 mm

Table 6.2. Instrumentation for US Pipe TR-XTREME™ Joint Axial Pull Test 3 (completed)

| | | |
|---|---|---|
| Southwest Side of Pipe, Outside Test Basin | String Pot for Axial Displacement of Bell Section | SP_SW |
| Southeast Side of Pipe, Outside Test Basin | String Pot for Axial Displacement of Bell Section | SP_SE |
| Northwest Side of Pipe, Outside Test Basin | String Pot for Axial Displacement of Spigot Section | SP_NW |
| Northeast Side of Pipe, Outside Test Basin | String Pot for Axial Displacement of Spigot Section | SP_NE |
| North End, Northwest Corner, Top | Load Cell | LC_NWS_top |
| North End, Northwest Corner, Top | Load Cell | LC_NWN_top |
| North End, Northeast Corner, Top | Load Cell | LC_NES_top |
| North End, Northeast Corner, Top | Load Cell | LC_NEN_top |
| North End, Southwest Corner, Top | Load Cell | LC_SWS_top |
| North End, Southwest Corner, Top | Load Cell | LC_SWN_top |
| North End, Southeast Corner, Bottom | Load Cell | LC_SES_top |
| North End, Southeast Corner, Bottom | Load Cell | LC_SEN_bot |
| Joint Crown | DCDT | dcdt_C |
| Joint East Springline | DCDT | dcdt_E |
| Joint West Springline | DCDT | dcdt_W |

## 6.3 Soil Placement and Compaction Data

The soil used during the pull-through tests was crushed, washed, glacio-fluvial sand produced by RMS Gravel consisting of particles mostly passing the ¼ in. (6.35 mm) sieve. Eight in. (200 mm) of compacted sand was placed in the test basin, followed by the pipe section, followed by roughly 8-in. (200-mm)-thick lifts until there was a 30 in. (0.76 m) cover of compacted sand above the pipe crown.

Every layer was compacted to the same extent and moistened with water in a similar way to achieve uniformity. Dry density measurements for each layer at four representative locations were obtained using a Troxler Model 3440 densitometer. The measurement locations were near the northwest (NW), northeast (NE), southwest (SW), and southeast (SE) corners of the north test basin. Moisture content measurements were obtained using both soil samples and the densitometer at the same locations. The target value of dry density was $\gamma_{dry}$ = 106 lb/ft$^3$ (16.65 kN/m$^3$) at a moisture content of w = 4.0 %.

Experience with the nuclear densitometer at Cornell has shown that the moisture measurements taken with the device are not as accurate as moisture measured using traditional methods such as moisture tins and oven drying. The Troxler makes two fundamental measurements. In direct transmission mode, which is used in this testing program, the Troxler uses gamma radiation from the Cesium-137 (Cs-137) to measure the total density of the material. The radiation backscattered to the detector from the source lowered into the soil is measured. The higher the measured backscatter, the greater the density of the material. The Americium-241: Beryllium (Am-241:Be) source neutrons detect the amount of hydrogen. Increasing amounts of hydrogen means a reduced energy of the neutrons returning to the detector. More hydrogen is an indicator of more moisture. Thus, the two fundamental measurements are 1) the total density, expressed in user-selected units, such as lb/ft$^3$, and 2) amount of water again expressed in user-selected units, such as lb/ft$^3$.

The average unit weight and moisture content data for the three axial pull tests are presented in Tables 6.3 through 6.8. For Test 1 the average dry unit weight was 106.6 lb/ft$^3$(16.75 kN/m$^3$) with an average water content of 4.7%. For Test 2 the average dry unit weight was 105.2 lb/ft$^3$ (16.53 kN/m$^3$), with an average water content of 4.8%. For Test 3 the average dry unit weight was 106.8 lb/ft$^3$, with an average water content of 4.3%. Repeatable unit weights and water contents were achieved in all tests, which are consistent with other large-scale tests conducted at Cornell. Table 6.9 lists the average results for all of the tests.

The angle of shearing resistance of the soil, based on correlations with soil unit weight established at Cornell, was 41-42°. The soil strength properties are representative of a well-compacted dense sand.

Table 6.3. Soil Dry Unit Weight Data for Pull Test 1

| | Dry Unit Weight ($lb/ft^3$) at Measurement Location | | | | | |
|---|---|---|---|---|---|---|
| Lift Number | NW | NE | SW | SE | Average | Std. Dev. |
| 1 | 107.5 | 107.4 | 107.3 | 108.1 | 107.6 | 0.4 |
| 2 | 105.6 | 105.9 | 107.1 | 106.5 | 106.3 | 0.7 |
| 3 | 105.1 | 105.6 | 107.0 | 105.9 | 105.9 | 0.8 |
| 4 | 106.4 | 106.7 | 106.6 | 106.9 | 106.6 | 0.2 |
| 5 | 106.8 | 106.0 | 106.7 | 107.4 | 106.7 | 0.6 |
| | | | | | | |
| Global | | | | | 106.6 | 0.8 |

1 $lb/ft^3$ = 0.157 $kN/m^3$

Table 6.4. Moisture Tin Water Content Data for Pull Test 1

| | Moisture Tin Water Content, w (%) at Measurement Location | | | | | |
|---|---|---|---|---|---|---|
| Lift Number | NW | NE | SW | SE | Average | Std. Dev. |
| 1 | 4.1 | 4.6 | 4.6 | 4.4 | 4.4 | 0.2 |
| 2 | 4.8 | 5.1 | 4.8 | 4.6 | 4.8 | 0.2 |
| 3 | 5.7 | 4.8 | 5.2 | 4.8 | 5.1 | 0.4 |
| 4 | 4.4 | 4.6 | 4.9 | 5.0 | 4.7 | 0.3 |
| 5 | 4.3 | 4.6 | 4.5 | 5.0 | 4.6 | 0.3 |
| | | | | | | |
| Global | | | | | 4.7 | 0.4 |

1 $lb/ft^3$ = 0.157 $kN/m^3$

Table 6.5. Soil Dry Unit Weight Data for Pull Test 2

| | Dry Unit Weight ($lb/ft^3$) at Measurement Location | | | | | |
|---|---|---|---|---|---|---|
| Lift Number | NW | NE | SW | SE | Average | Std. Dev. |
| 1 | 104.8 | 105.3 | 104.5 | 105.6 | 105.1 | 0.5 |
| 2 | 104.7 | 106.1 | 105.0 | 105.4 | 105.3 | 0.6 |
| 3 | 104.6 | 106.6 | 105.1 | 105.9 | 105.6 | 0.9 |
| 4 | 105.7 | 105.2 | 104.6 | 105.9 | 105.3 | 0.6 |
| 5 | 105.7 | 104.8 | 104.2 | 105.1 | 105.0 | 0.6 |
| | | | | | | |
| Global | | | | | 105.2 | 0.6 |

1 $lb/ft^3$ = 0.157 $kN/m^3$

Table 6.6. Moisture Tin Water Content Data for Pull Test 2

| | Moisture Tin Water Content, w (%) at Measurement Location | | | | | |
|---|---|---|---|---|---|---|
| Lift Number | NW | NE | SW | SE | Average | Std. Dev. |
| 1 | 6.2 | 4.8 | 5.0 | 4.7 | 5.2 | 0.7 |
| 2 | 5.0 | 4.8 | 4.7 | 4.7 | 4.8 | 0.1 |
| 3 | 4.8 | 4.8 | 4.8 | 4.8 | 4.8 | 0.0 |
| 4 | 4.8 | 4.8 | 5.2 | 4.4 | 4.8 | 0.3 |
| 5 | 4.5 | 4.5 | 4.9 | 4.5 | 4.6 | 0.2 |
| | | | | | | |
| Global | | | | | 4.8 | 0.4 |

1 $lb/ft^3$ = 0.157 $kN/m^3$

Table 6.7. Soil Dry Unit Weight Data for Pull Test 3

| | Dry Unit Weight ($lb/ft^3$) at Measurement Location | | | | | |
|---|---|---|---|---|---|---|
| Lift Number | NW | NE | SW | SE | Average | Std. Dev. |
| 1 | 107.8 | 107.7 | 107.8 | 106.6 | 107.5 | 0.6 |
| 2 | 106.3 | 107.2 | 106.6 | 106.0 | 106.5 | 0.5 |
| 3 | 106.8 | 107.5 | 106.1 | 105.8 | 106.5 | 0.8 |
| 4 | 106.8 | 107.6 | 104.6 | 107.4 | 106.6 | 1.4 |
| 5 | 108.5 | 106.1 | 107.1 | 106.7 | 107.1 | 1.0 |
| | | | | | | |
| Global | | | | | 106.8 | 0.9 |

1 $lb/ft^3$ = 0.157 $kN/m^3$

Table 6.8. Moisture Tin Water Content Data for Pull Test 3

| | Moisture Tin Water Content, w (%) at Measurement Location | | | | | |
|---|---|---|---|---|---|---|
| Lift Number | NW | NE | SW | SE | Average | Std. Dev. |
| 1 | 4.0 | 4.6 | 3.6 | 4.1 | 4.1 | 0.4 |
| 2 | 4.6 | 3.9 | 4.2 | 5.0 | 4.5 | 0.5 |
| 3 | 4.3 | 4.4 | 4.4 | 4.6 | 4.4 | 0.1 |
| 4 | 4.4 | 4.1 | 5.5 | 4.2 | 4.6 | 0.7 |
| 5 | 3.7 | 4.0 | 4.4 | 4.5 | 4.1 | 0.4 |
| | | | | | | |
| Global | | | | | 4.3 | 0.4 |

1 $lb/ft^3$ = 0.157 $kN/m^3$

Table 6.9. Average Soil Dry Unit Weights and Moisture Contents for Pull Tests

| | Dry Unit Weight | | Water Content | |
|---|---|---|---|---|
| Test | (lb/ft3) | Std. Dev ($lb/ft^3$) | (%) | Std. Dev (%) |
| 1 | 106.6 | 0.8 | 4.7 | 0.4 |
| 2 | 105.2 | 0.6 | 4.8 | 0.4 |
| 3 | 106.8 | 0.9 | 4.3 | 0.4 |

1 $lb/ft^3$ = 0.157 $kN/m^3$

## 6.4 Axial Pull Forces and Displacements

Figure 6.3 shows the pull force vs. north end displacement for the three tests, at increasingly larger displacement scales. Tests 1 and 2 were designed so that pullout forces and displacements applied from the north end of the specimen would cause the spigot to pull from the bell until the weld bead on the spigot was engaged with the bell mouth, after which both sections of pipe would be pulled through the soil. This trend can be seen clearly in Figure 6.3. For displacements to about 2.1 in., the pullout force stabilized at about 2 kips (8.9 kN) for Tests 1 and 2, after which the bell and spigot moved together as increasingly larger pullout forces were mobilized. The large pullout force was generated by soil reaction at the bell as it was pulled through the soil.

In Test 3 pullout force and displacement were applied to the bell end of the pipe so that axial resistance to pullout was generated at all times by the bell pulling through the soil in combination with frictional resistance mobilized between the soil and pipe surface. In this test, the pipe specimen south of the joint was not long enough to mobilize enough soil shear resistance for the bell end to pull from the spigot. Hence, the joint did not expand, or open, as it did in Tests 1 and 2.

As shown in Figures 6.3 a) and b), the pullout force in Test 1 increased to about 3.2 kips (14.2 kN) at 0.2 in. (5.1 mm) of displacement, which corresponds to a force virtually the same as mobilized in Test 3 at similar displacement. The force dropped rapidly in Test 1 to about 2 kips as the spigot started to pull from the bell of the joint.

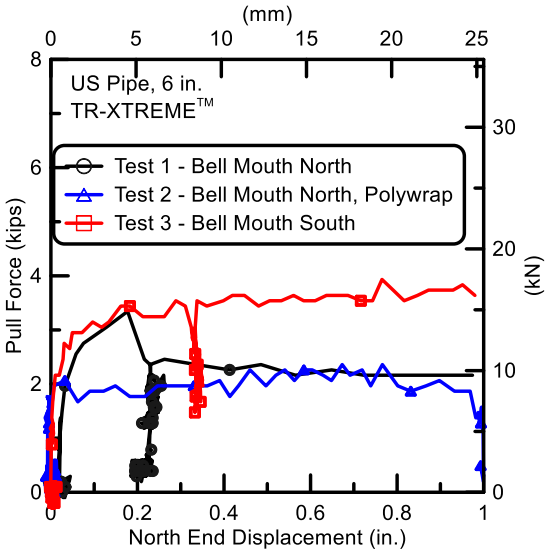


a) Up to 1 in. (25.4 mm) Displacement

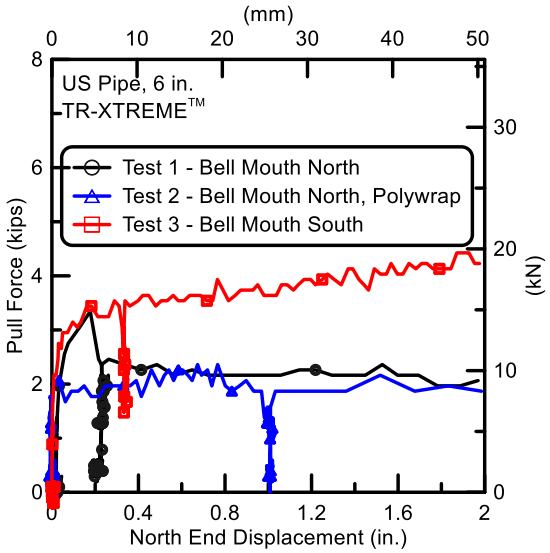


b) Up to 2 in. (50.8 mm) Displacement

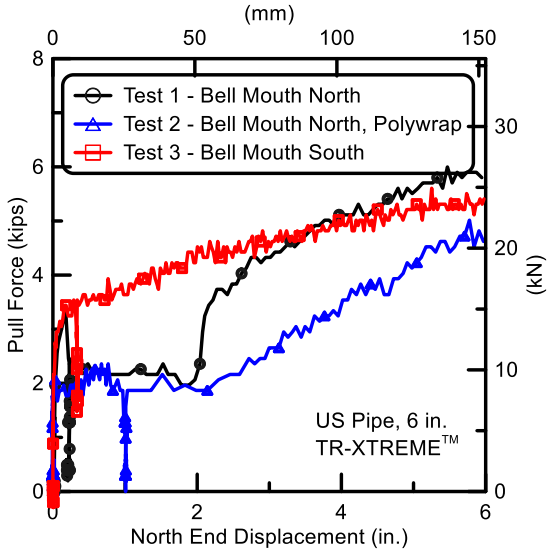


c) Up to 6 in. (152.4 mm) Displacement

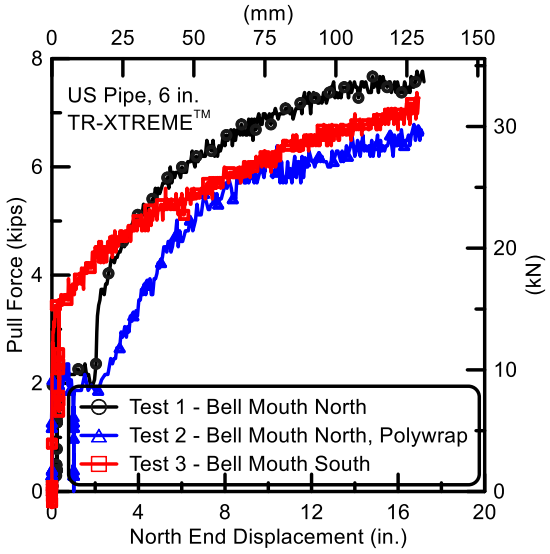


d) Up to 18 in. (457.2 mm) Displacement

Figure 6.3. Axial Pull Force vs. North End Displacement

Figure 6.4 corroborates the interpretation of test results given above. It shows the string pot measurements at the south end of the test section vs. those at the north end. Once the Test 1 displacement reached approximately 2.1 in. (53.2 mm), the weld bead on the spigot end engaged the bell mouth. There was a corresponding rapid increase in axial resistance, with. the south and north end displacements increasing at equal rates. In Test 2, which had polywrap, both the south and north ends moved together to a displacement of 0.7 in. (17.8 mm) Then, the spigot pulled from the bell at constant force until an additional displacement of 2 in. (50.8 mm) was imposed. At this stage in the loading, the weld bead was engaged fully with the bell and both pipe sections moved together. In Test 3 the south and north ends moved equally from the beginning of the test because the joint did not open.

A direct comparison between Tests 1 and 2 (see in particular Figures 6.3c) and d) shows that the polywrap reduced the axial pullout force by about 15% or more at displacements exceeding 4 in. when compared with unwrapped pipe under similar burial conditions. The force reduction is caused by reduced shear transfer between soil and pipe because of the polyethylene wrap.

It is noteworthy that the pullout resistances are within about 5% for Tests 1 and 3 at large displacements on the order of 16 in. (406 mm). Thus, there is little difference between the ultimate pullout forces associated with the flat and curved ends of the bell oriented towards the direction of movement. The force vs displacement data show that the ultimate pullout resistance is mobilized more rapidly with displacement when the flat end of the bell is oriented toward the direction of movement, thus contributing to a stiffer reaction.

Test 3 had DCDTs installed on the bell at the crown and east and west springlines. Figure 6.5 shows that there was very little DCDT movement at the bell; a maximum of about 0.1 in. (2.5 mm) at pull force of roughly 7 kips (31.1 kN). Figure 6.6 shows that the DCDTs began slight movement as the north end was displaced, and moved uniformly. At 1 in. (25.4 mm) of north end movement the DCDTs only showed about 0.5 in. (12.7 mm) displacement. As described previously, this response is consistent with the fact that insufficient soil shear transfer was available in the test specimen south of the joint to result in opening of the joint.

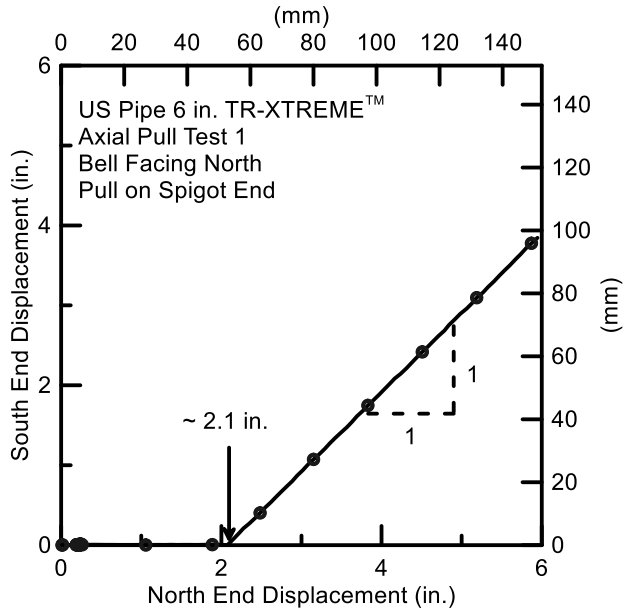


a) Test 1

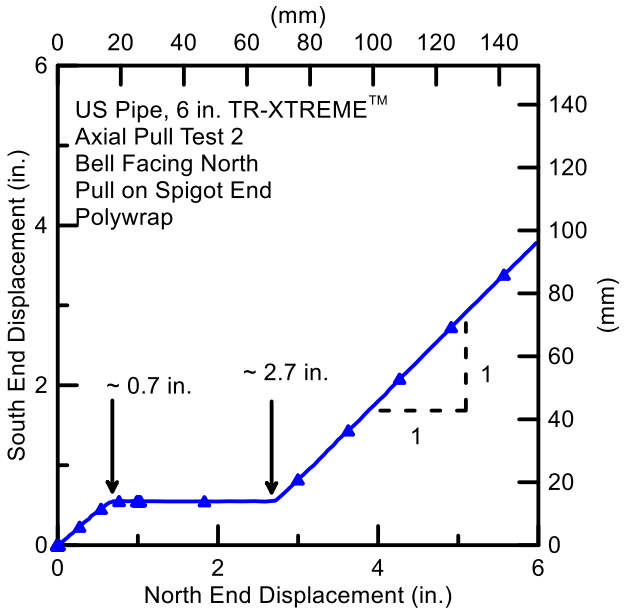


b) Test 2

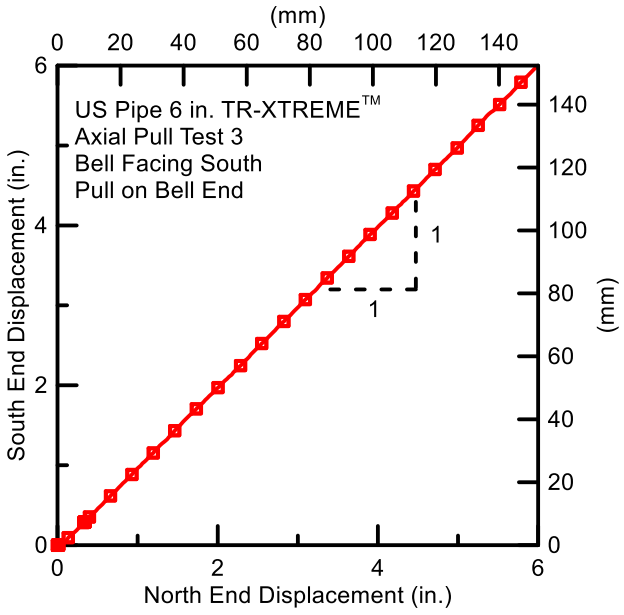


c) Test 3

Figure 6.4. South vs. North End Displacements

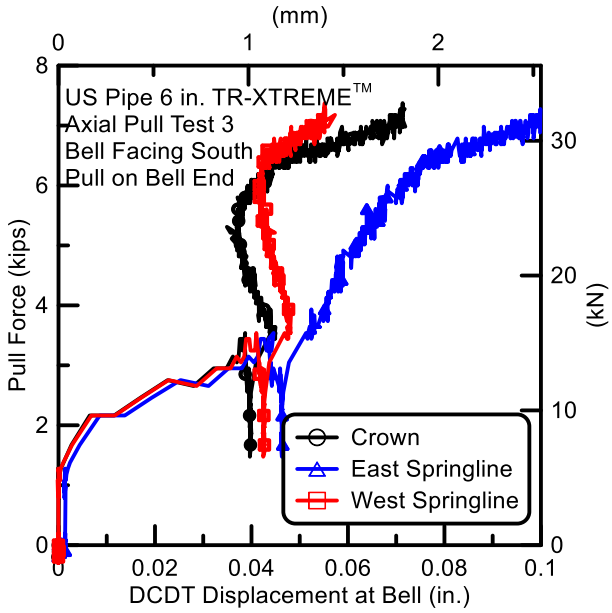


Figure 6.5. Pull Force vs. DCDT Displacement for Test 3

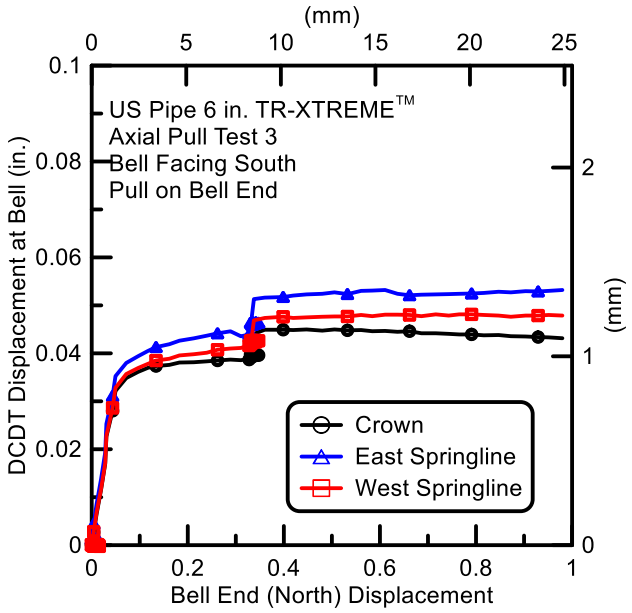


Figure 6.6. DCDT Displacement vs. North End Displacement for Test 3

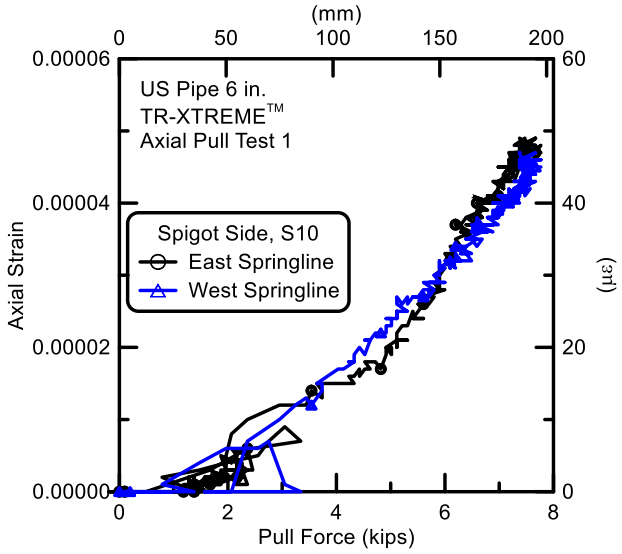


Figure 6.7. Spigot Axial Strains at Springlines vs. Pull Force for Test 1

## 6.5 Strains

In all tests, strain gages were installed on the spigot and bell end sections. The gages were orientated to measure axial strains, and were calibrated to be sensitive at the microstrain level. Figure 6.5 shows the axial strains measured at S10 (see Figure 6.2) for Tests 1 at the E and W springline locations. At a pullout force of about 2.1 kips (9.3 kN), corresponding to opening of the joint (see Figure 6.1b), the average axial pipe strain near the joint was very low, at about 2-3 microstrain (με), indicating low axial force.

The measurements therefore show that the pullout force was resisted by about 2 kips (8.9 kN) of soil shear resistance against axial pipe movement north of the S10 strain gages. This force agrees well with the soil shear resistance force, calculated theoretically on the basis of soil/pipe interface resistance and soil stress conditions consistent with the test preparation.

## 6.6 Conclusions for Axial Soil Resistance Tests

Table 6.10 lists the pipe orientations, bell mouth direction, and pull directions for the three tests. In the tests, the bell mouth was facing north in Tests 1 and 2, and south in Test 3. Test 2 was wrapped in polywrap. Thus, comparisons to Test1 and 2 are useful in assessing the effect of polywrap. Comparisons of Test 1 and 3 indicate differences in the direction of the bell. The pull forces for the three tests are tabulated in Table 6.11. The force for the polywrap pipe (Test 2) is smaller than that for Test 1. At large pull out, the difference between the polywrap and unwrapped pipe decreases.

The axial soil resistance tests confirm axial slip of the TR-XTREME™ joint under conditions in which sufficient soil/pipe shear resistance is mobilized either side of the joint to exceed the force required to initiate joint slip. Once the spigot bead becomes fully engaged with the bell mouth, additional resistance to pullout is mobilized from soil reaction at the bell as it is pulled through the soil. The test results provide excellent data with which to quantify the axial pullout loads and displacements when there is relative movement between the adjacent soil and pipelines with 6-in. (150-mm) TR-XTREME™ joints.

Table 6.10. Pipe Orientations, Bell Mouth Direction, and Pull Directions

| Test | South Pipe | North Pipe | Bell Mouth Facing | Pull From |
|---|---|---|---|---|
| 1 | Bell | Spigot | North | North |
| 2[a] | Bell | Spigot | North | North |
| 3 | Spigot | Bell | South | North |

a – Test 2 had polywrap

Table 6.11. Pull Forces for All Tests

| North End Displacement (in.) | Pull Force (kips) | | |
|---|---|---|---|
| | Test 1 | Test 2 | Test 3 |
| 0.1 | 2.9 | 1.9 | 3.9 |
| 0.2 | 2.2 | 1.8 | 3.6 |
| 1 | 2.1 | 1.8 | 3.7 |
| 2 | 2.1 | 1.8 | 4.3 |
| 4 | 5.1 | 3.5 | 5.0 |
| 8 | 6.5 | 5.6 | 5.8 |
| 12 | 7.2 | 6.1 | 6.4 |
| 16 | 7.5 | 6.5 | 6.9 |

1 in. = 25.4 mm; 1 kip = 4.48 kN

The test results show that the polywrap reduced the axial pullout force by about 15% or more at displacements exceeding 4 in. (102 mm) when compared with unwrapped pipe under similar burial conditions. The reduced axial force is caused by the lower interface resistance between the soil and polyethylene wrap when compared with the interface resistance between soil and ductile iron pipe.

There is less than 10% difference between the ultimate pullout forces associated with the flat and curved ends of the bell oriented towards the direction of movement. The force vs. displacement data show that the ultimate pullout resistance is mobilized more rapidly when the flat end of the bell is oriented toward the direction of movement, thus contributing to a stiffer reaction.

# Section 7

# Large-Scale Testing of Fault Rupture Effects

## 7.1 Introduction

This section presents the results of a large-scale test of fault rupture effects on a ductile iron pipeline, provided by US Pipe, composed of ductile iron pipe with TR-XTREME™ joints. All testing was performed in the large-scale test basin at the Cornell University Large Scale Lifelines Testing Facility during September 2014 It should be noted that the term "rotation" in this section is equivalent to "deflection" as used commonly in the field and commercial pipeline information.

## 7.2 Test Configuration and Procedure

Figure 7.1 is a plan view of the test layout, which shows the fault rupture plane and approximate locations of the four actuators generating ground failure. The pipeline consisted of five pipe segments connected with TR-XTREME™ joints. The objective of the test was to impose abrupt ground deformation on the pipeline, which was identical to left lateral strike slip fault rupture and representative of the most severe ground deformation that occurs along the margins of liquefaction-induced lateral spreads and landslides. The pipeline was constructed to evaluate its capacity to accommodate full-scale fault movement through the simultaneous axial pullout at four different joints. Measuring simultaneous performance of multiple joints allows for confirmation that the pipeline will respond to ground failure as intended, understand the complex interaction among the different joints, and determine the maximum ground deformation and axial pipeline load that can be sustained before joint leakage.

The pipeline was buried in the Cornell large-scale test basin in partially saturated sand that was compacted to have an average friction angle of 42º, equivalent in strength to that of a medium dense to dense granular backfill. The pipeline was laid out so that the spigot at each joint could pull from the bell approximately 2.3 in. (58.4 mm) before the spigot bead made contact with the restraining clips. Approximately 0.5 in. (12.5 mm) was available for compression at each joint. The depth of burial to top of pipe was 2.5 ft (0.76 m). During the test, the south part of the basin remained stationary, while the north part was displaced to the north and west by large-stroke actuators to cause soil rupture and slip at the interface between the two parts of the test basin.

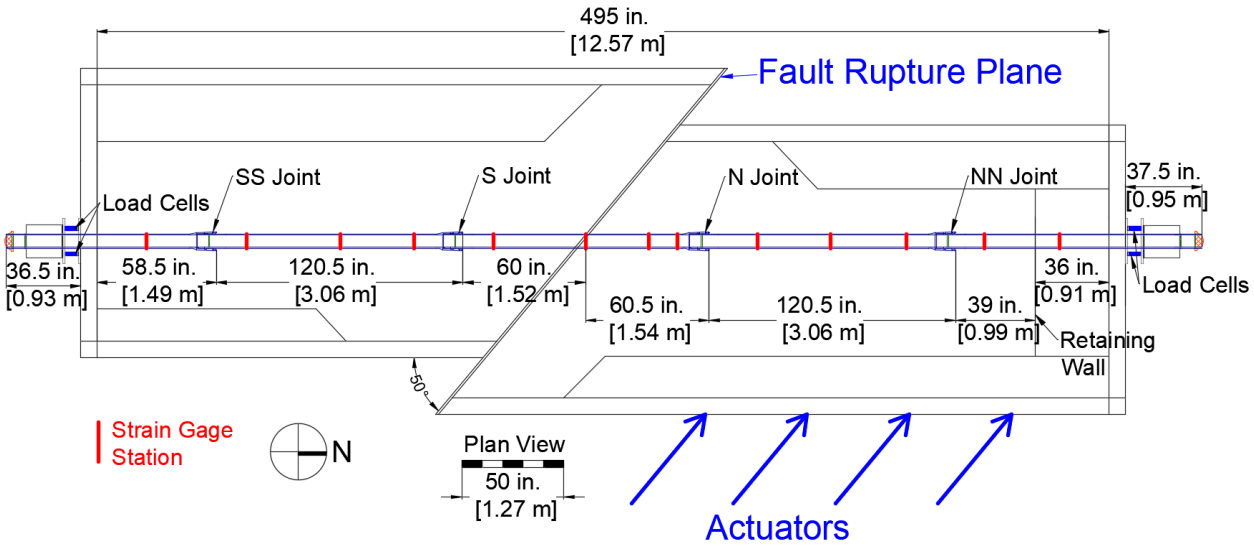


Figure 7.1. Plan View of US Pipe Ductile Iron Pressurized Pipe Centered Specimen in Test Basin

A 120.5-in. (3.06-m)-long pipe section was placed directly over the fault, with an intersection angle of 50°. Two identical 120.5-in. (3.06 m) pipes were installed to the north and the south of the center pipe. The simulated fault rupture caused both tensile and bending strains in the pipeline. The length of the pipeline buried in soil, also described as "test portion," was approximately 39 ft (11.89 m) long.

A wooden retaining wall was constructed at the north end inside the test basin to support the soil. The test basin was filled with compacted sand, so that the depth to the pipe crown was 30 in. (0.76 m). The retaining wall was 3 ft (0.91 m) away from end the box.

The pipe was pressurized with water to approximately 80 psi (552 kPa). The north (movable) portion of the test basin is connected to four MTS hydraulic actuators with load cells controlled by a MTS Flextest GT controller. All actuators were operated in synchronized displacement control. The general test procedure, after all soil placement and instrumentation was installed was:

a) Verify pipe internal pressure,
b) Move the test basin 1 in. (25.4 mm) at a rate of 12 in./minute (305 mm/minute),
c) Verify data collection, and system integrity
e) Begin moving basin again in multiple 10 in. (254 mm) increments until pipe failure.

At a fault displacement of roughly 19.0 in. (0.48 m) there was an abrupt pipe rupture at the bell near the south joint causing the internal pressure to drop to zero. The test was then stopped.

## 7.3 Instrumentation

Figure 7.1, a plan view of the test layout, shows the locations of the instruments along the test pipeline. The instrumentation consisted of strain gages at thirteen locations (gage planes) along the pipeline, load cells at the ends of the pipeline and direct current differential transformers (DCDTs) to measure joint displacements.

Sixty-four strain gages were installed in thirteen locations along the pipeline to measure strains and to evaluate axial forces and bending moments. Strain gages were positioned at the crown (C) and invert (I), and at the east (E) and west (W) springlines of the pipe. Table 7.1 provides the number of strain gage station locations with respect to the fault and joints. Strain gage locations were chosen on the basis of the expected deformed shape and axial behavior of the pipeline as determined from axial pull tests performed at Cornell University as well as the results of finite element analyses of the test. Strain gage stations 232 and -215 were intended to provide measurements of the end loads. Strain gage stations -45, 0, 31 and 45 are important to determine the deformed shape of the pipeline. Strain gage stations close to the joints, -166, -84, 84, 157 and 195, were placed to assess strain concentration near the joints. Table 7.1 provides locations and coding for the thirteen gage planes.

Three DCDTs were placed at each joint to measure the joint pullout and rotation, as well as spigot to bell face relative movement. Table 7.2 provides the locations and the labeling of the joint DCDTs to measure joint pullout and rotation, two DCDTs were mounted on the east and west springlines of the bell. In Figure 7.2 below shows the setup of a group of springline DCDTs.

The spigot is inserted into the bell approximately 2.3 in. (58.4 mm). After the instrumentation is installed, a protective shielding was then wrapped around the joint. Figure 7.3 is an overview of the pipe joint with the protective shielding.

Eight calibrated load cells were positioned at the ends of the test basin. Table 7.3 provides the locations and the labeling of the load cells.

Figure 7.2 Setup of Springline DCDTs


Figure 7.3. Pipe Joint with the Protective Shielding

Table 7.1. Strain Gage Locations and Coding System for US Pipe Ductile Iron Pressurized Pipe Test

| Gage Station | Gages | Distance from Fault | Distance from Closest Joint Bell Face |
|---|---|---|---|
| -215 | ST-215E-A-East Springline, Longitudinal<br>ST-215C-A-Crown, Longitudinal<br>ST-215W-A-West Springline, Longitudinal<br>ST-215I-A-Invert, Longitudinal | 215 in. (5.46 m) south | 34.5 in. (0.88 m) south of south-south joint |
| -166 | ST-166E-A-East Springline, Longitudinal<br>ST-166C-A-Crown, Longitudinal<br>ST-166W-A-West Springline, Longitudinal<br>ST-166I-A-Invert, Longitudinal | 166 in. (4.22 m) south | 14.5 in. (0.37 m) north of the south-south joint |
| -120 | ST-120E-A-East Springline, Longitudinal<br>ST-120C-A-Crown, Longitudinal<br>ST-120W-A-West Springline, Longitudinal<br>ST-120I-A-Invert, Longitudinal | 120 in. (3.05 cm) south | 60 in. (0.15 m ) south of the south joint |
| -84 | ST-84E-A-East Springline, Longitudinal<br>ST-84C-A-Crown, Longitudinal<br>ST-84W-A-West Springline, Longitudinal<br>ST-84I-A-Invert, Longitudinal | 84 in. (2.13 m) south | 24 in. (0.61 m) south of the south joint |

Table 7.1. Strain Gage Locations and Coding System for US Pipe Ductile Iron Pressurized Pipe Test (continued)

| Gage Station | Gages | Distance from Fault | Distance from Closest Joint Bell Face |
|---|---|---|---|
| -45 | ST-45E-A-East Springline, Longitudinal<br>ST-45C-A-Crown, Longitudinal<br>ST-45W-A-West Springline, Longitudinal<br>ST-45I-A-Invert, Longitudinal<br>ST-45E-C-East Springline, Circumferential<br>ST-45C-C-Crown, Circumferential<br>ST-45W-C-West Springline, Circumferential<br>ST-45I-C-Invert, Circumferential | 45 in. (1.14 m) south | 15 in. (0.38 m) north of the south joint |
| 0 | ST 0E-A-East Springline, Longitudinal<br>ST 0C-A-Crown, Longitudinal<br>ST 0W-A-West Springline, Longitudinal<br>ST 0I-A-Invert, Longitudinal | 0 | 60 in. (0.15cm) north of the south joint |
| 31 | ST 31E-A-East Springline, Longitudinal<br>ST 31C-A-Crown, Longitudinal<br>ST 31W-A-West Springline, Longitudinal<br>ST 31I-A-Invert, Longitudinal | 31 in. (0.79 m) north | 29.5 in. (0.75 m) south of the north joint |
| 45 | ST 45E-A-East Springline, Longitudinal<br>ST 45C-A-Crown, Longitudinal<br>ST 45W-A-West Springline, Longitudinal<br>ST 45I-A-Invert, Longitudinal | 45 in. (1.14 m) north | 15.5 in. (0.39 m) south of the north joint |
| 84 | ST 84E-A-East Springline, Longitudinal<br>ST 84C-A-Crown, Longitudinal<br>ST 84W-A-West Springline, Longitudinal<br>ST 84I-A-Invert, Longitudinal<br>ST 84E-C-East Springline, Circumferential<br>ST 84C-C-Crown, Circumferential<br>ST 84W-C-West Springline, Circumferential<br>ST 84I-C-Invert, Circumferential | 84 in. (2.13 m) north | 23.5 in. (0.60 m) north of the north joint |
| 120 | ST 120E-A-East Springline, Longitudinal<br>ST 120C-A-Crown, Longitudinal<br>ST 120W-A-West Springline, Longitudinal<br>ST 120I-A-Invert, Longitudinal | 120 in. (3.05 m) north | 59.5 in. (0.15 m) north of the north joint |
| 157 | ST 157E-A-East Springline, Longitudinal<br>ST 157C-A-Crown, Longitudinal<br>ST 157W-A-West Springline, Longitudinal<br>ST 157I-A-Invert, Longitudinal | 157 in. (3.99 m) north | 24 in. (0.61 m) south of the north-north joint |

Table 7.1. Strain Gage Locations and Coding System for US Pipe Ductile Iron Pressurized Pipe Test (completed)

| Gage Station | Gages | Distance from Fault | Distance from Closest Joint Bell Face |
|---|---|---|---|
| 195 | ST 195E-A-East Springline, Longitudinal<br>ST 195C-A-Crown, Longitudinal<br>ST 195W-A-West Springline, Longitudinal<br>ST 195I-A-Invert, Longitudinal | 195 in. (4.95 m) north | 14 in. (0.36 m) north of the north-north joint |
| 232 | ST 232E-A-East Springline, Longitudinal<br>ST 232C-A-Crown, Longitudinal<br>ST 232W-A-West Springline, Longitudinal<br>ST 232I-A-Invert, Longitudinal<br>ST 232E-C-East Springline, Circumferential<br>ST 232C-C-Crown, Circumferential<br>ST232W-C-West Springline, Circumferential<br>ST 232I-C-Invert, Circumferential | 232 in. (5.89 m) north | 51 in. (0.13 m) north of the north-north joint |

Table 7.2. DCDT Locations and Labeling for US Pipe Ductile Iron Pressurized Pipe Test

| Location | Displacement Measurement Device | Type and Stroke |
|---|---|---|
| South-South Joint | SS Disp E – East Springline | DCDT ± 2 in. |
| | SS Disp C – Crown | DCDT ± 2 in. |
| | SS Disp W – West Springline | DCDT ± 2 in. |
| South Joint | S Disp E – East Springline | DCDT ± 2 in. |
| | S Disp C – Crown | DCDT ± 2 in. |
| | S Disp W – West Springline | DCDT ± 2 in. |
| North Joint | N Disp E – East Springline | DCDT ± 2 in. |
| | N Disp C – Crown | DCDT ± 2 in. |
| | N Disp W – West Springline | DCDT ± 2 in. |
| North-North Joint | NN Disp E – East Springline | DCDT ± 2 in. |
| | NN Disp C – Crown | DCDT ± 2 in. |
| | NN Disp W – West Springline | DCDT ± 2 in. |

1 in. = 25.4 mm

Table 7.3. Load Cell Location and Labeling for US Pipe Ductile Iron Pressurized Pipe Test

| Location | Load Cell |
|---|---|
| South End | SW Top – Outer, West, Top<br>SE Top – Outer, East, Top<br>SW Bot – Outer, West, Bottom<br>SE Bot – Outer, East, Bottom |
| North End | NW Top – Outer, West, Top<br>NE Top – Outer, East, Top<br>NW Bot – Outer, West, Bottom<br>NE Bot – Outer, East, Bottom |

## 7.4 Soil Preparation and Compaction Data

The soil used during the test was crushed, washed, glacio-fluvial sand produced by RMS Gravel consisting of particles mostly passing the ¼ in. (6.35 mm) sieve. Figure 7.4 is a grain size distribution of the RMS graded sand. Eight inches (203 mm) of compacted sand was placed in the test basin, followed by the pipe sections, followed by approximately 8-in. (203-mm)-thick lifts until there was 30 in. (0.76 m) cover of compacted sand above the pipe crown. Every layer was compacted to the same extent and moistened with water in a similar way to achieve uniformity. Dry density measurements were taken for each layer using a Troxler Model 3440 densitometer. Moisture content measurements were obtained using both soil samples and the densitometer at the same locations. The target value of dry density was $\gamma_{dry}$ = 106 lb/ft$^3$ (16.7 kN/m$^3$) and the target value of moisture content was w = 4.0 %, corresponding to an angle of shearing resistance (friction angle) of the sand of approximately 42º.

Eight measurements of dry unit weight and moisture content were made for each soil lift. Figure 7.5 shows the approximate location of each measurement location. There were four measurement positions in the north portion of the test basin and four in the south portion. Table 7.4 lists the dry unit weights. Table 7.5 provides the moisture contents. The global average dry unit weight was 106.7 lb/ft$^3$ (16.8 kN/m$^3$) with a standard deviation of 2.5 lb/ft$^3$ (0.4 kN/m$^3$). The global average moisture content was 3.9% with a standard deviation of 1.1%. The angle of shearing resistance of the soil, based on correlations with soil unit weight established at Cornell, was 41-42°. The soil strength properties are representative of a well-compacted dense sand.

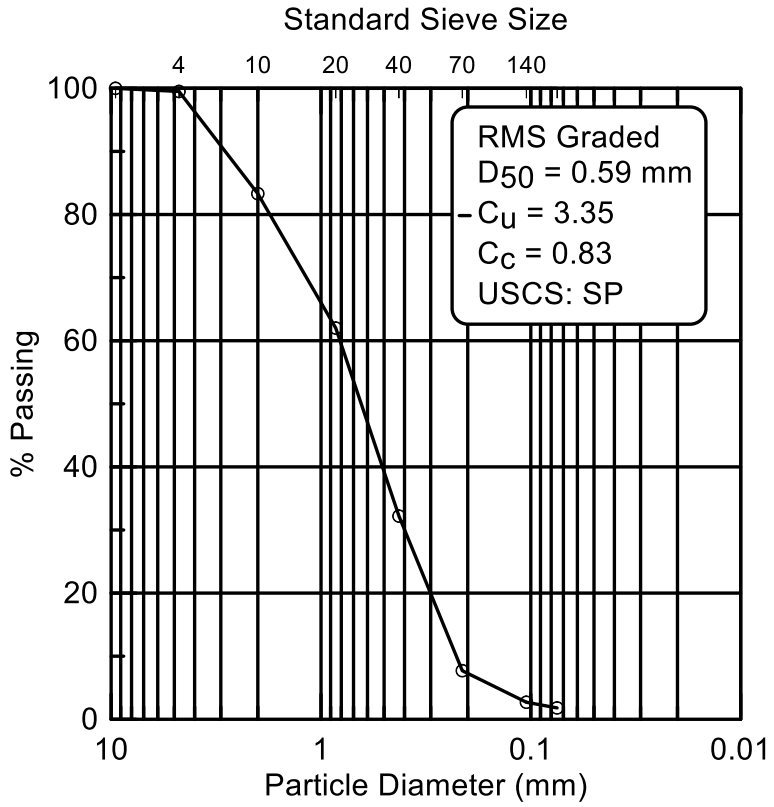


Figure 7.4. Particle Size Distribution of RMS Graded Sand

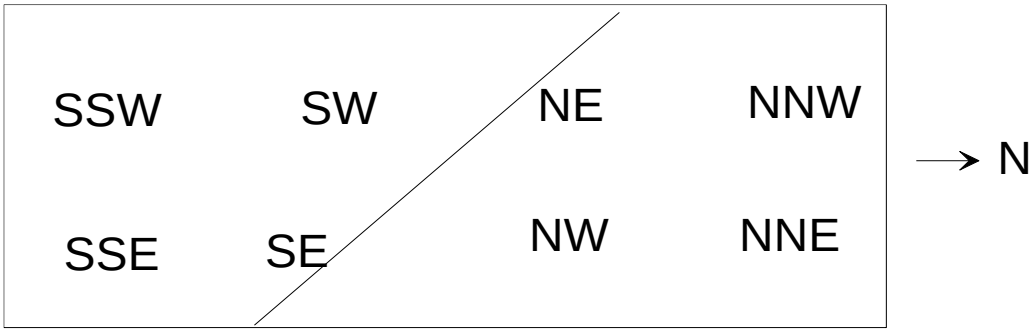


Figure 7.5. Plan View of Locations for Compaction Measurements

Table 7.4. Dry Unit Weights for US Pipe Ductile Iron Pressurized Pipe Test

| | Dry Unit Weights ($lb/ft^3$)[a] | | | | |
|---|---|---|---|---|---|
| Location | Lift 1 | Lift 2 | Lift 3 | Lift 4 | Lift 5 |
| NNW | 103.7 | 105.8 | 102.8 | 107.8 | 107.8 |
| NW | 106.0 | 106.2 | 106.8 | 104.7 | 112.1 |
| SSW | 106.7 | 107.4 | 105.2 | 106.0 | 106.7 |
| SW | 105.7 | 110.8 | 104.0 | 104.4 | 110.3 |
| SE | 106.3 | 107.9 | 106.3 | 106.6 | 113.0 |
| SSE | 103.9 | 109.0 | 107.0 | 106.4 | 106.9 |
| NE | 105.6 | 105.2 | 107.9 | 104.9 | 111.3 |
| NNE | 102.6 | 105.8 | 107.3 | 104.1 | 108.3 |
| Average | 105.1 | 107.3 | 105.9 | 105.6 | 109.5 |
| Stdev | 1.6 | 1.9 | 1.8 | 1.4 | 2.4 |
| Global Average | | | | | 106.7 |
| Global Stdev | | | | | 2.5 |

1 ($lb/ft^3$) = 0.1571 $kN/m^3$

Table 7.5. Moisture Tin Water Content Data for US Pipe Ductile Iron Pressurized Pipe Test

| | Moisture Tin Water Content, w (%) | | | | |
|---|---|---|---|---|---|
| Location | Lift 1 | Lift 2 | Lift 3 | Lift 4 | Lift 5 |
| NNW | 3.4 | 2.5 | 6.8 | 1.8 | 3.3 |
| NW | 3.4 | 4.3 | 3.1 | 4.1 | 2.8 |
| SSW | 4.1 | 3.7 | 3.3 | 4.9 | 5.8 |
| SW | 4.9 | 2.3 | 4.9 | 4.9 | 4.3 |
| SE | 3.4 | 2.4 | 4.1 | 3.4 | 4.1 |
| SSE | 4.4 | 2.5 | 3.9 | 3.8 | 2.7 |
| NE | 4.3 | 4.8 | 4.4 | 3.8 | 4.6 |
| NNE | 4.7 | 2.4 | 3.9 | 6.1 | 3.1 |
| Average | 4.1 | 3.1 | 4.3 | 4.1 | 3.8 |
| Stdev | 0.6 | 1.0 | 1.2 | 1.3 | 1.1 |
| Global Average | | | | | 3.9 |
| Global Stdev. | | | | | 1.1 |

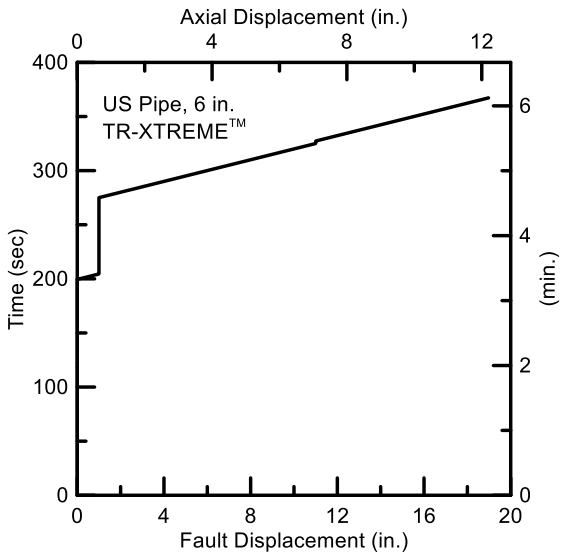


Figure 7.6 Fault Displacement vs. Time

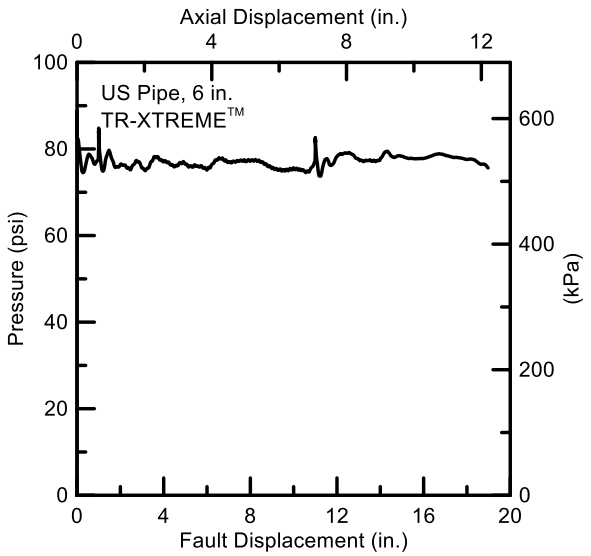


Figure 7.7. Internal Pipe Pressure vs. Fault Displacement

## 7.5 Test Basin Movements

Four actuators are connected between the movable portion of the test basin and the modular reaction wall in the laboratory. From south to north, the actuators are called short-stroke actuator 1 (SSA1), short-stroke actuator 2 (SSA2), long-stroke actuator 1 (LSA1), and long-stroke actuator 2. (LSA2). Each SSA actuator has a displacement range of ± 2 ft (± 0.61 m) for a total stroke of 4 ft (1.22 m) and load capacity of 100 kips (445 kN) tension and 145 kips (645 kN) compression. Each LSA actuator has a displacement range of ± 3 ft (0.91 m) for a total stroke of 6 ft (1.83 m) and load capacity of 63 kips (280 kN) tension and 110 kips (489 kN) compression.

Figure 7.6 shows the average displacement of the four actuators, which equals the fault displacement, with respect to time. The axial displacement imposed on the pipeline by fault displacement, $d_f$, is shown along the top horizontal axis. It is equal to $d_f \cos\beta$, for which $\beta$ is the angle of intersection between the pipeline and the fault.

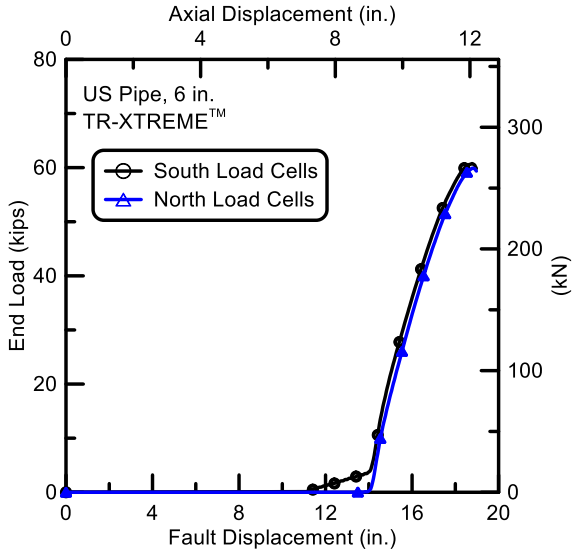


Figure 7.8 South and North Load Cells vs. Fault Displacement

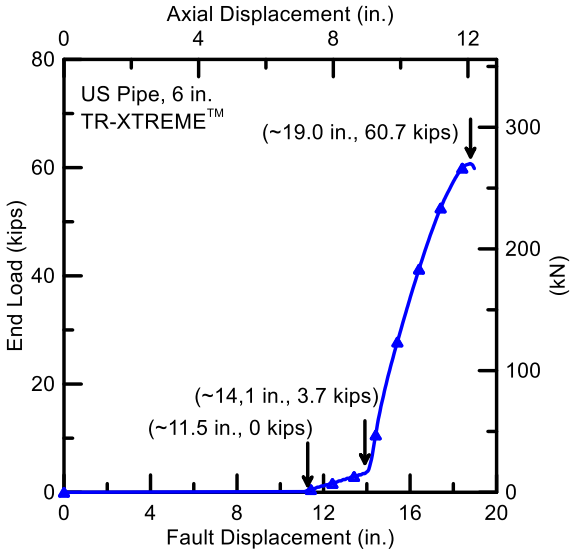


Figure 7.9 Average End Loads vs. Fault Displacement

## 7.6 Pipe Internal Pressure

The pipe was initially pressurized to 80 psi (552 kPa) before any basin movement. Each movement of the basin caused the pipe to increase slightly in overall length, causing the pressure to fluctuate slightly. Figure 7.7 shows the pipe internal pressure vs. fault displacement. At a fault displacement of roughly 19.0 in. (483 mm) there was a sudden loss of pressure in the pipe. This fault displacement corresponds to 12.2 in. (310 mm) of axial pipeline displacement. At this point the test was stopped and the water drained from the pipe.

## 7.7 End Loads

The end tensile loads were measured with four load cells at the south end of the test basin and four load cells at the north end. The sum of the four load cells at each end gives the total load at that end. Figure 7.8 shows the total load at the south and north ends of the test basin vs. fault displacement. The loads at the south end began to increase at a fault displacement of approximately 11.5 in. (292 mm), but the loads at the north end did not begin to increase until a fault displacement of 13.5 in. (343 mm). Thus, there was about 2 in. (50 mm) more fault displacement necessary to initiate load transfer to the north pipe end than the south. This additional 2 in. (50 mm) of fault displacement corresponds to an additional 1.3 in. (32.6 mm) axial test basin movement to begin load transfer to the

north end. After the north end loads begin to increase, the loads at the south and north ends are in excellent agreement.

Figure 7.9 shows the average end loads vs. fault displacement. Again, neither the south nor north ends show loads until substantial movement has taken place. At an average fault displacement of 14.1 in. (356 mm) and average load of 2.4 kips (10.7 kN) there is a sharp increase in the rate at which the end loads are increasing. This "displacement transition point" corresponds to an axial basin displacement of 9.1 in. (229 mm). As discussed in Section 7.8, this transition point represents 9.1 in. (231 mm) of axial pipeline extension, which is very close to the sum of the 2.3 in. (58.4 mm) pullout settings for the four TR-XTREME™ joints.

The outside diameter of the pipe was OD = 6.9 in. (175.3 mm) and the average measured wall thickness was $t_w$ = 0.3 in. (7.62 mm). This gives a pipe wall cross-sectional area of A = 6.22 in.$^2$ (4012.9 mm$^2$). The average Young's modulus of the ductile iron was E = 22650 ksi (156.2 GPa). This was determined from several tensile coupon tests. Using the average crown and invert strains at the gage stations and multiplying the strain times AE gives the force, F, in the pipe. The distribution of axial force along the pipe, calculated as $F = \varepsilon AE$, is shown in Figures 7.10 and 7.11.

Figure 7.11 shows that the axial forces in the pipe near the load cell locations are consistent with forces measured by the load cells. Both figures show that the load along the pipeline went up as the fault displacement increased. The load increased rapidly from 12 in. (305 mm) to 15 in. (381) of fault displacement. All four joints attained spigot bead contact with the restraining clips at 14 in. (356 mm) of fault displacement. When the pipe failed, the maximum load of 86.3 kips (384 kN) occurred at 31 in. (0.79 m) north of the fault, which is consistent with the axial pullout forces previously measured and reported for tension tests on the TR-XTREME™. The force at the spigot near the south joint dropped sharply between 18 in. (457 mm) and 19 in. (483 mm) of fault displacement because the circumferential deformation of the pipe caused the corruption of the axial strain gages.

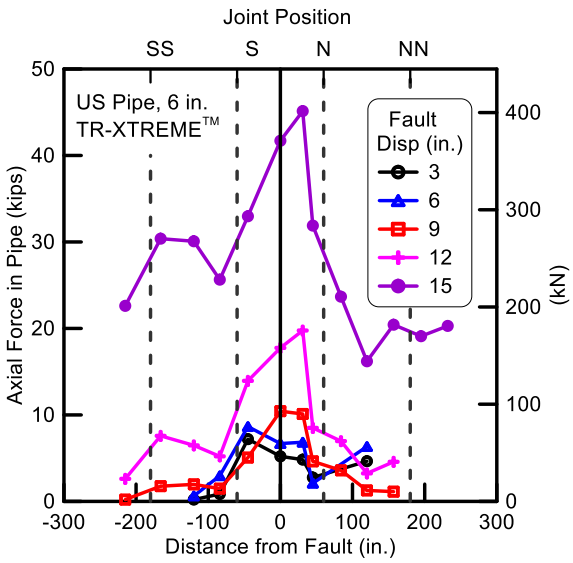


Figure 7.10. Axial Force in Pipe vs. Distance from Fault up to 15 in. (381 mm) Displacement

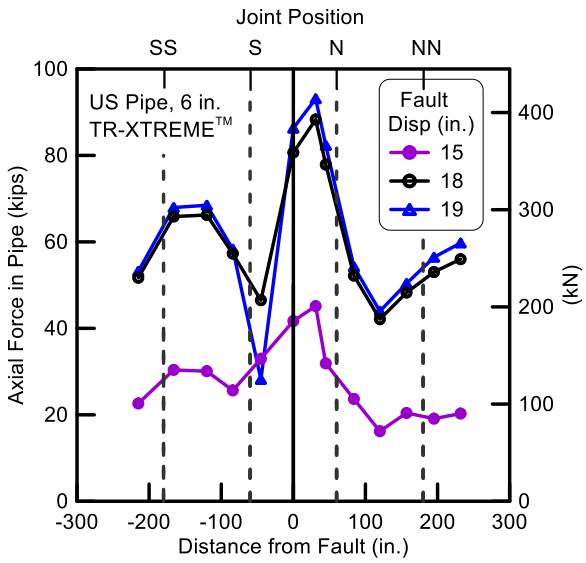


Figure 7.11. Axial Force in Pipe vs. Distance from Fault from 15 in. (381 mm) Displacement to Failure

## 7.8 Joint Movements and Rotations

The joint movements at the crown and east and west springlines of the south-south (SS), south (S), and north (N) and north-north (NN) joints are shown in Figures 7.12 to 7.15, respectively, and the collective movements of all joints are presented in Figure 7.16. Joint rotations are provided in Figure 7.17. The joint pullout movements and rotations were measured by the instrumentation described in Section 7.3 and shown in Table 7.2. In aggregate the measurements confirm that the pipeline was successfully able to accommodate fault rupture through axial displacements and rotations at all four joints. Moreover, the measurements provide a comprehensive and detailed understanding of how the movement was accommodated at each joint, the sequence of movements, and combined axial pullout and rotation at each joint.

During the first 6.8 in. (173 mm) of test basin displacement, most of the movement was taken up by the north and the south joints. After the north and the south joints were extended such that the spigot bead at each joint was in contact with the restraining clips, the north-north and the south-south joints slipped into spigot bead contact with the restraining clips. All four joints were extended to spigot bead contact with the restraining clips when the fault displacement reached the 14 in. (356 mm) transition point (see Section 7.7), after which additional movements were measured with the largest opening at the south joint.

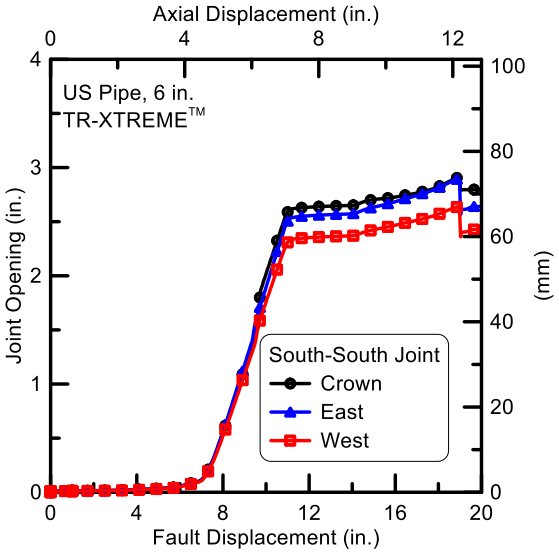


Figure 7.12. Displacements of South-South Joint

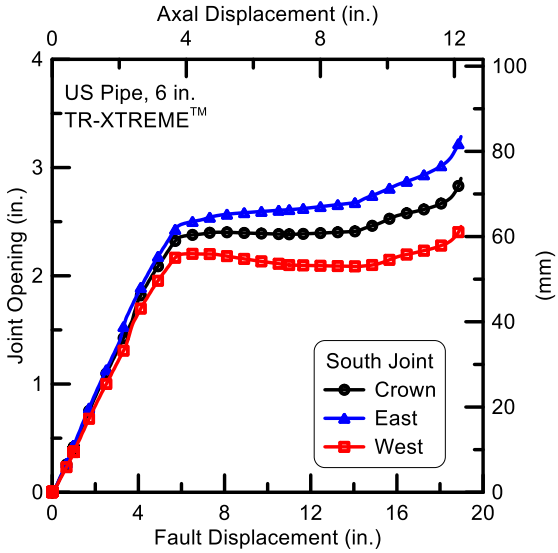


Figure 7.13. Displacements of South Joint

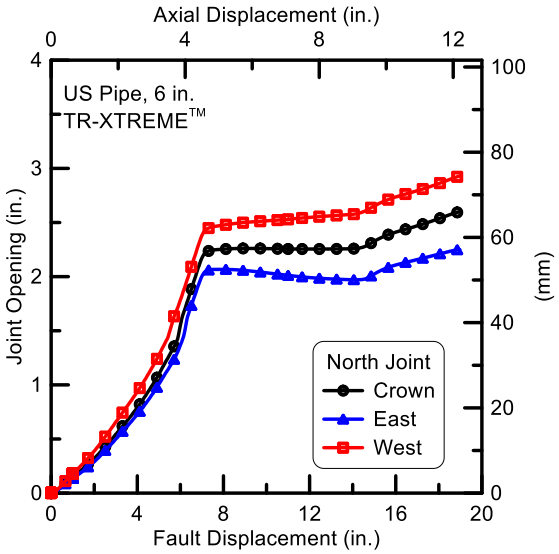


Figure 7.14 Displacements of North Joint

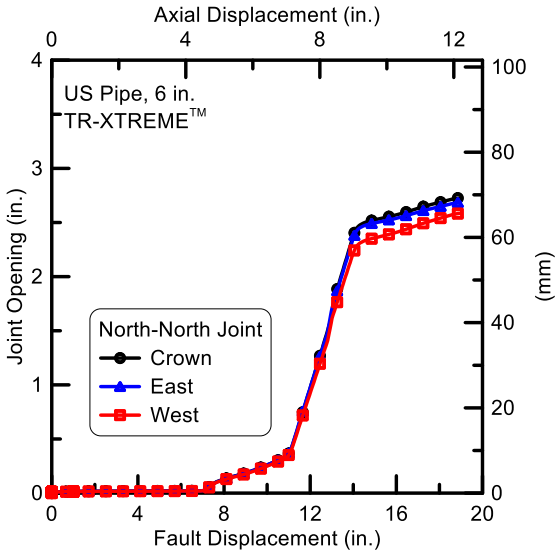


Figure 7.15. Displacements of North-North Joint

Figure 7.16 shows the average joint opening of all four joints vs. fault displacement. The south joint began to open first, followed by the north joint and then the south-south and north-north joints. At a fault displacement of approximately 19.0 in. (483 mm), the south joint failed, corresponding to an additional 3 in. (75 mm) beyond the transition point when all joints were extended to a condition of spigot bead/restraining clip contact.

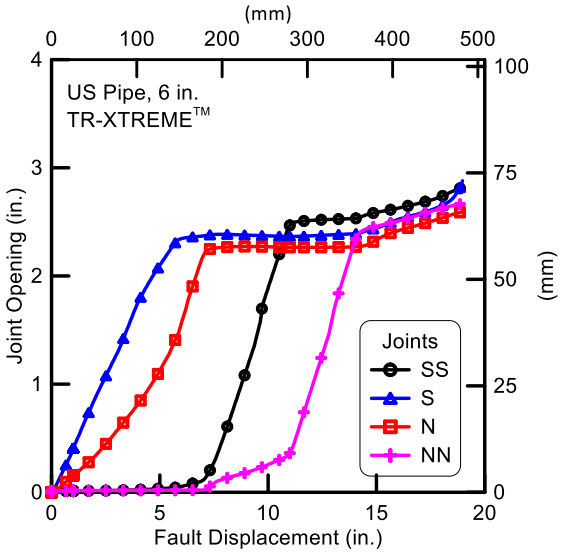


Figure 7.16. Average Joint Openings for All Joints vs. Fault Displacement

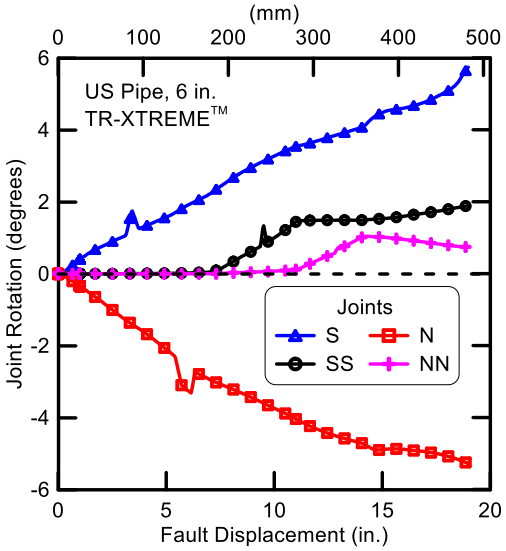


Figure 7.17. Joint Rotations vs. Fault Displacement

Joint rotation is calculated from the DCDT measurements at each joint as:

$$\text{Joint Rotation } (\text{deg}) = \tan^{-1}\left(\frac{180}{\pi}\frac{\text{East DCDT Displacement- West DCDT Displacement}}{\text{Separation Distance between the DCDTs Centerlines}}\right) \qquad (7.1)$$

The rotations of the four joints are shown in Figure 7.17. The north and the south joints, closest to the fault, had opposite joint rotations and accommodated most of the fault offset with maximum rotations of nearly 6 degrees. The joint rotations at the south-south and north-north joints were small, especially for the north-north joint, on the order of one to two degrees.

## 7.9 Bending Strains

Figures 7.18 and 7.19 present the measured bending strains in the pipeline, corresponding to fault displacements of 6 in. (152 mm), 12in. (305 mm), 15 in. (381 mm), and 18 in. (457 mm), respectively. The bending strains were calculated at each strain gage station as one half the difference between the springline strains. The plan view of the pipeline is similar to that in Figure 7.1, and the locations of the joints are indicated by the dashed lines.

The bending strains increase as the fault displacement becomes successively larger, with a maximum measured bending strain of about 600 με at 18 in. (457 mm) of fault displacement. In all cases, the strains are relatively low compared to the yield strength of the ductile iron pipe. Using the ductile iron properties for the TR-XTREME™ joints used in the Cornell testing program, the maximum measured tensile bending stress is 13.6 ksi (93.8 MPa). When added to axial tensile stress at the location of maximum bending strain, the total maximum tensile stress is approximately 25 ksi (172.4 MPa) which is less than half the yield stress of 52.5 ksi (362.0 MPa) and about 60% of the proportional limit stress of 42 ksi (289.6 MPa). Hence, the maximum stresses sustained by the pipeline, corresponding to the largest pipeline deformation, were well within the elastic range of pipeline behavior.

Because bending strains and joint rotations were measured during the test, it is possible to plot the moment vs. rotation response of the south and north joints closest to the fault and compare the data with the moment vs. rotation relationship previously measured and reported for TR-XTREME™ joints during four-point bending tests. Figure 7.20 presents the moment and rotation data for the south and north joints closest to the fault, pertaining to fault displacements of 3 in. (75 mm), 6 in. (152 mm), 9 in. (227 mm), 12 in. (305 mm), 15 in. (381 mm), and 18 in. (457 mm). The data compare very well with the average moment vs. rotation relationship for the two joints tested previously in the four-point bending tests.

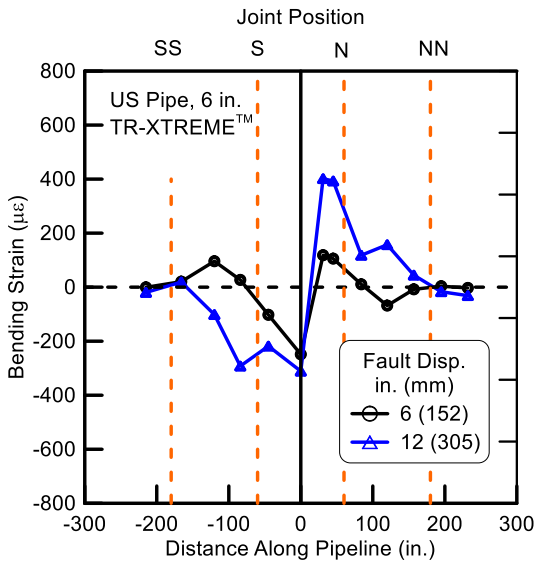


Figure 7.18. Bending Strains at 6 and 12 in. (152 and 305 mm) of Fault Displacement

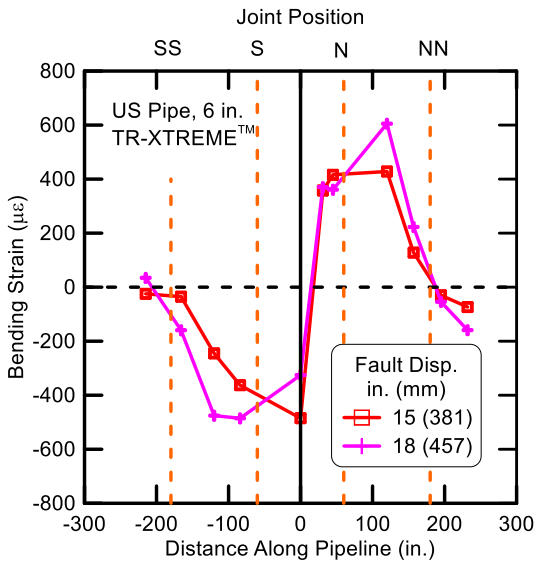


Figure 7.19. Bending Strains at 15 and 18 in. (381 and 457 mm) of Fault Displacement

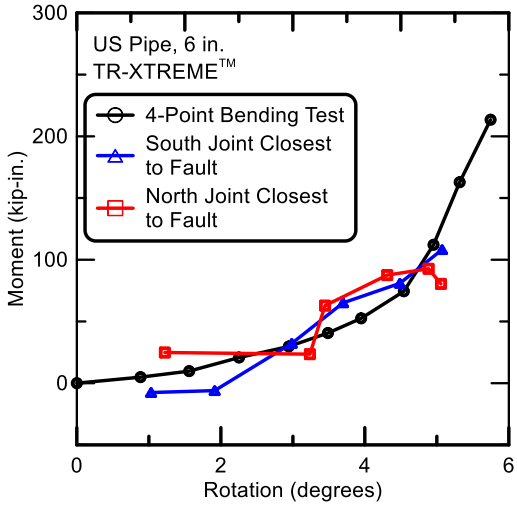


Figure 7.20. Comparison of Moment vs. Rotation Measurements during the Split Basin Test with Previously Measured Moment vs. Rotation Relationships during Bending Tests

## 7.10 Summary of Large-Scale Testing

A 39-ft (11.9-m)-long, five-piece section of a ductile pipeline was tested at the Cornell Large-Scale Lifelines Facility. The pipe had four joints, equally spaced about a 50º fault. The pipe was instrumented with sixty-four strain gages installed at thirteen locations along the pipeline to measure strains and to evaluate axial forces and bending moments. Strain gages were positioned at the crown (C), invert (I) east (E) springline, and west (W) springline of the pipe. There were three DCDTs at each joint to measure joint and restraint movements and to evaluate joint rotation. Four load cells were placed outside the test basin at each end, reacting between the test basin structural frame and pipe end restraint to measure axial force. The pipe was pressurized to approximately 80 psi (552 kPa).

The pipe was placed on a bed of compacted sand, aligned, instruments checked, and then backfilled with compacted sand to a depth of cover of 30 in. (762 mm) above the pipe crown. The test basin's north section was displaced along a 50º fault at a rate of 2 in. (51 mm) per minute. The basin was displaced roughly 1 in. (25.4 mm), paused, and then put in motion again. At a fault displacement of roughly 19.0 in. (483 mm) there was an audible "pop," the pipe lost pressure, and the test was stopped. The 19.0 in. (483 mm) fault displacement corresponds to 12.2 in. (310 mm) of axial extension of the test basin and pipe. Following excavation, a fracture was observed at the west springline of the bell of the south joint.

Figure 7.21 shows the fault rupture at pipe failure. Figure 7.22a shows the deformed pipe partially excavated after the test, including the failed south joint, and Figure 7.22b is a close-up photo of the south joint with the protective DCDT covering. The fractured south joint without the protective shield is shown in plan and elevation views in Figures 7.23a and 7.23b respectively.

The end forces at the south and north end of the test basin were about 60 kips (267 kN). The axial force in the pipe, as determined from the strain gage readings, was largest at 31 in. (0.790 m) north of the fault at 86.3 kips (384 kN), consistent with the axial pullout forces previously measured and reported for tension tests on the TR-XTREME™ joints.

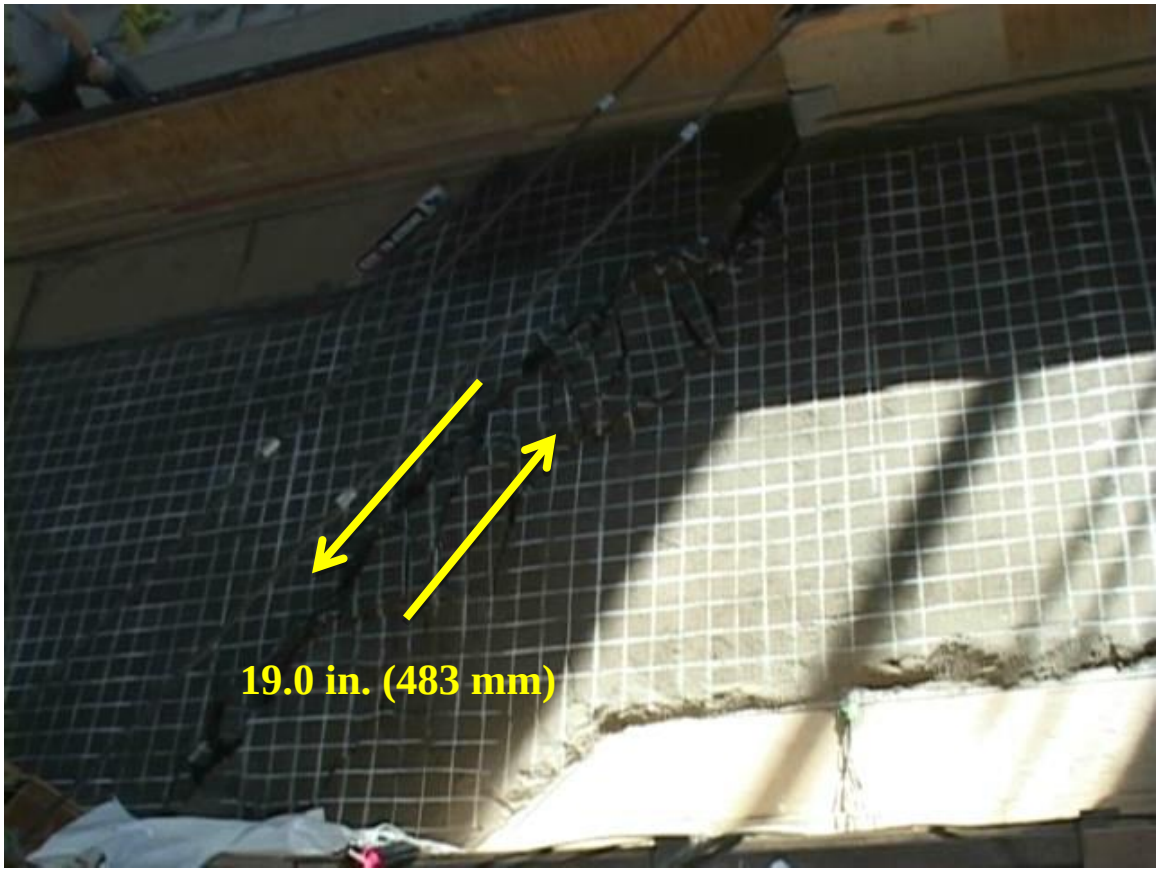


Figure 7.21. Fault Rupture at Pipe Failure

The test measurements confirm that the pipeline was successfully able to accommodate fault rupture through axial displacements and rotations at all four joints. Moreover, the measurements provide a comprehensive and detailed understanding of how the movement was accommodated at each joint, the sequence of movements, and combined axial pullout and rotation at each joint. The combined joint pullout displacements are 12.2 in. (310 mm), which exceeds the sum of the 2.3 in. (58.4 mm) spigot insertion length for all four joints. On average, the spigot at each joint pulled from the bell on the order of 3.05 in. (77 mm), thus confirming that significant additional pullout occurs beyond the slip required for the spigot bead to make contact with the restraining clips. This type of additional pullout capacity was observed at comparable levels of movement during previous tension testing of TR-XTREME™ joints. The maximum rotation measured at the joints closest to the fault was nearly six degrees, thus demonstrating the ability of the joints to sustain significant levels of combined axial pullout and rotation. The maximum stresses sustained by the pipeline, corresponding to the largest pipeline deformation, were well within the elastic range of pipeline behavior.

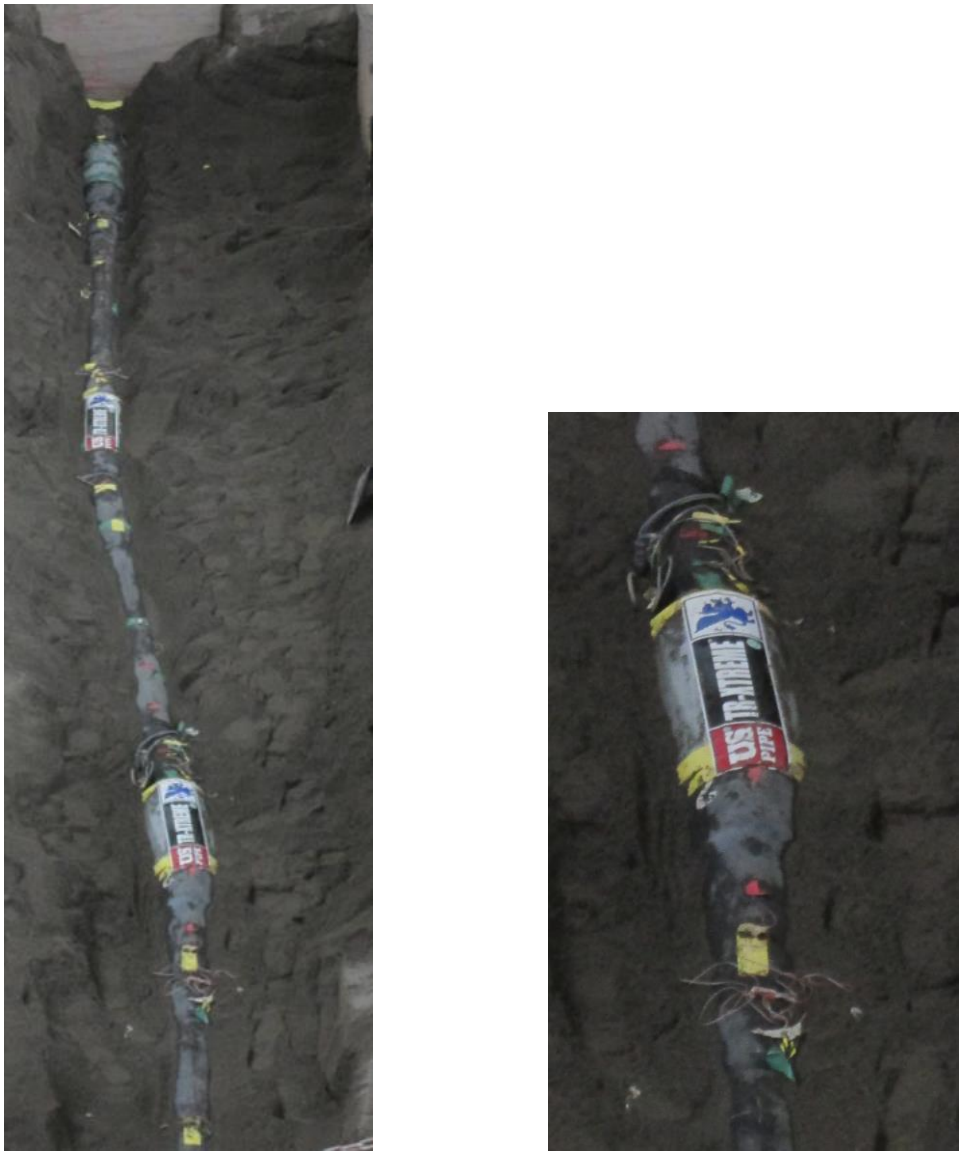

a) Deformed Pipe in Test Basin b) Failure at South Joint

Figure 7.22. Ruptured Pipe Following Test with the Protective Shield

The pipeline with TR-XTREME™ joints was able to accommodate significant fault movement through axial pullout and rotation of the joints. Fault rupture simulated in the large-scale test is also representative of the most severe ground deformation that occurs along the margins of liquefaction-induced lateral spreads and landslides.

a) Plan View of the South Joint

b) Elevation View of the South Joint from the West Springline

Figure 7.23. Ruptured Pipe Following Test without the Protective Shield

The amount of tensile strain that can be accommodated with pipelines with TR-XTREME™ joints will depend on the spacing of the pipeline joints. The pipeline used in the large-scale split-basin test was able to accommodate 12.2 in. (206 mm) of axial extension, corresponding to an average tensile strain of 2.61% along the pipeline. Such extension is large enough to accommodate the great majority of liquefaction-induced lateral ground strains measured by high resolution LiDAR after each of four major earthquakes during the recent Canterbury Earthquake Sequence in Christchurch, NZ (O'Rourke, et al., 2014). The test confirms that the TR-XTREME™ joints are able to sustain without leakage large levels of ground deformation through axial displacement and rotation of its joints under full-scale conditions of abrupt ground rupture.

## Section 8

## Summary

US Pipe has developed a hazard resistant ductile iron (DI) pipe joint, called the TR-XTREME™ joint. Sections of 6-in. (150-mm)-diameter pipes with the new joints were tested at Cornell University to 1) evaluate the stress-strain-strength characteristics of the DI, 2) evaluate the bending resistance and moment-rotation relationship of the joint for two positions of the locking clip segments, 3) determine the capacity of the joint in direct compression and tension, 4) investigate the axial soil resistance and pull-out capacity of the pipe-joint when buried in soil with and without a polywrap covering, and 5) evaluate the capacity of a 6 in. (150 mm) DI pipeline with TR-XTREME™ joints to accommodate fault rupture using the Cornell full-scale split-basin testing facility.

It should be noted that the term "rotation" in this report is equivalent to "deflection" as used commonly in the field and commercial pipeline information. Test results are summarized for tensile stress-strain-strength characteristics, bending test results, direct joint compression and tension, axial soil/pipe resistance, pipeline response to fault rupture, and significance of test results under the headings that follow.

### Tensile Stress-Strain- Strength Characteristics

The tensile test data for the DI specimens taken from the pipe with TR-EXTREME™ show similar tensile stress vs. strain characteristics as those of other US Pipe DI pipe. Given this similarity, there should be little to no difference in the mechanical performance of the pipe with this new joint relative to other pipe with similar geometric characteristics. Improvements in the casting and pipe fabrication are expected to result in pipeline response to large ground deformation that either equals or exceeds the TR-EXTREME™ jointed pipe response.

### Bending Test Results

Four-point bending tests were performed to evaluate the moment vs rotation relationships of the TR-XTREME ™ joints when the locking clips were at the 3 and 9 o´clock positions (Test A) and the 12 and 6 o´clock positions (Test B). Test A failed at an applied moment of 515 kip-in. (58.5 kN-m) and at an average rotation of 8.6 degrees. Test B failed at an applied moment of 480 kip-in. (7% lower than Test A) and at an average rotation of 9.1 degrees (6% higher than Test A). There is no significant moment – rotation difference for the two tests. The test results show that moments in the range of

the proportional limit, $M_{prop}$, and the yield moment, $M_{yield}$, were associated with loss of pressure and pipe leakage. Stress concentrations related to spigot-bead contact with the restraining clips are a likely source of local deformations leading to leakage at such moments.

**Direct Joint Compression and Tension**

The compressive testing showed that the TR-XTREME™ joint was able to accommodate axial loads to a compressive level at about the DI proportional limit. After this stress level was reached, progressive bending and local distortion of the pipe occurred. Axial loads of roughly 350 kips were applied to the joint. These results were similar to those from the four-point bending tests in which local deformation developed and subsequent leakage occurred after moments, corresponding to the proportional limit, were applied.

Two tension tests were performed on the US Pipe TR-XTREME™ joints. Tests T1 and T2 reached a maximum force of 83 kips (369.2 kN) at 2.75 in. (69.6 mm) of axial displacement and an axial load of 78 kips (346.0) at 2.72 in. (69.1 mm) of joint displacement, respectively. The joints began to leak at openings of 3.3 and 3.5 in. (83.8 and 88.9 mm) for T1 and T2, respectively. The overall behavior of T1 and T2 was nearly identical.

The onset of leakage was caused by forces generated between the spigot bead and restraining clips that deform the spigot inward a sufficient distance to allow the bead to slip past the clips, with attendant loss of water pressure. Similar to the compressive and four point bending test results for the US Pipe TR-XTREME™ joint, leakage occurred in the tensile tests when localized strains resulted in irrecoverable deformation. In this case, those strains are circumferential, and the irrecoverable deformation was reflected in shortening of the spigot diameter caused by forces between the spigot bead and clips.

**Axial Soil/Pipe Resistance**

The axial soil resistance tests confirm axial slip of the TR-XTREME™ joint under conditions in which sufficient soil/pipe shear resistance is mobilized either side of the joint to exceed the force required to initiate joint slip. Once the spigot bead engages the clips that, in turn, engage the bell mouth, additional resistance to pullout is mobilized from soil reaction at the bell as it is pulled through the soil. The test results provide excellent data with which to quantify the axial pullout loads and

displacements when there is relative movement between the adjacent soil and pipelines with 6-in. TR-XTREME™ joints.

The test results show that the polywrap reduced the axial pullout force by about 15% or more at displacements exceeding 4 in. (102 mm) when compared with unwrapped pipe under similar burial conditions. The reduced axial force is caused by the lower interface resistance between the soil and polyethylene wrap when compared with the interface resistance between soil and ductile iron pipe.

There is less than 10% difference between the ultimate pullout forces associated with the flat and curved ends of the bell oriented towards the direction of movement. The force vs. displacement data show that the ultimate pullout resistance is mobilized more rapidly when the flat end of the bell is oriented toward the direction of movement, thus contributing to a stiffer reaction.

**Pipeline Response to Fault Rupture**

A 39-ft (11.9-m)-long, five-piece section of a DI pipeline with TR-XTREME™ joints was tested at the Cornell Large-Scale Lifelines Facility. The pipe had four joints, equally spaced about a 50º fault. The pipe was pressurized to approximately 80 psi (552 kPa). The pipe was placed on a bed of compacted partially saturated sand, aligned, instruments checked, and then backfilled with compacted sand to a depth of cover of 30 in. (762 mm) above the pipe crown. The test basin's north section was displaced along a 50º fault at a rate of 12 in. (305 mm) per minute. At a fault displacement of roughly 19.0 in. (483 mm) there was an audible "pop," the pipe lost pressure, and the test was stopped. The 19.0 in. (483 mm) fault displacement corresponds to 12.2 in. (310 mm) of axial extension of the test basin and pipe. Following excavation, a fracture was observed at the west springline of the bell of the south joint.

The test measurements confirm that the pipeline was able to accommodate successfully fault rupture through axial displacements and rotations at all four joints. Moreover, the measurements provide a comprehensive and detailed understanding of how the movement was accommodated at each joint, the sequence of movements, and combined axial pullout and rotation at each joint. The combined joint pullout displacements are 12.2 in. (310 mm), which exceeds the sum of the 2.3 in. (58.4 mm) spigot insertion length for all four joints. On average, the spigot at each joint pulled from the bell on the order of 3.05 in. (77 mm), thus confirming that significant additional pullout occurs beyond the slip required for the spigot bead to make contact with the restraining clips. This type of additional pullout capacity was observed at comparable levels of movement during previous tension testing of

TR-XTREME™ joints. The maximum rotation measured at the joints closest to the fault was nearly six degrees, thus demonstrating the ability of the joints to sustain significant levels of combined axial pullout and rotation. The maximum stresses sustained by the pipeline, corresponding to the largest pipeline deformation, were well within the elastic range of pipeline behavior.

The pipeline with TR-XTREME™ joints was able to accommodate significant fault movement through axial pullout and rotation of the joints. Fault rupture simulated in the large-scale test is also representative of the most severe ground deformation that occurs along the margins of liquefaction-induced lateral spreads and landslides.

**Significance of Test Results**

The amount of tensile strain that can be accommodated with pipelines with TR-XTREME™ joints will depend on the spacing of the pipeline joints. The pipeline used in the large-scale split-basin test was able to accommodate 12.2 in. (206 mm) of axial extension, corresponding to an average tensile strain of 2.61% along the pipeline. Such extension is large enough to accommodate the great majority (over 99%) of liquefaction-induced lateral ground strains measured by high resolution LiDAR after each of four major earthquakes during the recent Canterbury Earthquake Sequence (CES) in Christchurch, NZ (O'Rourke, et al., 2014). These high resolution LiDAR measurements for the first time provide a comprehensive basis for quantifying ground strains caused by liquefaction on a regional basis. To put the CES ground strains in perspective, liquefaction-induced ground deformation measured in Christchurch exceed those documented in San Francisco during the 1989 Loma Prieta earthquake (e.g., O'Rourke and Pease, 1997; Pease and O'Rourke, 1997) and in the San Fernando Valley during the 1994 Northridge earthquake (e.g., O'Rourke, 1998). They are comparable to the levels of most severe liquefaction-induced ground deformation documented for the 1906 San Francisco earthquake, which caused extensive damage to the San Francisco water distribution system (e.g. O'Rourke and Pease, 1997; O'Rourke, et al., 2006).

The tests confirm that the TR-XTREME™ joints are able to sustain without leakage large levels of ground deformation through axial displacement and rotation. The test results are directly applicable to the performance of nominal 4-in. (100-mm), 6-in. (150-mm), and 8-in. (200-mm)-diameter US Pipe DI pipelines with TR-XTREME™ joints and representative of the behavior of these types of pipe and joints in all sizes.

## References


ASTM International (2013). "Standard Test Methods for Tension Testing of Metallic Materials", *ASTM Standards*. E8/E8M - 13a, 1 – 28.

AWWA (2009). "Ductile Iron Pipe, Centrifugally Cast for Water", *AWWA Standard*. ANSI/AWWA C151/A21.51-09.

O'Rourke, T.D. (1998). "An Overview of Geotechnical and Lifeline Earthquake Engineering", Geotechnical Special Publication No. 75, ASCE, Reston, VA, Proceedings of Geotechnical Earthquake Engineering and Soil Dynamics Conference, Seattle, WA, Aug. 1998, Vol. 2, pp.1392-1426.

O'Rourke, T.D. and J.W. Pease (1997). "Mapping Liquefiable Layer Thickness for Seismic Hazard Assessment", Journal of Geotechnical Engineering, ASCE, New York, NY, Vol. 123, No.1, January, pp. 46-56.

O'Rourke, T.D., A. Bonneau, J. Pease, P. Shi, and Y. Wang (2006). "Liquefaction Ground Failures in San Francisco" Earthquake Spectra, EERI, Oakland, CA, Special 1906 San Francisco Earthquake Vol. 22, No. 52, Apr., pp. 691-6112.

O'Rourke, T.D., Jeon, S-S., Toprak, S., Cubrinovski, M., Hughes, M., van Ballegooy, S., and Bouziou, D. (2014) "Earthquake Response of Underground Pipeline Networks in Christchurch, NZ", Earthquake Spectra, EERI, Vol. 30, No.1, pp. 183-204**.**

Pease, J.W. and T.D. O'Rourke (1997), "Seismic Response of Liquefaction Sites", Journal of Geotechnical Engineering, ASCE, New York, NY, Vol. 123, No. 1, January, pp. 37-45.